2019

Seismic performance of prefabricated bridge piers supported on pile foundations

Zhao Cheng
Iowa State University

Seismic performance of prefabricated bridge piers supported on pile foundations

by

Zhao Cheng

A dissertation submitted to the graduate faculty

in partial fulfillment of the requirements for the degree of

DOCTOR OF PHILOSOPHY

Major: Civil Engineering (Structural Engineering)

Program of Study Committee:
Sri Sritharan, Co-major Professor
Jeramy C. Ashlock, Co-major Professor
Steven J. Hoff
Jon Matthew Rouse
Jennifer Shane

The student author, whose presentation of the scholarship herein was approved by the program of study committee, is solely responsible for the content of this dissertation. The Graduate College will ensure this dissertation is globally accessible and will not permit alterations after a degree is conferred.

Iowa State University

Ames, Iowa

2019

TABLE OF CONTENTS

Page

LIST OF FIGURES

Page

LIST OF TABLES

Page

ACKNOWLEDGMENTS

I would like to specifically acknowledge and thank my major professor, Dr. Sri Sritharan, for his much valued input and guidance throughout my doctoral study. I greatly appreciate my co-major professor, Dr. Jeramy C. Ashlock for his contributions to the study present here. I also thank Dr. Steven Hoff, Dr. Jon Matthew Rouse, and Dr. Jennifer Shane for generously serving as members of my committee.

The research presented in this dissertation was funded by Iowa Highway Research Board (IHRB) and Federal Highway Administration State Transportation Innovation Council (STIC). The financial support and are greatly acknowledged.

I would like to express my thanks to Owen Steffens, Douglas Wood, and many others who helped conduct the extensive experimental efforts utilized in this study.

I would like to thank my parents for teaching me the value of hard work and graciously encouraging me throughout this journey. Finally, I would like to recognize and thank my wife, Yao Liu, who has supported me each step along this journey.

ABSTRACT

Using prefabricated components has been continuously gaining momentum in bridge constructions because of its numerous advantages over conventional cast-in-place construction methods. However, there are few, if any, projects that have utilized prefabricated components to construct the entire bridge piers because the seismic sufficiency of such structures has not been adequately addressed. Therefore, the studies in this dissertation were conducted to investigate the prefabricated bridge pier systems suitable for seismic regions. A pier system consisting of precast column, precast pile cap, and pile foundation was developed. For this system, the prefabricated components are integrally connected utilizing column socket connection and pile pocket connections that are preformed in the pile cap with corrugated steel pipes. An experimental study was performed using eight specimens that modeled the full-scaled connection interfaces, demonstrating that side shear strength in the column socket connection is sufficient to transfer large vertical loads from the column to the pile cap. An outdoor test was subsequently conducted on the column-pile cap-pile system at a cohesive soil site. A half-scale test unit was constructed on the foundation consisted of four vertical steel piles and four battered steel piles. To evaluate the system performance as well as the behaviors of various connections and pile foundation, the test unit was subjected to different combinations of vertical and lateral loads. Throughout the test, the socket and pocket connections maintained fixity with the formation of a plastic hinge in the column, evidencing that the system can ensure life safety and collapse prevention during earthquake events. Along with the results of numerical analysis, the battered piles were found to subject to larger axial forces but less bending moments than the vertical piles.

Following the successful development and investigation of the prefabricated column-pile cap-pile system, the controlled rocking pile foundation (CRPF) system with replaceable bar fuses was studied through a numerical approach. The CRPF system allows the pile cap to rock on the pile foundation and dissipates seismic energy through the inelastic deformations of the bar fuses connecting the pile cap and piles, thereby achieving additional seismic performance objectives such as immediately openings after an earthquake, shorter repair times, and lower repair costs. Analysis results indicated that, subjected to a severe earthquake, the CRPF system showed negligible residual displacement and maintained elastic behavior except the bar fuses as designed. The damaged fuses can be rapidly replaced to recover the bridge seismic resistance after the earthquake.

CHAPTER 1. INTRODUCTION

Background

"*To produce a safe bridge that is aesthetically pleasing, and satisfies all functionality requirements at a cost acceptable to the owner*," said Dr. Man-Chung Tang, a notable bridge engineer, regarding the mission of bridge design.

Bridges are constructed to create stable and permanent connections crossing over physical obstacles such as a body of water, valley, or road. By spanning two or more far-off points and eventually reducing the distance between them, bridges have been influencing people's culture and changing the day-to-day way in which people live, work, and relate to one another. The history of bridges started in ancient times. Like any human construction, different types of bridges have been constructed throughout their history as materials and technologies advanced. Nowadays, the girder bridge is the most commonly utilized bridge form throughout the United States and the world (Barker & Puckett 2013).

The structural components in a typical girder bridge (Figure 1.1) fall into two categories: superstructure that provides the horizontal spans and substructure that supports horizontal spans (AASHTO 2012). The loads acting on the bridge deck are carried by the supporting girders in the superstructure, mainly through their bending capacity. As prestressed concrete technologies rapidly developed after World War II, prestressed concrete girders became popular for the highway bridges. Possible span lengths of current prestressed concrete girders range from 12 to 61 m (40 to 200 ft) (Barker and Puckett 2013).

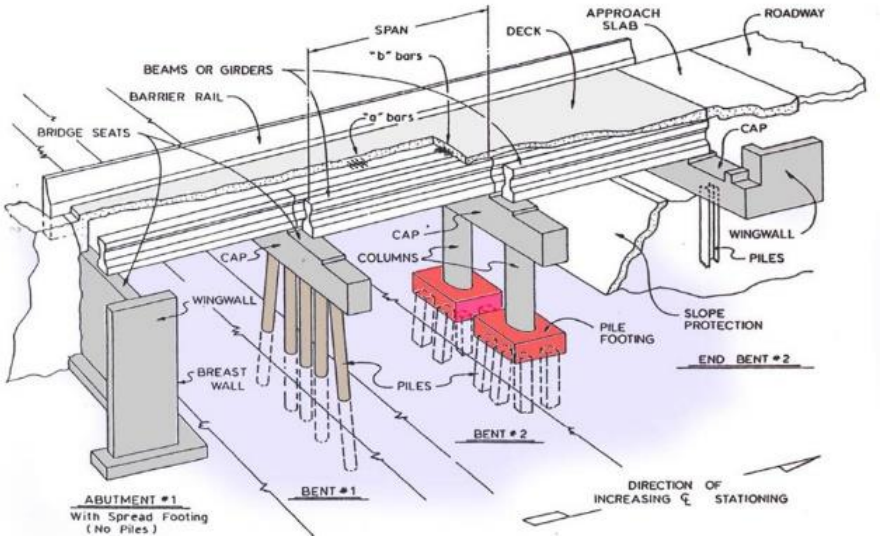

Figure 1.1 *Typical girder bridge components*

Piers in girder bridges support the superstructures vertically at their intermediate points and transfer loads to the foundations. Nowadays, piers are predominantly constructed using reinforced concrete. Although piers are traditionally designed to mainly carry gravity loads, these days it is common to take the high lateral seismic loads into account. Many types of piers have been built, and they can be distinguished by their framing configuration: column bent, pile bent, hammerhead, or pier wall. Selection of the type of piers should be based on functional, structural, esthetical, and geometric requirements. Often times, pier types are mandated by transportation agencies or owners. Among the different pier configurations, the column bent pier (Figure 1.2), consisting of a bent cap and supporting columns, has a lower construction cost. Geometry of the column bent pier is suitable to support either a steel or prestressed concrete girder superstructure. The reinforced concrete column bent is by far the most popular type of pier used in girder bridges (Wang 2014).

Figure 1.2 *Typical column bent pier in the girder bridge*

Foundation is part of bridge substructure, transferring loads from the bridge structure to the ground. In instances where the soil near the ground surface is not competent enough to carry the design loads, deep foundation involving deeper geologic materials is merited. Steel driven piles are extensively used for the deep foundation in highway girder bridges (Ma and Deng 2014). They are typically driven in groups, and capped with a thick reinforced concrete mat, commonly referred to as pile cap, to provide a suitable footing for bridge piers.

Prefabricated for Girder Bridge

Rising traffic congestion is a global phenomenon, from Los Angeles to Beijing, from London to Mumbai (INRIX 2018). Traffic delay associated with congestion induces not only direct costs relating to the value of fuel and time wasted, but also indirect costs referring to freight and business fees from company vehicles idling in traffic. One source of traffic congestion is the designation of work zones, which accompany construction activities on the highway. These have been cited by travelers as one of the most frustrating conditions on their trips (Cambridge Systematics, Inc. and Texas Transportation Institute 2005). As bridges are a critical component of the highway system, any bridge-related activities such as construction, repair, or basic maintenance will disrupt traffic. Transportation agencies are therefore

seeking methods for delivering high-quality bridge projects in reduced construction time. Because prefabricated bridge components are manufactured off-site and assembled on-site, they offer potential time-savings in construction. The prefabricated components also have a high product quality due to being repetitively produced in a controlled environment, which reduces the need for maintenance and repair. Furthermore, limiting on-site work improves safety for both the traveling public and construction workers and reduces environmental impacts. For these reasons, transportation agencies have been gradually embracing prefabricated technologies for highway bridge projects.

As the most commonly used prefabricated products, precast concrete components have been an integral part of bridge construction for many years. In girder bridges, they are used in a variety of locations. Precast girders are extensively used throughout the United States and the world, which are typically made composite with deck slab (Figure 1.3). Precast concrete has also been used in bridge substructure. Figure 1.4 shows examples of precast bent cap and precast abutment.

Figure 1.3 *Precast girders made composite with deck in the Magnolia Bridge, Louisiana*

Figure 1.4 *Precast bent cap (Lake Belton Bridge, Texas) and precast abutment (Davis Narrows Bridge, Maine)*

As manufacturing processes and construction technologies advanced, systems, or even full bridges, were constructed by assembling precast concrete components to address both the needs for fast project delivery as well as a high-quality product. Precast deck that is composed of a series of precast concrete panels (Figure 1.5) can produce full precast superstructure through composite connections to the supporting precast girders. An example of advancements that occurred with the implementation of precast concrete substructure is the US 6 Bridge over Keg Creek, Iowa (AASHTO 2011). The project (Figure 1.6) utilized precast concrete bent caps and columns, precast concrete abutments, and grouted splice couplers for connecting precast components. With the precast system and associated construction technologies, the mobility impact time due to the project was shortened from approximately six months to a total time of only two weeks. The I-5 Grand Mound Bridge (Figure 1.7) that was constructed with precast segmental columns, precast bent caps, and all precast superstructure, is a project that demonstrates the feasibility of full-precast girder bridge (ABC-UTC 2011).

Figure 1.5 *Full precast superstructure utilizing precast deck in the Mackey Bridge, Iowa*

Figure 1.6 *Precast substructure in the US 6 Bridge over Keg Creek, Iowa*

Figure 1.7 *Precast substructure and superstructure in the I-5 Grand Mound Bridge, Washington*

A critical factor for further promoting precast concrete for bridge projects lies in the connections between precast components. These connections should not only be easy to

construct, but they should also ensure dependable structural performance. Due to the lack of direct force transferring mechanisms between precast components, providing properly connections for precast bridges is challenging. Furthermore, if the bridges are located in seismic hazard zones, the seismic loads will make the design of connections more difficult.

Earthquake Damage to Bridges

The bridges in many regions worldwide with high population density are exposed to the risk of damage from earthquake (Figure 1.8). Earthquake damage to bridges that are located in these regions can cause severe consequences. Aside from the risk to people on or below the bridge, bridge closure in the immediate aftermath of an earthquake can cause vital links in the transportation system to be severed, impairing emergency response operations and resulting in post-earthquake economic impact (Moehle and Eberhard 2003).

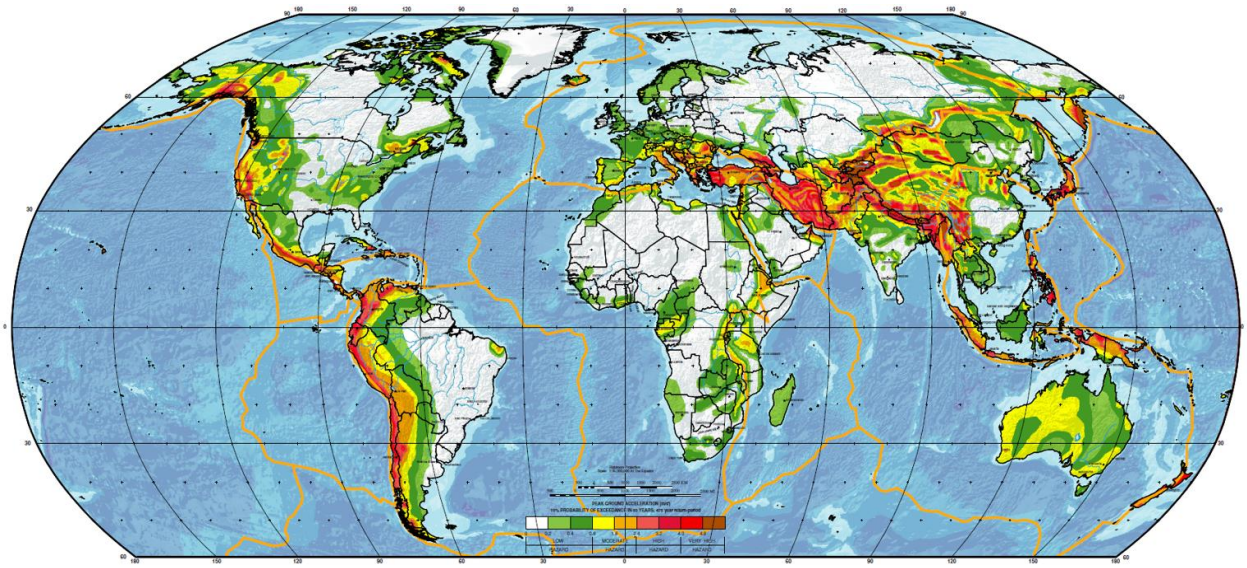

Figure 1.8 *Global seismic hazard map (GSHAP)*

The damages that each bridge has suffered because of an earthquake has varied with the characteristics of the ground motion and the construction details of the particular bridge. The following section briefly reviews the typical primary damages in past earthquakes that have triggered the collapse of bridges.

Figure 1.9 shows the examples of span unseating at movement joints. These simple spans were toppled from their supports either due to shaking or differential support movement associated with earthquake ground motion. Unseating has been a particular problem with short seating lengths that were common in older construction.

Figure 1.9 *Span unseating in the 1964 Niigate Earthquake (left) and the 1989 Loma Prieta Earthquake (right)*

In the bridges constructed prior to the 1970s, the amount and details of transverse reinforcement in columns provided negligible confinement to the concrete. As a result, the columns exhibited insufficient flexural ductility to withstand earthquakes, as shown in Figure 1.10. Shear failures of concrete bridge columns (Figure 1.11) have occurred in many earthquakes, which also ascribed to relatively light transverse reinforcement. Failures associated with improper termination or lap splices of longitudinal reinforcement in concrete bridge columns were identified in past earthquakes. The practice in Japan has been to cutoff some of longitudinal reinforcement at the mid height of column, leading to failure near the cutoff point, as shown in Figure 1.12. For construction convenience, column longitudinal reinforcement in old bridges was often lap-spliced or weld-spliced immediately above the foundation, where the regions experienced high flexural demand during earthquakes. Figure 1.13 shows damage to the base of a column, attributable to weld-splice failure, in the 1995

Kobe Earthquake. Concrete columns also failed due to inadequate anchorage of longitudinal reinforcement. An example is shown in Figure 1.14.

Figure 1.10 *Confinement failure of column in the 1971 San Fernando Earthquake*

Figure 1.11 *Shear failure of a column in the 1994 Northridge Earthquake*

Figure 1.12 *Failure of column with terminated longitudinal reinforcement in the 1995 Hyogo-Ken Nanbu Earthquake*

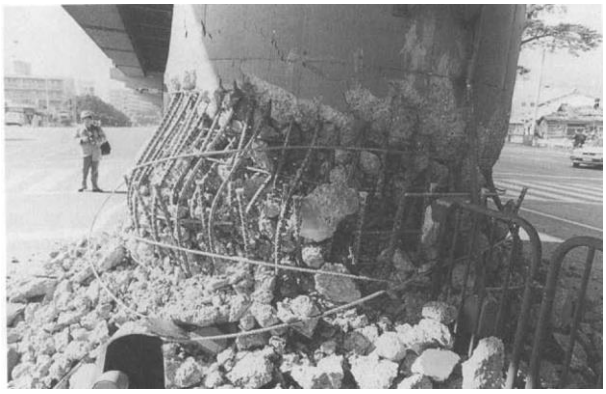

Figure 1.13 *Weld splice failure of column longitudinal reinforcement in the 1995 Kobe Earthquake*

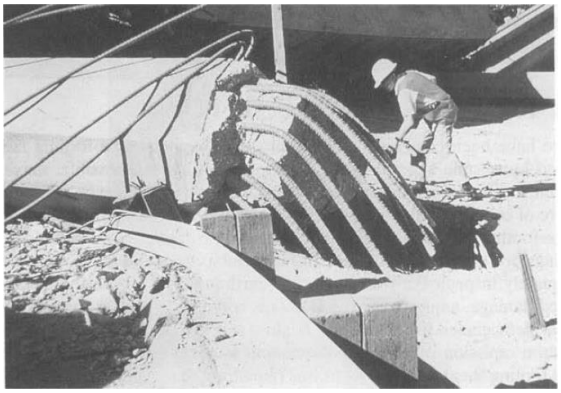

Figure 1.14 *Column failure due to longitudinal reinforcement pullout in the 1971 San Fernando Earthquake*

In reviewing earthquake damages to bridges, the majority tend to be direct consequences of the early elastic design philosophy that was uniformly adopted for bridge seismic design prior to the 1970s (Priestley et al. 1996).

Seismic Design Philosophy

Following several damaging earthquakes, particularly the 1971 San Fernando Earthquake, the procedure of bridge seismic design transitioned from the elastic design approach to the capacity design approach. With the early elastic design approach, the load demand produced by earthquake is simply taken as a lateral force that equals to a specified fraction of the permanent weight of the bridge, and the entire bridge was designed to remain

elastic when exposed to this lateral force. Designing bridges to respond elastically avoids damage, but is not economically feasible in moderate to high seismic regions because very large forces will be developed in the columns and foundations. Furthermore, there is a possibility that an earthquake larger than the design earthquake will occur during the service life of the bridge. In this case, the elastic design approach seriously underestimated the seismic displacement, and often led to incorrect moment patterns during earthquakes, which may cause catastrophic failure of bridges. The capacity design approach, unlike the elastic design approach, allows the bridges to be damaged in a certain manner, but without collapse of all or part of the bridge during the design earthquake. This would assure "life-safety" in an economical way. With this "no-collapse" philosophy, only ductile yielding is permitted in the selected members that are specifically designed and detailed. As a consequence, the yielding of these selected members places a cap on the forces in the rest of members during an earthquake greater than anticipated in the design. The ductile behavior of the yielded members keeps the bridge from collapsing, and other members of the bridge, referred to as capacity protected components, can be economically designed to remain elastic under the maximum resistance (i.e. capacity) of the yielded members rather than inertial force associated with the mass of the bridge.

Using the capacity design approach, yielding of selected members protects all the other bridge members against damage. The region pre-selected to experience yielding during the design earthquake is commonly referred to as the plastic hinge in earthquake engineering. Theoretically, a designer can locate the plastic hinge anywhere in the lateral load path of the bridge as long as the overall stability is provided. However, it is a practice in seismic design to keep plastic hinges above the ground or just below the ground line for post-earthquake

inspection and subsequent repair if necessary. For the girder bridge with column bent piers and steel driven pile foundations, the practices seek to locate plastic hinges at the ends of columns. Thus, the capacity protected components such as foundation, bent cap, superstructure, and their connections, need to be designed and detailed to remain essentially elastic when the column reaches its plastic moment capacity.

Seismic Resilient Structures

Bridges designed following the conventional capacity design approach would ensure life safety through forming the plastic hinges in preselected locations. However, they often sustain excessive damages and exhibit considerable residual drifts following major seismic events. The damaged bridges can disrupt traffic, necessitate time-consuming inspections, and may be difficult to repair. Addressing these issues, seismic resilient structures (such as rocking structures) have been developed to achieve additional seismic performance objectives such as mitigating economic losses, maintaining bridge functionality, and improving reparability.

Structures with rocking mechanism can suffer less damage, even experiencing large deformation for the duration of shaking. In addition, rocking structures have recentering capacity resulting from unbonded posttensioning or structural self-weight. Unlike conventional structures designed to form plastic hinges, the rocking structures exhibits a bilinear elastic behavior with minimal energy dissipation capacity, as shown in Figure 1.15. The softening in the slope of the load-displacement response is identified by the uplift of the structures with respect to their footings. As a result of the elastic behavior, energy dissipating elements are required for the rocking structures to provide sufficient hysteretic energy dissipation capacity. The combination of rocking mechanism and additional energy dissipating elements leads to a hysteresis behavior typically referred to as flag-shaped.

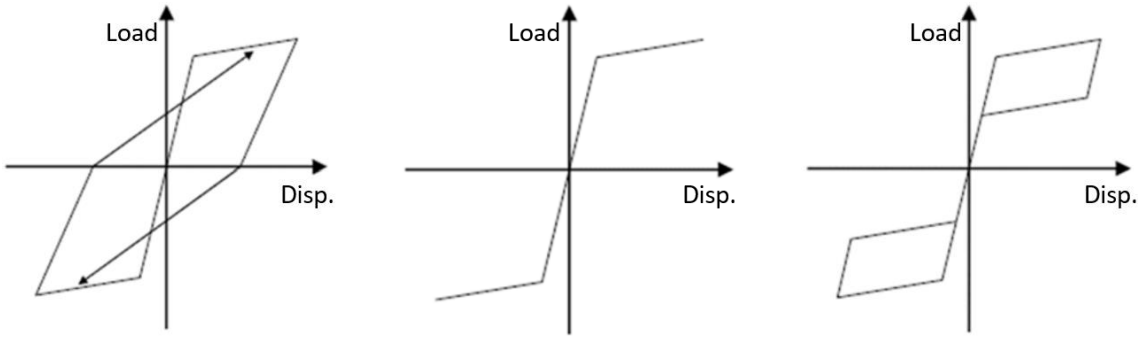

(a) conventional (b) bilinear elastic (c) flag-shaped

Figure 1.15 *Idealized hysteresis behavior of conventional plastic hinge system and rocking system*

Research Motivation

Based on the aforementioned seismic design philosophy, the capacity protected components should be designed and detailed based on an inelastic response. For the bridges attempting to profit from precast concrete technologies, these seismic requirements pose a challenge to the design of systems and connections between precast components. Historically, earthquake damage to the precast systems occurred mainly at the connections between the components because of poor detailing to withstand many cycles of load reversals (Kunze et al. 1965; Lew et al. 1971). Therefore, the concept of "emulative" is commonly accepted for designing seismic connections in precast bridges, which requires the connections between precast components to be designed and detailed to act as a conventional concrete construction joint. Transportation agencies, industry, and academia have been successfully developing a number of connection details for precast bridge members that are emulating cast-in-place connections, promoting the use of precast concrete in the bridge industry (Marsh et al. 2011). However, the precast column bent pier with steel pile foundation was seldom, if ever, encountered in practice because of the lack of the structurally dependable and easy-to-construct connections for precast pile cap to connect precast column

and steel piles. During a moderate-to-high earthquake, plastic hinges are often pre-selected to form in the columns. The column-to-foundation connections thereby would experience the high moment and shear demands induced by the column plastic hinging mechanism, superimposed on an axial load in the column. In the pile foundation, each single pile would be subject to a considerable combination of axial load, shear, and bending moment that are induced by both gravity and column plastic hinging mechanism. These seismic demands (Figure 1.16) make the design of connections in precast pile cap more challenging. In addition, the difficulty in experimentally testing a soil-foundation-structure system causes a lack of information on the system behavior of precast column bent pier with steel H-pile foundation, particularly under earthquake excitation.

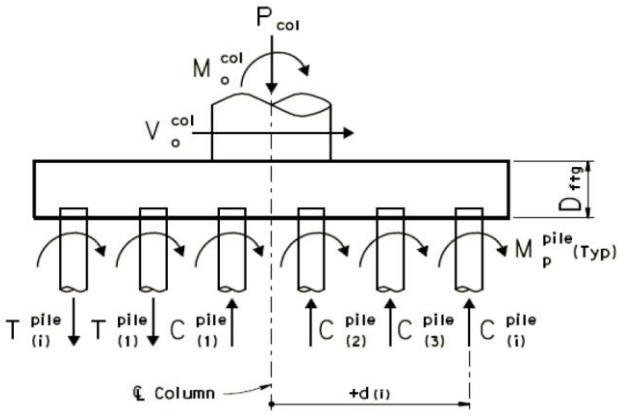

Figure 1.16 *Demands for column-to-pile cap and pile cap-to-pile connections*

Further than ensuring life safety, numerous efforts have been made to develop rocking piers for bridges. In addition to the pier column with internal unbonded prestressing tendons, bridge piers supported on shallow foundations would also mobilize rocking behavior at their footings, utilizing the weight of superstructures as the recentering force. The advantages of the rocking shallow foundation include sufficient recentering capacity, significant energy dissipation, well-defined moment capacity. However, this type of system

has relatively low bearing capacity, may experiences the residual settlement and rotation due to the permanent deformation of underlying soils, and is difficult to repair after an earthquake. In order to facilitate the uniform application of rocking systems, new structures with less concern regarding the soil conditions, improved reparability, and adequate energy dissipation are necessary.

Research Summary

Challenges to the incorporation of precast column bent pier with steel pile foundation include a lack of proper connections between precast components and an absence of research related to behavior of a soil-foundation-structure system, particularly under earthquake excitation. These issues have been addressed in the study presented in this dissertation. Following the comprehensive evaluation of many types of connecting methods that are potentially suitable for constructing precast column bent pier, the alternative connections were identified for study with the considerations of structural performance, constructability, and durability. Details of the proposed connection have been optimized through a series of experimental tests. A half-scaled test unit representing the precast column bent pier with steel H-pile foundation utilizing the proposed connection details has been subsequently tested under cyclic reversed loading at an outdoor test site in order to adequately account for the soil-foundation-structure interaction. To further understand soil-foundation interaction, the pile foundation in the test unit has been loaded alone to failure, and a nonlinear finite element model has been developed to simulate the system behavior of precast column bent piers with different pile foundation configurations. In the context of above described experimental and analytical works, the study presented in this dissertation will promote and advance the use of precast concrete for routine bridge construction, especially in seismic hazard zones.

This dissertation also presents a controlled rocking pile foundation (CRPF) system, which consists of the pile cap supported on the piles that are connected to the footing using the replaceable bar fuses. When subjected to strong earthquake ground motions, the system allows the pile cap rock on the pile foundation and dissipates seismic energy through the inelastic deformations of the fuses. Following the conceptual design of the CRPF system, an analytical model was developed for a bridge pier utilizing the CRPF system to investigate its seismic response. Another model was established for a pier designed to develop a plastic hinge in its column. Both the two models were subjected to the static cyclic loads, dynamic free vibrations, and earthquake ground motions, and their responses were compared. The results indicated the advantages of the CRPF system over conventional designed bridge piers.

Dissertation Layout

Following the introductory chapter, Chapter 2 reviews the literatures on the topics related to the study presented in this dissertation, such as policy and design for precast column bent pier, current state of the knowledge about connecting methods for precast components, design of steel pile foundation, rocking structures, and analysis techniques that have been used to analyze structure, in particular nonlinear pile response while satisfying simultaneously the appropriate nonlinear response of the soil. Chapters 3, 4, 5 and 6 are written as journal articles. Chapter 3 presents the experimental investigation of the proposed column-to-pile cap connections in sustaining axial load. The experimental test of a precast column bent pier with steel pile foundation for design validation and strength evaluation is presented in Chapter 4. Chapter 5 presents the pile foundation behavior under the combination of gravity and lateral loading. Chapter 6 details the development and numerical analysis of the CRPF system. Chapter 7 concludes the dissertation and provides a summary of the research results.

References

ASSTO. (2011). *IA: US 6 Keg Creek Bridge*. Retrieved from America's Transporation Awards: https://americastransportationawards.org/past-projects/2012-2/ia-us-6-keg-creek-bridge/. Accessed April 2018.

AASHTO. (2012). *LRFD* Bridge *Design Specifications, 6th Edition*. Washington, D.C.

ABC-UTC. (2011). *I-5 / US 12 Bridge at Grand Mound*. Retrieved from ABC Project Database: http://*utcdb*.fiu.edu/bridgeitem?id=273. Accessed April 2018.

Barker, R. M., and Puckett, J. A. (2013). *Design of highway bridges: An LRFD approach*. John wiley & sons.

Cambridge Systematics, Inc. and Texas Transportation Institute. (2005). *Traffic congestion and reliability: trends and advanced strategies for congestion mitigation* (No. FHWA-HOP-05-064). United States. Federal Highway Administration.

INRIX. (2018, Feburary). *INRIX Global Traffic Scorecard*. Retrieved from INRIX: http://inrix.com/scorecard/. Accessed April 2018.

Kunze, W. E., Sbarounis, J. A., and Amrhein, J. E. (1965). *Behavior of Prestressed Concrete Structures During the Alaskan Earthquake*. Portland Cement Association.

Lew, H. S., Leyendecker, E. V., and Dikkers, R. D. (1971). *Engineering aspects of the 1971 San Fernando earthquake* (Vol. 40). US National Bureau of Standards.

Ma, Y., and Deng, N. (2014). Deep Foundations. In W.F. Chen, & L. Duan, *Bridge Engineering Handbook: Substructue Design.* CRC Press.

Marsh, M. L., Wernli, M., Garrett, B. E., Stanton, J. F., Eberhard, M. O., and Weinert, M. D. (2011). *NCHRP Report 698: Application of Accelerated Bridge Construction Connections in Moderate-to-High Seismic Regions*. Transportation Research Board, Washington, DC.

Moehle, J. P., and Eberhard, M. O. (2003). Earthquake Damage to Bridges. In W.F. Chen, & L. Duan, *Bridge Engineering: Seismic Design.* CRC Press.

Priestley, M. N., Seible, F., and Calvi, G. M. (1996). *Seismic design and retrofit of bridges*. John Wiley & Sons.

Wang, J. (2014). Piers and Columns. In W.F. Chen, and L. Duan, *Bridge Engineering Handbook: Substructure Design.* CRC Press.

CHAPTER 2. LITERATURE REVIEW

Accelerated Bridge Construction (ABC) and Precast Elements

Accelerated bridge construction (ABC) can be defined as bridge construction that uses innovative planning, design, materials, and construction methods in a safe and cost-effective manner to reduce the onsite construction time that occurs when building new bridges or replacing and rehabilitating existing bridges (Culmo 2011). The successes of a number of projects in Iowa and other states prove that ABC techniques offer many advantages over traditional cast-in-place (CIP) bridge construction, which include, but are not limited to accelerated project delivery, improved construction quality, low life-cycle costs, minimal environmental impacts, improved work-zone safety, and reduced traffic disruptions. The available ABC methods are in two main categories: (1) offline construction that constructs the bridge away from the final location and then moves the completed bridge into place through self-propelled modular transporter (SPMT), lateral sliding, longitudinal launching, or a crane based system, and (2) online construction that constructs the bridge in its final location using prefabricated bridge elements and systems (PBES) (UDOT 2017). Among these methods, online construction using prefabricated elements is the most common strategy for implementing ABC.

Prefabricated elements, especially precast concrete elements, have been an essential part of bridge construction for many years. Being constructed in a controlled environment, these elements normally achieve higher quality. The un-restrained condition during curing (i.e., no contact with previously cast concrete) reduces, and in most cases, eliminates shrinkage cracking, thereby minimizing long term deterioration of the concrete (Culmo 2011). Given the considerations of transportation, fabrication, and construction, the height

and width of each precast element, including projecting reinforcing, are recommended to less than 3.0 m (10 ft) and 4.3 m (14 ft), respectively (UDOT 2017). In addition, the elements need to be sized based on the weight limits of the available equipment and the proposed shipping routes. Designers should carefully consider the constructability when using precast elements. Some effective methods to improve the constructability include providing repetitive and simple details, minimizing the number of connections, and providing as much tolerance in the system as possible. Based on the "emulating" principles, the design of individual elements can follow traditional LRFD design specifications as if they were constructed using CIP techniques. Precast elements can be used for all components in bridges. Due to the interests of this study, only precast frame piers will be discussed in the following section.

Precast Bridge Pier

Most bridge piers can be grouped into frame pier, T-pier, pile bent, or diaphragm pier, as shown in Figure 2.1 (Iowa DOT 2018). Among these pier configurations, frame pier is the usual selections for typical pretensioned prestressed concrete beam (PPCB) or continuous welded plate girder (CWPG). If a bridge is not required to be designed for vehicular collision force and ice load, the frame pier is preferred because of low construction cost (Iowa DOT 2018). A frame pier typically consists of a bent cap, columns, and foundation under each column. In Iowa, considering site conditions and economy, it often is appropriate to use steel H-piles for pier foundation (Iowa DOT 2018).

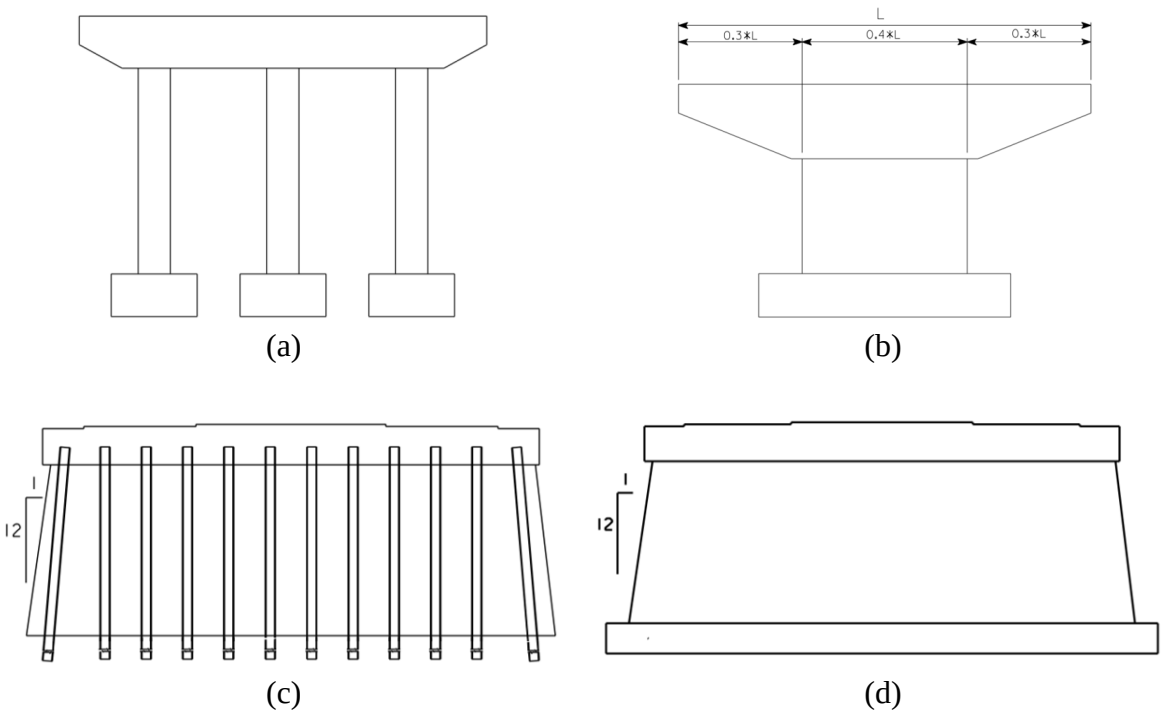

Figure 2.1 *Bridge piers: (a) frame pier, (b) T-pier, (c) pile bent, and (d) diaphragm pier*

Due to the difficulty of forming and pouring the bent cap and column in height, construction of a frame pier can be challenging. Using precast elements can eliminate the on-site forming, and save significant time during construction. With precast technologies, a typical frame pier can be constructed in as little as two days once the footings are in place (Culmo 2011). Several state agencies have utilized precast elements in the construction of frame piers. The Iowa DOT has successfully accomplished the construction of the U.S. 6 Bridge over Keg Creek with precast columns and precast bent caps (Figure 2.2). The Texas Department of Transportation (TxDOT) introduced precast reinforced bent caps in the 1990s, and has developed precast pretensioned bent cap designs in recent years. Full precast frame piers were constructed for Riverdale Road Bridge over I-84 in Utah. The Washington State DOT has successfully implemented precast columns and precast bent caps with CIP spread footings. To address the challenges from site constraints, precast elements can be used for the

construction of foundation. The New Hampshire DOT and the Utah DOT have developed the precast spread footings for bridge construction. However, none of the precast pier has been constructed on the pile foundation.

(a) (b)

Figure 2.2 *Precast frame piers for (a) U.S. 6 Bridge over Keg Creek and (b) U.S. 12 Bridge over I-5 at Grand Mound*

Connections for Precast Bridge Piers

The connections between precast elements are the most critical parts in ABC projects. These connections should not only be easy-to-construct, but they should also ensure structurally dependable performance. Most ABC projects are based on the concept of "emulation design", which requires the precast connections to be designed and detailed to act as a cast-in-place construction joint. Another strategy for connecting precast elements is providing a connection with a strength lower than that of the adjacent components, while still ensuring sufficient energy dissipation and strength to maintain the integrity of the bridge.

The successes in past projects (Culmo 2009) and extensive research projects (Marsh et al. 2011; Restrepo et al. 2011) showed the feasibility of adequately connecting precast bent caps and precast columns in bridge construction. A commercial grouted splice coupler is the most common connection method. Other methods, such as a bar coupler connection, grouted

duct connection, pocket connection, or hybrid connection with post-tension technology, are also practical selections. Aside from the connection between precast bent caps and precast columns, the column-to-footing connection is a critical element to successfully implement a precast frame pier. If the piles are used as the foundation, the pile cap-to-pile connection is required as well. The following sections describe the findings from the literatures and practices on the connections for precast column and pile.

Column-to-Footing Connections

Using the force transfer mechanism, the connections suitable for a precast column can be classified as bar coupler connection, grouted duct connection, socket connection, and jointed connection.

Bar coupler connection

A bar coupler works as a connection by splicing the reinforcing bars from column and footing. Several styles of couplers, as illustrated in Figure 2.3, are commercially available. Among these couplers, grouted splice sleeve and headed bar with mating sleeve are used for connecting a column and footing. Figure 2.4 shows the typical connection details using grouted splice sleeves (UDOT 2017). A grout bed using non-shrink grout is prepared before the column is placed. Reinforcing bars extending from the footing or the column are grouted into splice sleeves. Another type of bar coupler connection is shown in Figure 2.5 (Haber et al. 2014). Vertical reinforcing bars with headed ends project from the footing and the column. After placing the column on the footing, the link bars are connected by mating sleeves to the bars projecting from the column and footing. Spiral reinforcement is then put around the link bars, and the connection is completed by casting concrete around the splice region at the column base.

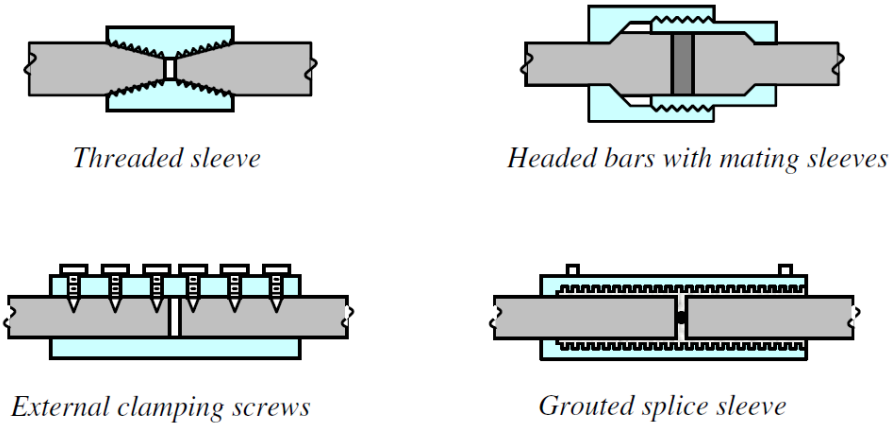

Figure 2.3 *Types of bar couplers (Marsh et al. 2011)*

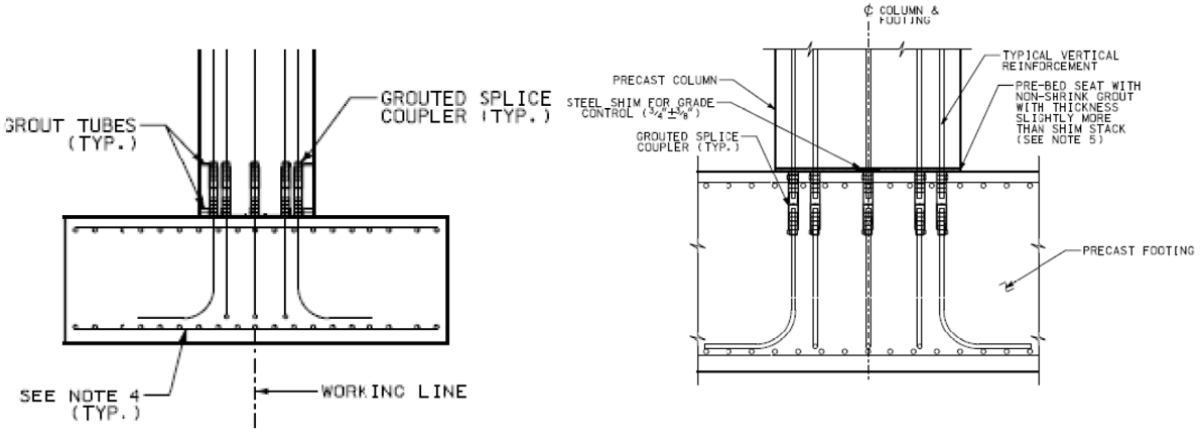

Figure 2.4 *Connection details using grouted splices sleeves*

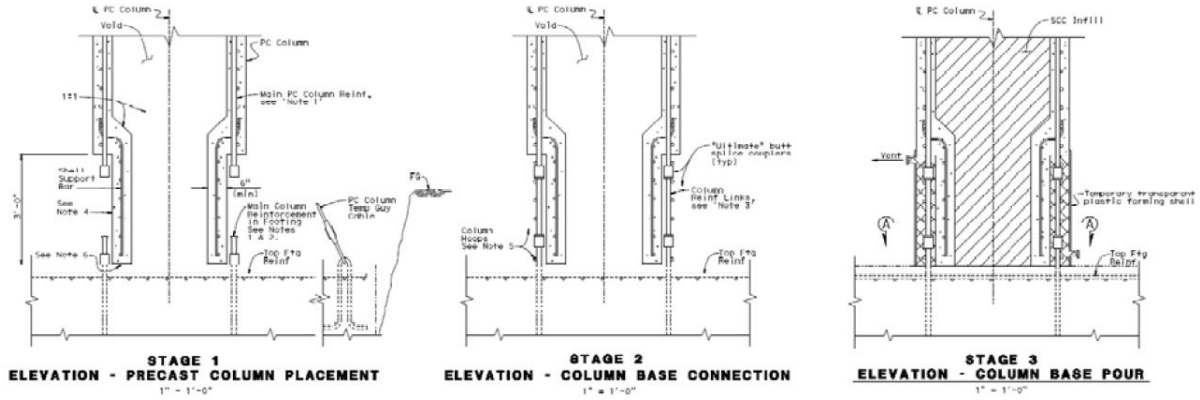

Figure 2.5 *Column-to-footing connections with bar couplers*

For the bar coupler connections, the force transfer mechanism is straightforward, but the main challenges are cost, tolerance, and potential conjunction due to the larger diameter

of the couplers. Designers can mitigate the cost by minimizing the number of couplers through using large diameter reinforcing bars. Tolerance is a challenge because all projected bars must be aligned in the field. To help with this, template can be used to position the bars and couplers during fabrication of the column and footing. In order to reduce conjunction, it is preferred to embed the coupler into the footing and use larger bars to reduce the number of couplers required. The tests conducted with these connections (Haber et al. 2014) showed that the strain concentration occurred either above or below the couplers, depending on their locations.

Grouted duct connection

In a grouted duct connection, reinforcing bars projecting from one member are grouted into ducts that are cast into the adjacent member. The force is transferred from the reinforcing bars to the concrete surrounding the ducts. A small number of larger bars are typically used for easier alignment and less conjunction. Due to the length required to anchor the large bars, ducts are typically cast into the column, as illustrated in Figure 2.6a. Using ultra high performance concrete (UHPC) to fill the ducts instead of grout requires shorter length to fully anchor the reinforcing bars, such that the ducts can be placed in the footing as shown in Figure 2.6b. Several tests (Matsumoto 2009; Pang et al. 2010) have been conducted on this type of connection, and preliminary design guidelines can be found in *PCI Design Handbook* (2004). Similar to the bar coupler connection, the challenges associated with grouted ducts are tolerance and potential conjunction.

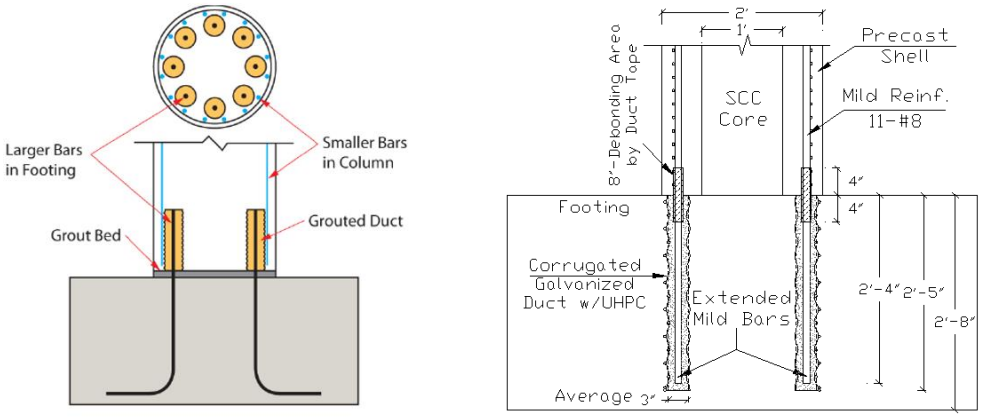

(a) (b)

Figure 2.6 *Column-to-footing connections with grouted ducts: (a) large bars with ducts Cast into column and (b) ducts placed in footing with UHPC infill*

Socket connection

A socket connection for joining precast column and footing can be constructed using one of the following two methods: (1) cast a CIP footing around the column, and (2) insert the column into a preformed socket in a CIP or precast footing and secure the connection using a grout closure pour. The surface of the column can be roughened to improve the shear transfer between members. The preformed socket can be accomplished using commercially available corrugated steel pipe (CSP) due to its low cost and variability in sizes. In addition to serving as stay-in-place formwork, CSP offers confinement effects for the connections and its corrugations support a robust load transfer mechanism. The column reinforcing bars in socket connections are fully encased, and the sockets are preformed oversized, enabling generous tolerance to be accommodated. The Washington State Department of Transportation (WSDOT) has developed and successfully implemented the socket connection that was suitable for a precast column with CIP spread footing, as shown in Figure 2.7 (Haraldsson et al. 2013). The option with precast footing has been investigated as well. Motaref et al. (2011) and Kavianipour et al. (2013) tested a precast bridge pier, in

which the columns were embedded into the reserved socket in a precast footing with high-strength grout infill (Figure 2.8a). The embedment length of the column in the footing socket was 1.5 times the column diameter. The authors reported that the embedment length was sufficient to develop full fixity at the column base. Mehrsoroush and Saiidi (2016) tested a pier model with precast columns and socket connections in the precast bent cap. In the model, the sockets were made using CSP and the column embedment length was 1.2 times the column diameter. Results showed that the configurations were adequate to develop moment connections and form plastic hinges in the columns. Another experimental studies (Mashal and Palermo 2015; Mohebbi et al. 2017) showed that the column embedment length can be shortened to 1.0 times the column diameter. As shown in Figure 2.8c, the socket on the precast footing was created by foam, and both the socket wall and base of the column were treated with exposed aggregate finish. The socket connection successfully formed the plastic hinges in the column with no damage to the footings.

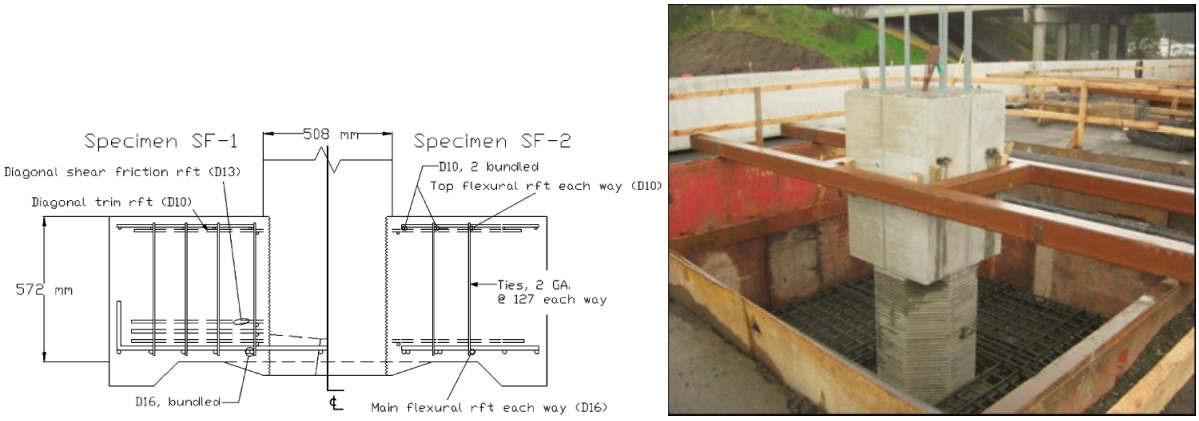

Figure 2.7 *Socket connections with CIP footings: (a) test specimen and (b) implementation over I-5 in Washington State*

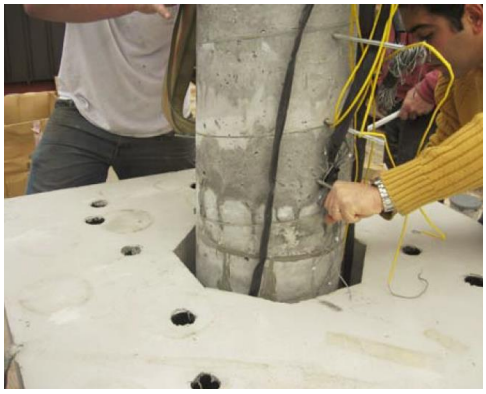

(a)

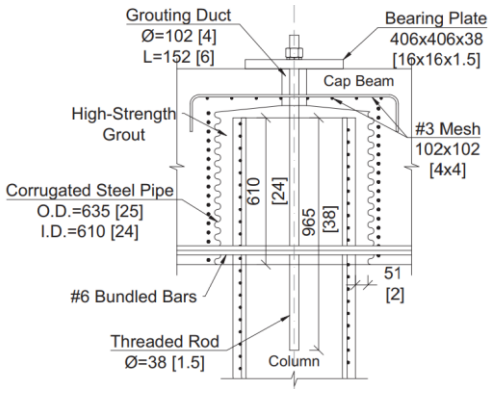

(b)

(c)

Figure 2.8 *Socket connections with precast members: (a) Motaref et al. (2011), (b) Mehrsoroush and Saiidi (2016), and (c) Mashal and Palermo (2015)*

Jointed connection

Jointed connections utilize unbonded post-tensioning tendon to connect a precast column with its footing. The post-tensioning tendon is designed to remain elastic for a drift at the design-level motion, allowing the column to re-center while not allowing the members to undergo plastic deformation. Keeping the tendon elastic provides very little energy dissipation capacity. Mild reinforcing bars or other innovative devices are installed for dissipating energy, and can be replaced after damage. Figure 2.9 illustrates examples of jointed connections utilizing unbonded post-tensioning. Note that these connections were experimental and have not been used on actual bridges. The challenges associated with a

jointed connection include cost, constructability, and durability. Also, this type of connection offers no advantage in non-seismic regions.

(a)

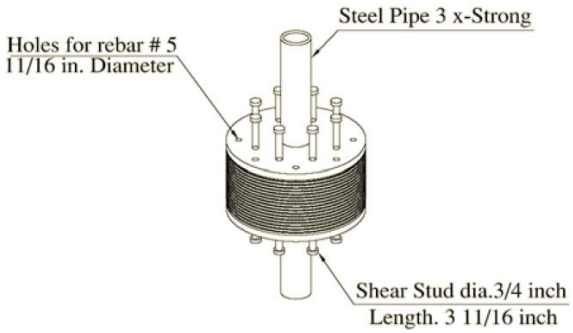

(b)

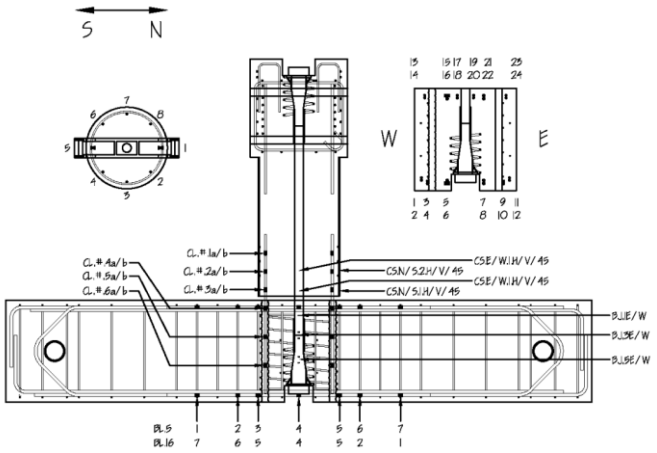

(c)

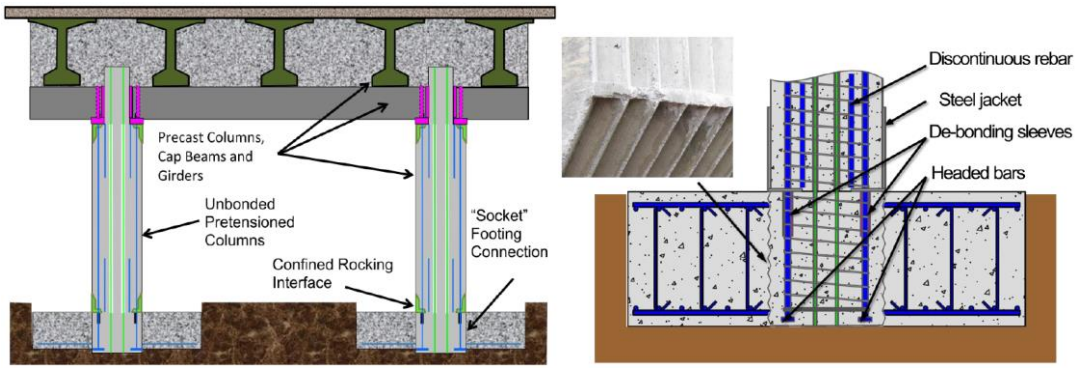

(d)

Figure 2.9 *Jointed connections: (a) Mashal and Palermo (2015), (b) Motaref et al. (2010), (c) Restrepo et al. (2011), and (d) Thonstad et al. (2016)*

Pile Cap-to-Pile Connection

Steel H-pile is a common foundation choice for bridges with frame piers. Pile foundations are normally capped with concrete footing in order to provide a stable platform to support the column. A pile group with a concrete cap is an indeterminate structure. In most cases (i.e., the piles are surrounded by competent soil), the lateral movement of the pile in a pile group with a concrete cap under lateral loads is very small. Therefore, moments in the pile-to-cap connection can be ignored. Even though the moment is often ignored in the design process, the experimental studies (Shama et al. 2002; Xiao et al. 2006) indicated that embedding the pile head into the cap, as it constructed in current practices, develops significant capacity to sustain a moment.

Few attempts have been made to implement precast pile cap in bridge construction. Only conceptual details have been developed for the connection of precast pile caps to steel H-piles, and one of them is from the PCI Northeast Bridge Technical Committee (Culmo, 2011). As shown in Figure 2.10a, leveling bolts are used in the corners of the precast cap to set grade, and concrete is poured through ports to fill the voids around the piles. Based on the research on precast abutment, another conceptual connection (Figure 2.10b) has been developed, similar to a socket connection, using CSP voids. The research findings showed that the connection with CSP can provide a large amount of strength to transfer the axial force of steel H-piles (Wipf et al., 2009).

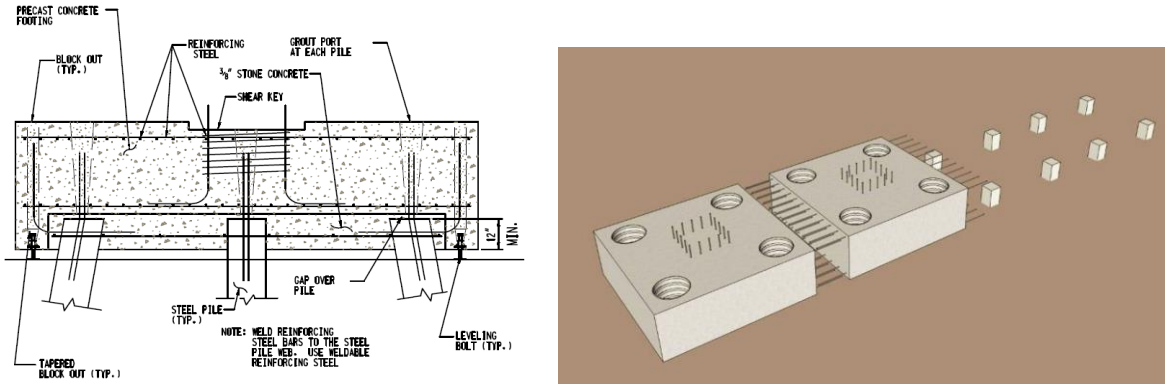

(a) (b)

Figure 2.10 *(a) Concept from the PCI Northeast Bridge Technical Committee and (b) concept using socket connection*

Wyoming DOT developed and implemented a connection for connecting precast concrete pier caps to steel H-piles when constructing the bridge over Crow Creek. To establish the connection, steel plates with shear studs are cast at the pile locations in the bottom of the pier cap. In the field, after the cap is set, the steel H-piles are welded to the steel plates, as shown in Figure 2.11.

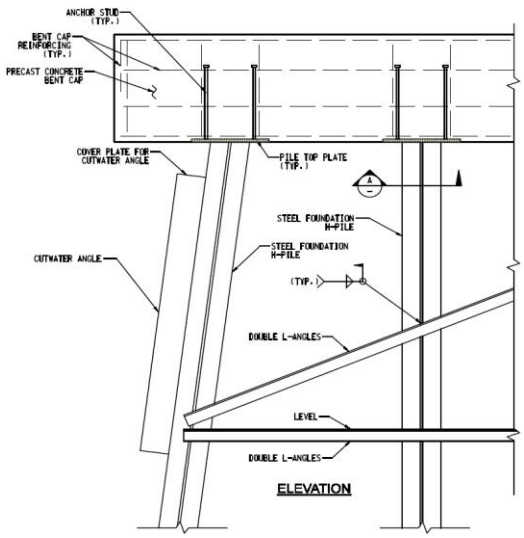

Figure 2.11 *Welded connection between precast cap and steel pile*

Construction of Socket Connection

Socket connection is an easy-to-construct detail. The socket on one member can be made using commercially available corrugated steel pipe (CSP). After inserting another member into the socket, the connection is secured by using a grout closure pour. The surface of the embedded member can be intentionally roughened to improve the force transfer between concrete and grout as they are cast separately. The following sections contain the information on the materials, the products, and the techniques that are required for establishing a structurally adequate and easy-to-construct socket connection.

Corrugated Steel Pipe (CSP)

Corrugated steel pipe (CSP) is an effective way to pre-form a socket in precast elements. In addition to serving as stay-in-place formwork, CSP offers a confinement effect for the connection and its corrugations provide a robust load transfer mechanism. Referring to the specifications for the culvert pipe (AASHTO 2017; UDOT 2017), the CSP used for creating socket shall meet the requirements of AASHTO M 218 (2016). Metallic coating is typically applied to improve the durability of CSP, but aluminum cladding is not allowed because aluminum is reactive with the surrounding concrete, leading to degradation of the connection over time (UDOT 2017). The seam types of standard CSP include annular corrugations with riveting or resistance spot welding and helical corrugations with lock seam or continuous welding. For establishing sockets, annular corrugations are preferred because any detail to convey water more efficiently is not recommended for structural applications (UDOT 2017). The corrugations of annular seams are 68-mm (2-2/3-in.) pitch by 13-mm (1/2-in.) depth and 76-mm (3-in.) pitch by 25-mm (1-in.) depth depending on CSP diameter. For the most common CSPs ranging from 305 mm to 2134 mm (12 in. to 84 in.), the corrugation pattern is 68 mm (2-2/3 in.) by 13 mm (1/2 in.), where 68 mm (2-2/3 in.) is

measured from crest to crest and 13 mm (1/2 in.) is from valley to crest. Commercially available CSPs have variability in sizes from 305 mm (12 in.) to 3658 mm (144 in.) measured on the inside crest of the corrugations. Designers should be aware of manufacturing tolerances when they choose the pipe to fit their projects. For the CSP used in bridge construction, the average inside diameter of the circular pipe shall not vary more than one percent or one-half inch, whichever is greater, from the nominal inside diameter (AASHTO 2016).

Grout

There are several different types of grouts. Among these grouts, cementitious grouts are inexpensive, generally easy to work with, and develop adequate strengths in reasonable time, making them suitable for bridge construction. These grouts are often pre-packaged and composed of hydraulic cement, fine aggregate and other ingredients. Most commercially available cementitious grout requires only the addition of water for use. The manufacturer may allow job site addition of specific amounts and types of aggregates for some uses. For securing socket connections, the grout is required to have the following desirable properties: fluid consistency, extended working time, high early strength, high strength, and non-shrink. The fluid consistency and extended working time provide the possibility to flow easily into tight clearance and large placements in bridge socket connections. High early strength (i.e., a compressive strength not less than 4000 psi at 1 day) allows the connections to gain strength quickly, such that the project can be completed in a short period. High strength of the grout ensures the strength of the finished connection. Ideally, non-shrink grout will not exhibit dimensional change in the plastic or hardened state. This property tends to reduce the crack that occurs at the interface between grout and precast elements and in grout itself, which improves the durability of connection. To recognize the suitable products, information of

cementitious grouts available in the market were scanned and sorted (Sritharan and Cheng, 2016). After reviewing the technical datasheets and several trial mixes, Rapid Set® ULTRAFLOW® 4000/8, referred to as "Ultraflow", is identified as one meeting the requirements for securing socket connection. This particular type is a fluid consistency, non-shrink, precision grout that provides extended working time up to 30 min., but then gains strength quickly after an hour and hits 4000 psi in 8 hours. In addition, the Ultraflow grout reaches a specified 28 days compressive strength of 8500 psi at fluid consistency. Any other products that have the comparable properties can be used for socket connection as well.

Concrete Surface Finishing Techniques

In the socket connection, the surface of the embedded element is often intentionally roughened. Different practical methods can be used to achieve different degrees of roughness. Exposed aggregate finish is popular, and deeper texture with regularized patterns can also be created by form liners. Chemical formwork retarders are very effective in exposing coarse aggregate. The application of retarder to the formwork prior to casting the concrete delays the surface cement paste from hardening. After hardening of the concrete mass, the retarded outer layer can be removed by high-pressure water washing. Acid etching is another technique to expose aggregate on the concrete surface. Unlike retarders that are applied prior to casting concrete, acid etching dissolves the surface cement paste after concrete harden. Note that acid etching is only for light to medium exposures, while formwork retarder can provide deep exposure where the coarse aggregate becomes the major surface feature (PCI 2007). Hardening concrete can also be mechanically roughened with sandblasting or bush hammering to produce an exposed aggregate texture. These finishing techniques are more labor intensive, and may soften the exposed aggregate (PCI 2007). Form liners are made of wood, steel, elastomeric, plastic, or polystyrene. A variety of surface

textures can be achieved by casting against form liners that are incorporated in or attached to the surface of formwork. Form liners are most suitable for flat surfaces.

Behavior of Piles Driven in Clay

Driven piles are structural members used to transmit the load to the soil gradually. In most cases, the piles are installed in group and subjected to both the axial and lateral loads. Numerous studies have been conducted to investigate and predict the behavior of piles. The following discusses the present state of the art.

Axial Capacity and Settlement of Driven Piles

The axial resistance of a steel driven pile includes tip resistance, side resistance, and the effective weight of the pile, while pile weight is usually ignored in practices. Generally, the displacement need to mobilize the side resistance is less than that required to mobilize the tip resistance. However, for determining the axial pile capacity, practices commonly assume that both the pile toe and the shaft have moved sufficiently with respect to the adjacent soil to simultaneously develop the full tip and side resistance. The most used methods for calculating the axial capacity of steel driven piles include the α-method, the Nordlund method, and the API method (Hannigan et al. 2016). Other empirical methods and CPT-based methods have also been developed (Jia 2018).

Settlement accompanying with axial loads is another critical factor of the pile foundation behavior. Several empirical procedures are available for determining settlement of single pile and pile group (Ma and Deng 2014; Hannigan et al. 2016). As an alternative, the force-settlement behavior can be achieved through the method using localized springs, called *t-z* method (Kraft et al. 1981; Resse and O'Neil 1988). Figure 2.12 illustrates the model used in the *t-z* method. In this method, the load transfers in side resistance and tip resistance are represented by a series of localized springs along the pile (*t-z* curves) and a

spring at the bottom of the pile (*Q-z* curve), respectively. The *t-z* method thereby allows the assessment of the pile load-settlement behavior as well as the load distributions along the pile by solving the differential equation for the pile and soil using a finite difference approach. For the analyses under static loading, the behavior of these springs may vary from linearly elastic to nonlinear hysteretic, and the pile can be modeled as a continuous beam-column, either linear or nonlinear.

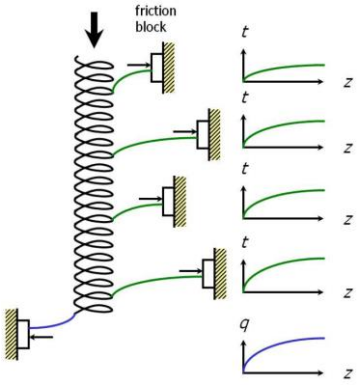

Figure 2.12 *Model used for t-z method*

API (2002) provides recommendations for generating static t-z curve and Q-z curve for driven piles. The typical t-z curves that API recommend are show in Figure 2.13. For driven piles in clay, value of the residual adhesion ratio (t_{max}/t_{RES}) can range from 0.7 to 0.9, which is a function of soil stress-strain behavior, stress history, pile installation method, pile load sequence and other factors. The maximum unit side resistance can be calculated from the following equation:

$$t_{max} = \alpha c_u \qquad \text{Equation 2-1}$$

where α = dimensionless factor and c_u = undrained shear strength of soil at calculation point.

The dimensionless factor, α, is calculated from the following equation:

$$\alpha = \begin{matrix} 0.5\psi^{-0.5} & for\ \psi \leq 1.0 \\ 0.5\psi^{-0.25} & for\ \psi > 1.0 \end{matrix} \qquad \text{Equation 2-2}$$

where $\psi = c_u/p_0'$ and p_0' = effective overburden pressure at the calculation point.

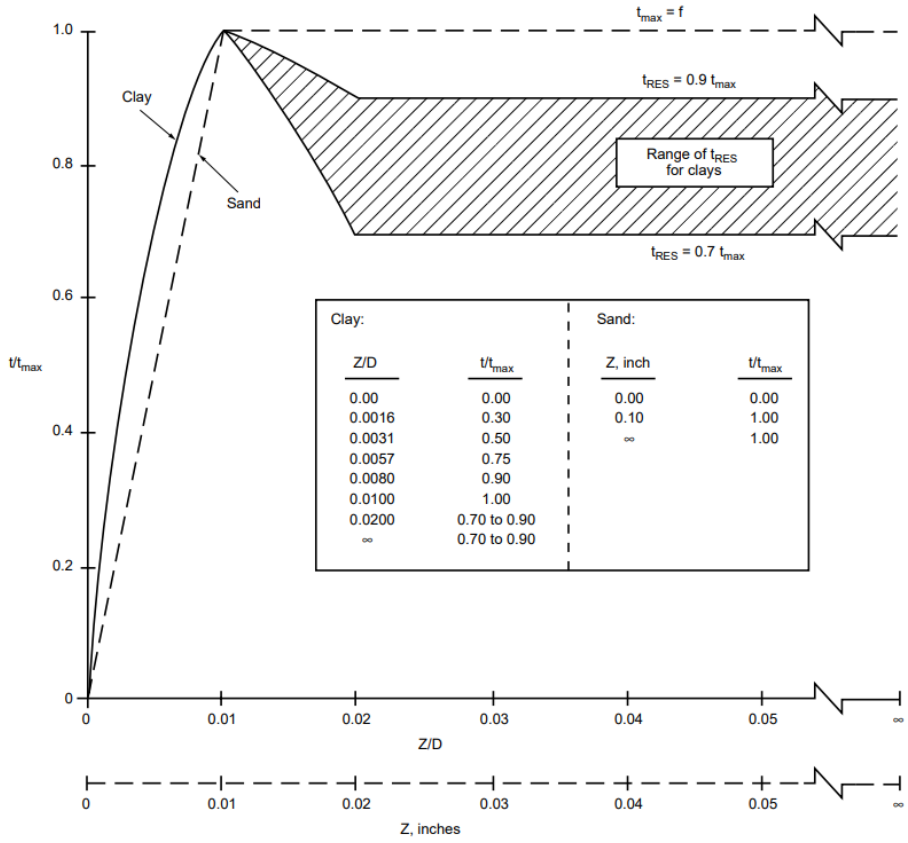

Figure 2.13 *Typical t-z curves*

Figure 2.14 shows the typical static *Q-z* curve for both sand and clay following the API approach (API 2002). The suggested maximum unit tip resistance, Q_p, for clay is calculated from the following equation:

$$Q_p = 9c_u \qquad \text{Equation 2-3}$$

where c_u = undrained shear strength of soil at the tip of the pile.

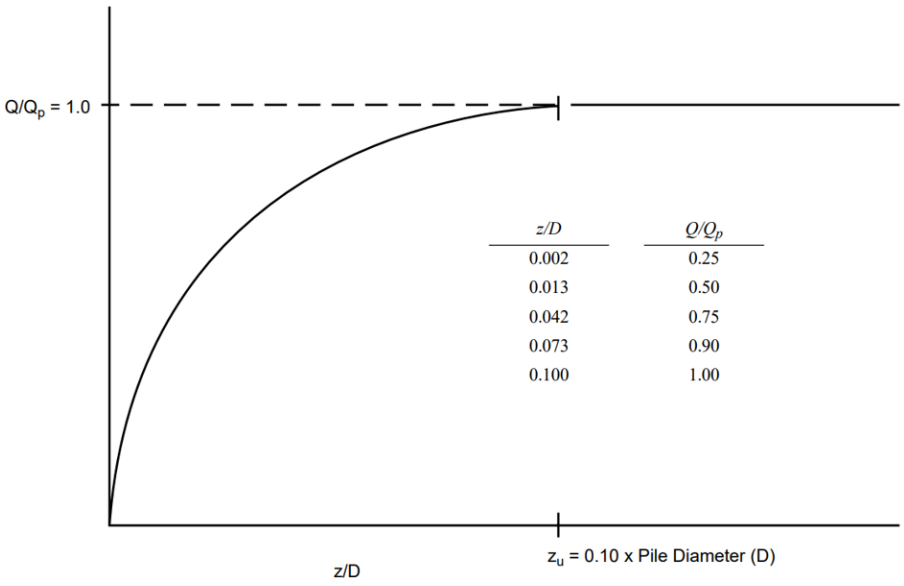

Figure 2.14 *Typical Q-z curves*

Lateral Capacity and Deflection of Driven Pile

The pile behavior under lateral loads depends on pile stiffness and strength, soil stiffness and strength, as well as pile head fixity. Numerous methods have been developed for analyzing laterally loaded piles. In the 1960s, Broms (1964a and 1964b) made the recommendations to estimate the ultimate lateral capacity of a pile, which is based on the assumption that the pile is short and rigid. Some researches implement three-dimensional, nonlinear finite elements to account soil-pile interaction in a fully-coupled manner. The most commonly used method is the *p-y* method, in which soil is not continuum but be represented as a series of localized nonlinear springs (*p-y* curves) along the pile (Figure 2.15). To recognize the nonlinear response characteristics of pile, nonlinear beam-column elements can be used for modeling the piles. By solving the differential equations describing the behavior of the beam-column with nonlinear supports (Hetenyi, 1946), *p-y* method provides deflection, bending moment, shear force, and soil response over the length of the lateral loaded piles.

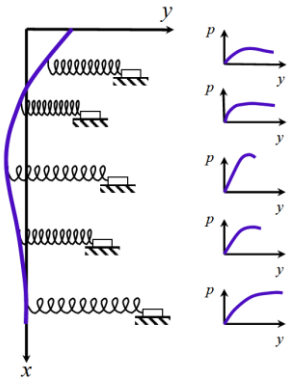

Figure 2.15 *Model used for p-y method*

Proper *p-y* curves are essential to obtain the acceptable results from the *p-y* method. Ideally, *p-y* curves should be generated from full-scale lateral load tests on instrumented test piles. In the absence of experimentally data, it is possible to use empirical *p-y* formulations that have been proposed in the literature for different types of soils. For driven pile in clay, the recommended characteristic shape and formulations of *p-y* curves are shown in Figure 2.16.

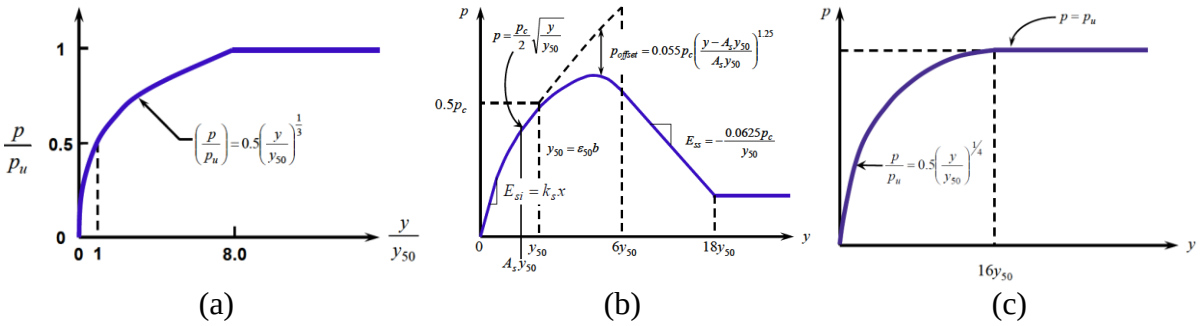

(a) (b) (c)

Figure 2.16 *Characteristic shape of p-y curves for static loading in (a) soft clay (Matlock 1970), (b) stiff clay with free water (Resse et al. 1975), and (c) stiff clay without free water (Resse and Wlech 1975)*

The *p-y* formulations are originally developed for circular pile and thus as a function of the diameter. The analytical studies (Ashour and Norris 2000; Resse and Van Impe, 2011) indicated that, for two piles have the same width perpendicular to the lateral load but

different shapes (i.e. circular and square), the square pile would induce a soil resistance higher than the circular pile because shear stresses could act on the sides of square section paralleling to the lateral load. To formulate the p-y curves for noncircular piles, the following equation can be used to solve for the equivalent diameter, D_e, of a rectangular section (Resse and Van Impe, 2011):

$$D_e = w\left[\frac{p_{uc} + 2(d - \frac{w}{2})f_z}{p_{uc}}\right] \qquad \text{Equation 2-4}$$

where w = width of the noncircular section, d = depth of the noncircular section, p_{uc} = ultimate resistance of a circular section with a diameter equal to w, and f_z = shear resistance along the sides of the rectangular shape at the depth z below the ground.

For the undrained strength approach for cohesive soils, the shearing resistance may be computed with the following equation:

$$f_z = \alpha c_u \text{ with } 0.5 \leq \alpha \leq 1 \qquad \text{Equation 2-5}$$

where α = shear strength reduction factor, which can be taken as 1 for steel H-pile loaded in strong axis and c_u = soil undrained shear strength.

The equivalent diameter, as computed by the above equations, will vary with the depth being selected. An average value of the equivalent diameters at a few depths can be used in making a solution.

Effects of Cyclic Loadings

The influence of cyclic loads is a function of magnitudes, cycles, and rate of loading, pile structural characteristics, and soil characteristics (API 2002). Repetitive axial loadings would cause a decrease in load-carrying resistance and an accumulation of settlement.

However, if the ratio of cyclic axial load amplitude to static axial pile capacity is below a threshold value, no axial pile capacity reduction needs to be considered. The threshold values, which is referred to as the critical level of repeated loading (CLRL), are ranged from 0.35 to 0.55 for normally consolidated clay, but from 0.85 to 1.0 for over-consolidated clay (Schwarz, 2002).

Cyclic lateral loads result in the loss of soil resistance as illustrated in Figure 2.17. For piles driven in clay with the presence of free water, the cyclic loading effect can be severe because of the subjection of the clay to repeated strains of large magnitude (Long, 1984), and scour from the enforced flow of water near the pile when water is above the ground surface (Reese et al. 1975; O'Neill and Dunnavant, 1984).

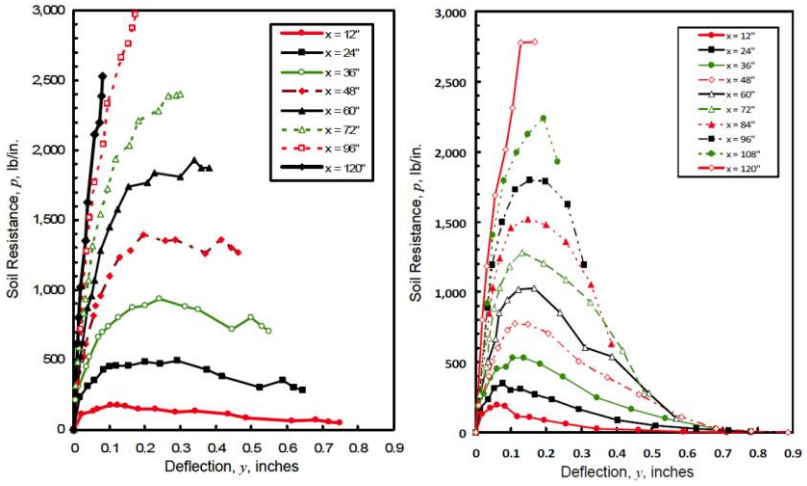

Figure 2.17 *p-y curves developed from static and cyclic load tests on pipe piles in submerged stiff clay (Resse et al., 1975)*

Effects of Pile Batter

Piles are sometimes driven on an intentional inclination, giving them a greater capacity and smaller deflection when subject to lateral loads. To account these effects in the *p-y* method, the foundational formulations for *p-y* curves need to be modified. The factor on

the ultimate soil resistance at the front of the pile where the pile is installed at an angle θ with the vertical was derived by Reese (1958) and is shown in following:

$$k_f = \frac{1}{1 + tan\theta} \qquad \text{Equation 2-6}$$

The factor on the soil resistance at the back of the pile following Reese approach is:

$$k_b = \frac{cos\theta}{\sqrt{2}\cos(45° + \theta)} \qquad \text{Equation 2-7}$$

The values of the soil resistance modifying factor as the batter angle were deduced from the results of the model tests (Awoskika and Reese 1971) and from results of full-scale tests (Kubo 1964). As shown in Figure 2.18, the agreement between the empirical curve following Reese approach and the experiments is generally achieved.

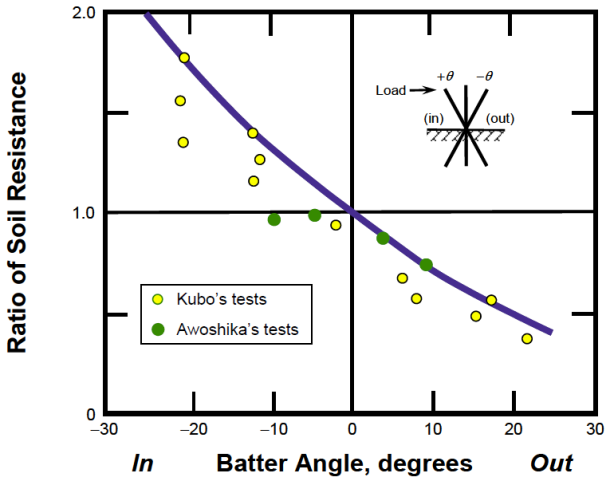

Figure 2.18 *Soil resistance factor for p-y curves for battered piles*

Group Effect

In most cases, piles are constructed in group to transmit the structural load to the soil. Although a pile group is composed of a number of individual piles, the resistance of a pile group is not always equivalent to the sum of all the piles as if they are individual piles. The pile group can produce greater moment resisting capacity because piles would form force

couples resulting from their axial resistances through the action of the pile cap. However, the capacity to withstand axial and lateral loads for a group of piles is often less than the sum of individual piles because of the interaction between piles. The amount of reduction depends on many factors such as the spacing between the piles, the deflection of the piles, and the type of soil. The interaction piles usually diminish for piles spaced at approximately 7-8 pile diameters (Ma and Deng 2014).

When the piles are clustered, the stresses transmitted by the piles to soil may overlap (Figure 2.19a), reducing the axial capacity of the piles. One way to account for the interaction between piles under axial load is to use the group efficiency factor, which is defined as the ratio of the axial capacity of a pile group to the sum of the axial capacity of all the individual piles. For pile group driven in stiff clay, the pile efficiency factor of 1.0 may be used (Hannigan et al., 2016). For pile group in soft to medium stiff clay, the group efficiency factor is usually less than 1.0, and the pile group under axial load tends to behave like a block (Figure 2.19b).

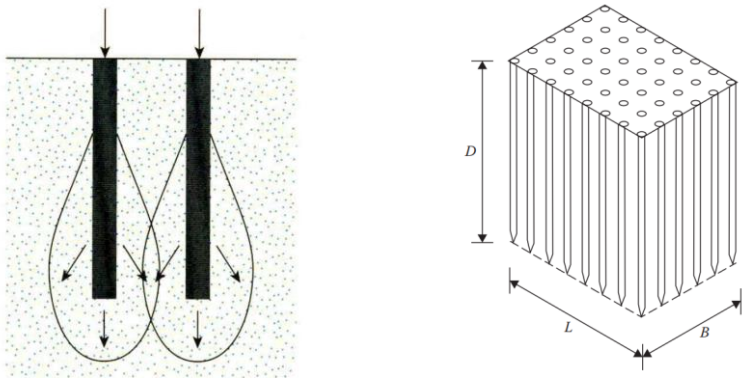

(a) (b)

Figure 2.19 *(a) Overlap of stress zones for pile group under axial load and (b) block failure model for pile group*

Under lateral load, as the piles are installed close to each other, the stressed zones of the piles in a pile group can overlap each other as shown in Figure 2.20 (Brown et al. 1988; Poulos, 1971; Rollins et al. 2006). This effect by far is not well defined. Generally, it is believed that the group effect depends on from a number of factors such as pile spacing, row position in the group, and soil type. The limited full scale load tests show the distribution of the load within a pile group (Meimon et al. 1986; Brown et al. 1987; Brown et al. 1988; Rollins et al. 1998; Christensen, 2006). In all of these tests, under a certain lateral load acting on the pile cap, the piles in the leading row exhibited the higher resistance than the piles in the subsequent rows, but individually these piles have lower resistances than a single pile. Another study (Ashour and Ardalan, 2011) demonstrated that the group effect develops from nothing where small deflections are present, and increases gradually with the deflection. When the laterally loaded piles are analyzed using the *p*-*y* method, the most common approach to incorporate the group effect is using a *p*-multiplier to adjust the single pile *p*-*y* curve, as suggested by Brown et al. (1988). With this approach, the soil resistance is scaled down by a constant factor (Figure 2.21). The *p*-multipliers for driven piles in clay back-calculated from selected pile group load tests and the default values used in a widely used analysis software are summarized in Table 2.1. In another approach, rather than defining *p*-multipliers for single pile *p*-*y* curve, an average *p*-multiplier for all piles in the group is used (Brown et al. 2001). Use of an average *p*-multiplier is justified for the cyclic reversed loads, converting leading rows of piles instantaneously into trailing rows.

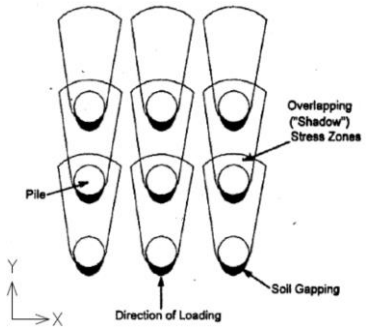

Figure 2.20 *Overlap of stress zones for pile group under lateral load*

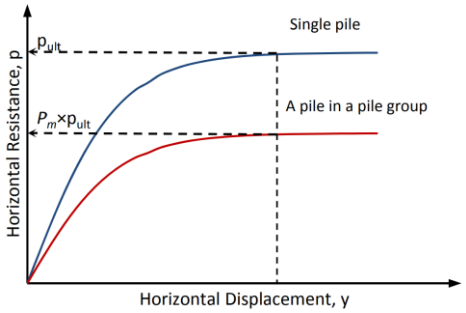

Figure 2.21 *Constant p-multiplier for single pile p-y curve*

Table 2.1 *P-multiplier values*

Reference	Soil properties	Pile spacing (/pile diameter)	1st row	2nd row	3rd row	4th row (5th row)
Cox et al. (1984)	soft clay	3	0.95	0.75	0.77	0.73 (0.72)
Meimon et al. (1986)	silty clay	3	0.9	0.5		
Brown et al. (1987)	stiff clay	3	0.7	0.5	0.4	
Rollins et al. (1998)	clayey silt	3	0.6	0.4	0.4	
Wilmington load test (Brown et al. 2001)	soft clay	3	0.8	0.4	0.2	0.3
Spring Villa load test (Brown et al. 2001)	silty clay	3	0.64	0.32	0.16	0.24
Rollins et al. (2006)	stiff clay	3.3	0.82	0.61	0.45	0.45 (0.51-0.46)
Cox et al. (1984)	soft clay	4	0.96	0.86	0.85	
Spring Villa load test (Brown et al. 2001)	silty clay	4	0.72	0.5	0.4	
Rollins et al. (2006)	stiff clay	4.4	0.9	0.88	0.69	
Rollins et al. (2006)	stiff clay	5.65	0.95	0.88	0.77	
Cox et al. (1984)	soft clay	6	1.01	0.92	0.92	
FB-MultiPier		3	0.8	0.4	0.3	0.3
FB-MultiPier		5	1.0	0.85	0.7	0.7

Rocking Bridge Pier

Structures with rocking mechanism offer the potentials to achieve the desired seismic performance objectives such as mitigating economic losses, maintaining bridge functionality, and improving reparability. Numerous studies have been conducted to develop rocking structures for bridges, including the columns with internal posttensioning tendons designed to rock at their ends, shallow foundations that are free to uplift, and rocking pile cap supported on pile foundation. Representative works are reviewed and summarized in the following sections.

Rocking Precast Column with Internal Prestressing Tendons

The rocking column utilizes unbonded prestressing tendons passing through the center of the column to provide recentering force. Hewes and Priestley (2002) tested two columns with a high aspect ratio and two columns with a low aspect ratio under cyclic lateral loading. As illustrated in Figure 2.22, each column was constructed with precast segments and the vertical posttensioned prestressing tendons passing through ducts located in the precast segments. Steel jackets were used to confine the end region of each column. All four column underwent large nonlinear displacements up to a drift ratio of 4% without experiencing significant strength degradation. Because of the restoring force provided by the prestressing tendons, the residual drift was minimal. Wang et al. (2008) extended the concepts of precast segmental construction and added bonded mild steel bars across the segment joints to increase the hysteretic energy dissipation capacity for the rocking column (Figure 2.23). The four large-scale column specimens showed ductile behavior and satisfactory hysteretic energy dissipation capacity under cyclic lateral loading. Ou et al. (2010) demonstrated that using high performance steel reinforcing bars as the energy dissipation components would achieve greater drift capacity, higher lateral strength, and

larger energy dissipation. To improve the reparability of the rocking pier, Mashal and Palermo (2019) tested the precast column with unbonded posttensioning tendons and the externally attached metallic dissipaters, as shown in Figure 2.24. Following many cycles of large drift ratios, there was no damage or residual displacement in the test unit.

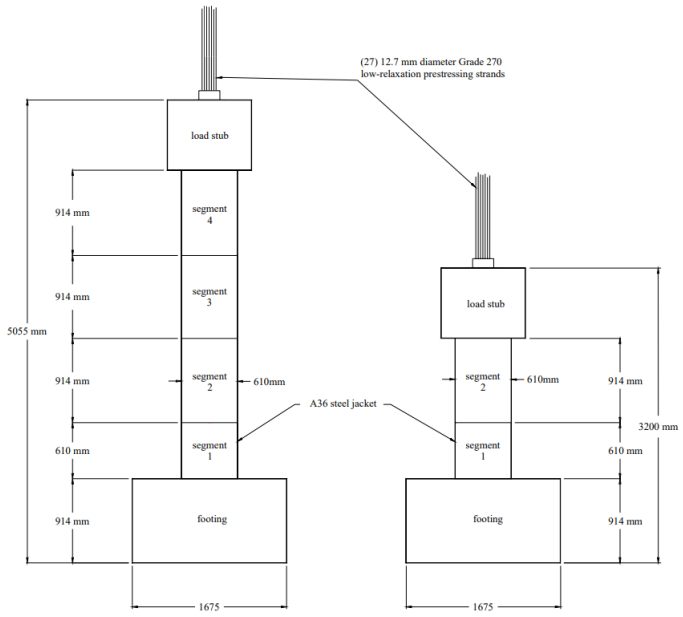

Figure 2.22 *Segmental column with prestressing tendons (Hewes and Priestley 2002)*

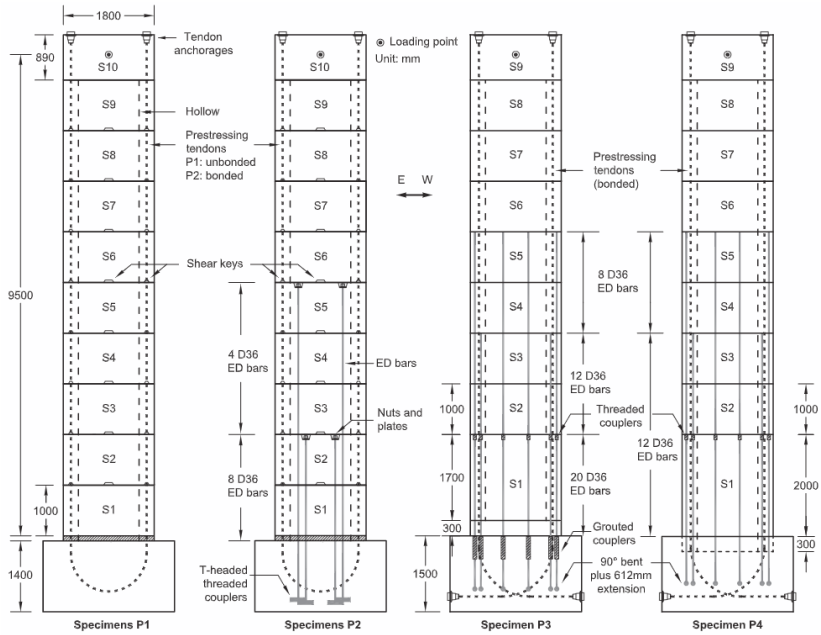

Figure 2.23 *Rocking column with internal energy dissipation bars (Wang et al. 2008)*

Figure 2.24 *Externally attached metallic dissipaters (Mashal and Palermo 2019)*

Rocking Shallow Foundation

Utilizing the structural self-weight as the recentering force, bridges with shallow foundation would mobilize rocking behavior at their footings. Espinoza and Mahin (2008) conducted a series of shaking table tests on a single column bridge column supported on the shallow foundation. For these tests, the underlying soil was modeled by a neoprene pad. Antonellis et al. (2015) tested the rocking shallow foundation placed inside a sand box using the large outdoor shake table. These test indicated that the rocking shallow foundation would reach a great peak drift ratio but exhibit minimal residual drift ratios.

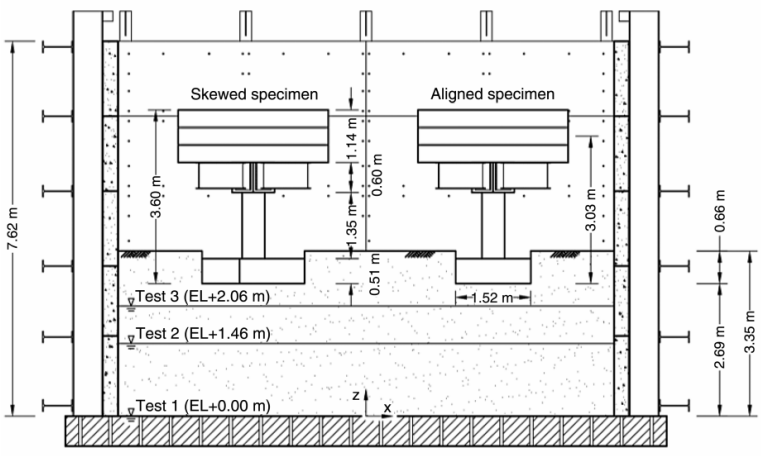

Figure 2.25 *Setup of shaking table test on rocking shallow foundation (Antonellis et al. 2015)*

Rocking Pile Foundation

Although the benefits of rocking shallow foundations have been widely explored, some hurdles impeding the use of this type of system still exist, such as relatively low bearing capacity, the potential settlement and residual rotation due to the permanent deformation of underlying soils, and the difficulty to repair after an earthquake. Addressing these issues, rocking pile foundation was developed. Allmond and Kutter (2012; 2013) conducted centrifuge tests to explore the behavior of the rocking foundation on unattached piles with different footing-pile connection details (Figure 2.26). These tests demonstrated the well performance of the rocking pile foundation during an intense shaking, even in poor soil conditions. Guan et al. (2018) tested two large-scale pile foundation models with a rocking pile foundation and a conventional foundation. Compared to the conventional foundation, the rocking pile foundation resulted in less damage in the piles and minimal residual drift, evidencing the feasibility of rocking pile foundation.

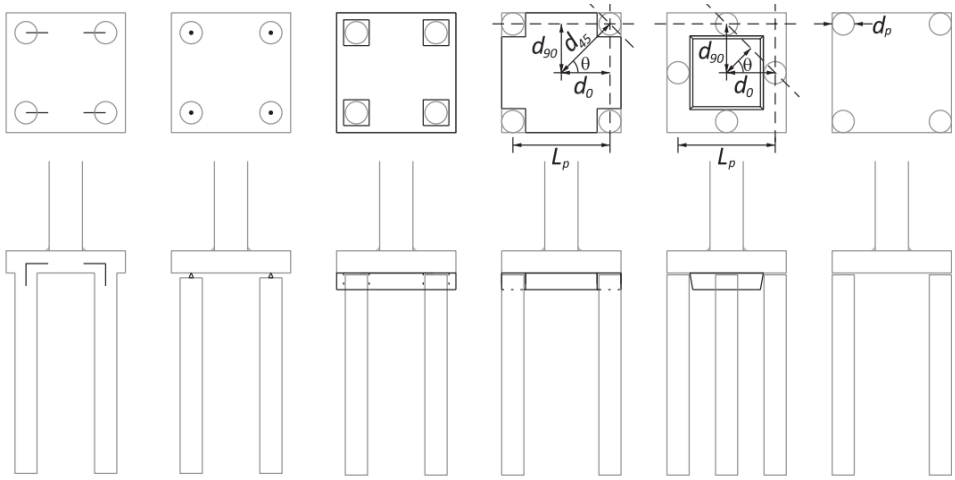

Figure 2.26 *Different footing-pile connection details (Allmond and Kutter 2012)*

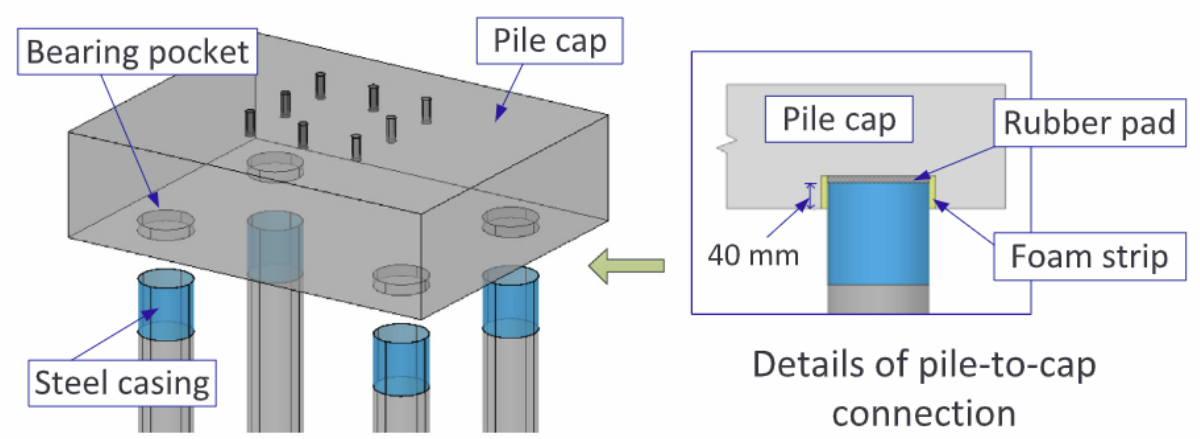

Figure 2.27 *Connection details for pile-to-pile cap connection (Guan et al. 2018)*

References

Allmond, J., and Kutter, B. L. (2012). "Centrifuge testing of rocking foundations on saturated and submerged sand: Centrifuge Data Report for JDA01." *UCD/CGMDR-12/01*, Univ. of California at Davis, Davis, CA.

Allmond, J., and Kutter, B. L. (2013). "Centrifuge testing of rocking foundations on saturated and submerged sand: Centrifuge Data Report for JDA02." *UCD/CGMDR-13/01*, Univ. of California at Davis, Davis, CA.

American Association of State Highway and Transportation Officials (AASHTO) (2017). *LRFD Bridge Design Specifications*, 8th Ed., Washington, DC.

American Association of State Highway and Transportation Officials (AASHTO) (2016). "Standard Specification for Steel Sheet, Zinc-Coated (Galvanized), for Corrugated Steel Pipe", *AASHTO M 218*, Washington, DC.

Antonellis, G., Gavras, A. G., Panagiotou, M., Kutter, B. L., Guerrini, G., Sander, A. C., and Fox, P. J. (2015). "Shake table test of large-scale bridge columns supported on rocking shallow foundations." *J. Geotech. Geoenviron. Eng.*, 141(5), 04015009.

API. (2002). *Recommended Practice for Planning, Designing and Constructing Fixed Offshore Platforms-Working Stress Design*. American Petroleum Institute.

Ashour, M., and Ardalan, H. (2011). "Employment of the P-Multiplier in Pile-Group Analysis." *Journal of bridge engineering*, 612-623.

Ashour, M., and Norris, G. (2000). "Modeling Lateral Soil-Pile Response Based on Soil-Pile Interaction*." Journal of Geotechnical and Geoenvironmental Engineering*, 420–428.

Awoshika, K., and Reese, L. C. (1971). *Analysis of Foundation with Widely-Spaced Batter*. Center for Highway Research, The University of Texas at Austin.

Broms, B. B. (1964a). Lateral Resistance of Piles in Cohesionless Soils. *Journal of the Soil Mechanics and Foundations Division*, 123–156.

Broms, B. B. (1964b). Lateral Resistance of Piles in Cohesive Soils. *Journal of the Soil Mechanics and Foundations Division*, 27–64.

Brown, D. A., Morrison, C., and Reese, L. C. (1988). Lateral Load Behavior of Pile Group in Sand. *Journal of Geotechnical Engineering*, 1261-1276.

Brown, D. A., O'Neill, M. W., Hoit, M., McVay, M., El Naggar, M. H., and Chakrabory, S. (2001). *Static and dynamic lateral loading of pile groups (NCHRP Report No. 461).* Washington, D.C.: Transportation Research Board, National Research Council.

Brown, D. A., Resse, L. C., and O'Neill, M. W. (1987). Cyclic Lateral Loading of a Large-Scale Pile Group. *Journal of Geotechnical Engineering*, 1326-1343.

Broms, B. B. (1964a). Lateral Resistance of Piles in Cohesionless Soils. *Journal of the Soil Mechanics and Foundations Division*, 123–156.

Broms, B. B. (1964b). Lateral Resistance of Piles in Cohesive Soils. *Journal of the Soil Mechanics and Foundations Division*, 27–64.

Brown, D. A., Morrison, C., and Reese, L. C. (1988). Lateral Load Behavior of Pile Group in Sand. *Journal of Geotechnical Engineering*, 1261-1276.

Brown, D. A., O'Neill, M. W., Hoit, M., McVay, M., El Naggar, M. H., and Chakrabory, S. (2001). *Static and dynamic lateral loading of pile groups (NCHRP Report No. 461).* Washington, D.C.: Transportation Research Board, National Research Council.

Brown, D. A., Resse, L. C., and O'Neill, M. W. (1987). Cyclic Lateral Loading of a Large-Scale Pile Group. *Journal of Geotechnical Engineering*, 1326-1343.

Christensen, D. S. (2006). *Full Scale Static Lateral Load Test of a 9 Pile Group in Sand.* Brigham Young University, Department of Civil and Environmental Engineering.

Cox, W. R., Dixon, D. A., and Murphy, B. S. (1984). Lateral-load tests on 25.4-mm (1-in.) diameter piles in very soft clay in side-by-side and in-line groups. *Laterally loaded deep foundations: Analysis and performance.* ASTM International.

Culmo, M. P. (2011). "Accelerated Bridge Construction- Experiences in Design, Fabrication and Erection of Prefabricated Bridge Elements and Systems." *FHWA-HIF-12-013, Federal Highway Administration,* U.S. Department of Transportations, Washington, DC.

Culmo, M. P. (2009). "Connection details for prefabricated bridge elements and systems." *FHWA-IF-09-010, Federal Highway Administration,* U.S. Department of Transportations, Washington, DC.

Espinoza, A., and Mahin, S. A. (2008). "Shaking table and analytical investigation of reinforced concrete bridge piers with foundations allowed to uplift during earthquakes." *Rep. No. UCB/SEMM-08/03*, Dept. of Civil and Environmental Engineering, Univ. of California, Berkeley, CA.

Guan, Z., Chen, X., and Li, J. (2018). "Experimental investigation of the seismic performance of bridge models with conventional and rocking pile group foundations." *Eng. Struct.*, 168, 889-902.

Haber, Z. B., Saiidi, M. S., and Sanders, D. H. (2014). "Seismic performance of precast columns with mechanically spliced column-footing connections", *ACI Structural Journal*, 111(3), 639-650.

Hannigan, P. J., Rausche, F., Likins, G. E., Robinson, B. R., and Becker, M. L. (2016). *Desing and Construction of Driven Pile Foundations (FHWA-NHI-16-009).* Washington, DC: Federal Highway Administration (FHWA).

Haraldsson, O.S., Janes, T.M., Eberhard, M.O., and Stanton, J.F. (2013). "Seismic resistance of socket connection between footing and precast column", *J. Bridge Eng.*, 18(9), 910-919.

Harry, P. G. (1971). Behavior of Laterally Loaded Piles: II-Pile Groups. *Journal of the Soil Mechanics and Foundations Division*, 733-751.

Hetenyi, M. (1946). *Beams on Elastic Foundation.* University of Michigan Press.

Hewes, J. T., and Priestley, M. J. N. (2002). "Seismic design and performance of precast concrete segmental bridge columns." *Rep. No. SSRP2001/25*, California Dept. of Transportation, Sacramento, CA.

Iowa DOT (Iowa Department of Transporatation) (2018). *LRFD Bridge Design Manual*, Ames, IA.

Jia, J. (2018). *Soil Dynamics and Foundation Modeling.* Springer Nature.

Kavianipour, F. and Saiidi, M.S. (2013). "Experimental and analytical seismic studies of a four-span bridge system with composite piers", CCEER-13-17, Center for Civil Engineering Earthquake research, *Department of Civil and Environmental Engineering, University of Nevada, Reno*, Reno, NV.

Kraft, L. M., Focht, J. A., and Amerasinghe, S. F. (1981). Friction Capacity of Piles Driven into Clay. *Journal of Geotechnical Engineering*, 1521-1541.

Kubo, K. (1964). *Experimental Study of the Behavior of Laterally Loaded Piles.* Japan: Transportation Technology Research Institute.

Long, J. H. (1984). *The Behavior of Vertical Piles in Cohesive Soil Subjected to Repetitive Horizontal Loading.* Austin, Texas: The University of Texas.

Ma, Y., and Deng, N. (2014). Deep Foundations. In W.-F. Chen, and L. Duan, *Bridge Engineering Handbook: Substructure Design.* CRC Press.

Mashal, M., and Palermo, A. (2019). Low-Damage Seismic Design for Accelerated Bridge Construction. Journal of Bridge Engineering, 24(7), 04019066.

Mashal, M., and Palermo, A. (2015). "High-Damage and Low-Damage Seismic Design Technologies for Accelerated Bridge Construction." *Structures Congress*, 549-560

Marsh, L. M., Wernli, M., Garrett, B. E., Stanton, J. F., Eberhard, M. O., and Weinert, M. D. (2011). "Application of accelerated bridge construction connections in moderate-to-high seismic regions." *Rep. 698, National Cooperative Highway Research Program (NCHRP)*, Transportation Research Board, Washington, DC.

Matlock, H. (1970). Correlations for design of laterally loaded piles in soft clay. *Proceedings of the II Annual Offshore Technology Conference*, (pp. 577-594). Houston, Texas.

Matsumoto, E. (2009). Emulative Precast Bent Cap Connections for Seismic Regions: Grouted Duct and Cap Pocket Test Results, Design and Construction Specifications, Design Examples, and Connection Details. Report No. ECS-CSUS-2009-05. California State University, Sacramento.

Mehrsoroush, A. and Saiidi, M.S. (2016). "Cyclic response of precast bridge piers with novel column-base pipe pins and pocket cap beam connections", *J. Bridge Eng.*, 21(4): 04015080.

Meimon, Y., Baguelin, F., and Jezequel, J. F. (1986). Pile group behaviour under long time lateral monotonic and cyclic loading. *the 3rd InternationalConference on Numerical Methods on Offshore Piling*, (pp. 285-302). Inst. Francais du Petrole, Nantes, France.

Mohebbi, A., Saiidi, M.S., and Itani, A. (2017). "Development and seismic evaluation of pier system w/pocket connections, CFRP tendons, and ECC/UHPC columns", CCEER-17-02, Center for Civil Engineering Earthquake research, *Department of Civil and Environmental Engineering, University of Nevada, Reno*, Reno, NV.

Motaref, S., Saiidi, M.S., and Sanders, D. (2011). "Seismic response of precast bridge columns with energy dissipating joints", CCEER-11-01, Center for Civil Engineering Earthquake research, *Department of Civil and Environmental Engineering, University of Nevada, Reno*, Reno, NV.

Motaref, S., Saiidi, M. S., and Sanders, D. (2010). Experimental Study of Precast Bridge Columns with Built-in Elastomer. In Transportation Research Record: Journal of the Transportation Research Board, No. 2202, Transportation Research Board of the National Academies, Washington, DC, pp. 109–116.

O'Neill, M. W., and Dunnavant, T. W. (1984). *A Study of the Effects of Scale, Velocity, and Cyclic Degradability on Laterally Loaded Single Piles in Overconsolidated Clay.* Houston, Texas: Department of Civil Engineering, University of Houston-University Park.

Ou, Y. C., Tsai, M. S., Chang, K. C., and Lee, G. C. (2010). "Cyclic behavior of precast segmental concrete bridge columns with high performance or conventional steel reinforcing bars as energy dissipation bars." *Earthquake Eng. Struct. Dyn.*, 39(11), 1181–1198.

Pang, J. B. K., Eberhard, M. O., and Stanton, J. F. (2010). Large-Bar Connection for Precast Bridge Bents in Seismic Regions. Journal of Bridge Engineering, 15(3), pp. 231–239.

Precast/Prestressed Concrete Institute (PCI) (2014). "Precast and prestressed concrete." *Precast/Prestressed Concrete Institute*, Chicago, IL.

Precast/Prestressed Concrete Institute (PCI). (2007). "Architectural Precast Concrete Manual, Section 3.5", *Precast/Prestressed Concrete Institute*, Chicago, IL.

Reese, L. C. (1957). Discussion of " Soil Modulus for Laterally Loaded Piles by B. McClelland and Jr., J.A. Focht". *Journal of the Soil Mechanics and Foundations Division*, 21-43.

Reese, L. C., and O'Neil, M. W. (1988). *Drilled Shafts: Construction Procedures and Design Methods.* McLean, VA: U.S. Department of Transportation, Federal Highway Administration.

Reese, L. C., and Van Impe, W. F. (2011). *Single Piles and Pile Group under Lateral Loading.* CRC Press.

Reese, L. C., and Welch, R. C. (1975). Lateral Loading of Deep Foundations in Stiff Clay. *Journal of the Geotechnical Engineering Division*, 633-649.

Reese, L. C., Cox, W. R., and Koop, F. D. (1975). Field testing and analysis of laterally loaded. *Proceedings of the VII Annual Offshore Technology Conference*, (pp. 672-690). Houston, Texas.

Restrepo, J. I., Tobolski, M. J., and Matsumoto, E. E. (2011). "Development of a precast bent cap system for seismic regions." *Rep. 681, National Cooperative Highway Research Program (NCHRP)*, Transportation Research Board, Washington, DC.

Rollins, K. M., Olsen, K. G., Jensen, D. H., Garrett, B. H., Olsen, R. J., and Egbert, J. J. (2006). Pile Spacing Effects on Lateral Pile Group Behavior: Analysis. *Journal of Geotechnical and Geoenvironmental Engineering*, 1272-1283.

Rollins, K. M., Peterson, K. T., and Weaver, T. J. (1998). Lateral load behavior of full scale pile group in clay. *Journal of Geotechnical Engineering*, 468–478.

Schwarz, P. (2002). *Beitrag zum Tragverhalten von Verpresspfählen mit kleinem.* Lehrstuhl und Prüfamt für Bodenmechanik und Felsmechanik der Technischen Universität München.

Shama, A. A., Marder, J. B., and Aref, A. J. (2002). "Seismic performance and retrofit of steel pile to concrete cap connections." *ACI Struct. J.*, 99(1), 51–61.

Sritharan, S. and Cheng, Z. (2016). "Accelerated Bridge Construction (ABC) – Substructure: Grout." ⟨http://sri.cce.iastate.edu/ABC-Guidelines/Grout%20New.html⟩ (Sep. 30, 2017)

Thonstad, T., Mantawy, I. M., Stanton, J. F., Eberhard, M. O., and Sanders, D. H. (2016). "Shaking table performance of a new bridge system with pretensioned rocking columns." *Journal of Bridge Engineering*, 21(4), 04015079.

Utah Department of Transportation (UDOT) (2017). *Structural Design and Detail Manual, UDOT SDDM*, Taylorsville, UT.

Wang, J. C., Ou, Y. C., Chang, K. C., and Lee, G. C. (2008). "Large-scale seismic tests of tall concrete bridge columns with precast segmental construction." *Earthquake Eng. Struct. Dyn.*, 37(12):1449–1465.

Wify, T., Klaiber, W., and Hockerman, S. (2009). Precast Concrete Element for Accelerated Bridge Construction: Laboratory Testing of Precast Substructure Components, Boone County Bridge (CTRE Project 06-262). Ames, IA: Bridge Engineering Center, Iowa State Univeristy

Xiao, Y., Wu, H., Yaprak, T. T., Martin, G. R., and Mander, J. B. (2006). "Experimental studies on seismic behavior of steel pile-to-pile-cap connections", *J. Bridge Eng.*, 11(2), 151-159.

CHAPTER 3. SIDE SHEAR STRENGTH OF PREFORMED SOCKET CONNECTIONS SUITABLE FOR VERTICAL PRECAST MEMBERS

A paper published in the ASCE Journal of Bridge Engineering

(February 18, 2019, DOI: 10.1061/(ASCE)BE.1943-5592.0001391)

Zhao Cheng, S.M.ASCE[1] and Sri Sritharan, Ph.D., M.ASCE[2]

[1]Graduate Research Assistant, Dept. of Civil, Construction, and Environmental Engineering, Iowa State Univ., Ames, IA 50011. E-mail: zcheng@iastate.edu

[2]Wilkinson Chair of Interdisciplinary Engineering, Dept. of Civil, Construction, and Environmental Engineering, Iowa State Univ., Ames, IA 50011 (corresponding author). E-mail: sri@iastate.edu

Abstract

Use of precast substructure in Accelerated Bridge Construction (ABC) has been gaining popularity due to its advantages over traditional cast-in-place (CIP) construction. When using vertical precast members (e.g., columns and piles) in bridge substructure construction, they must be connected to the adjoining members (e.g., bent cap, pile cap, and abutment) reliably. To accomplish this goal and promote ease of construction, the preformed socket connection has been suggested. This connection is established by inserting the vertical precast member inside a preformed socket in the precast adjoining member and filling the socket with non-shrink, high-strength grout. Using specimens that modeled the full-scaled connection interfaces, this paper experimentally evaluates the side shear strength of preformed socket connections with various connection parameters. Test results show that side shear mechanism in the preformed socket connections can provide significant resistance, facilitating transfer of large vertical loads. This paper also includes recommendations for the socket connections and appropriate stress limits.

Keywords: Accelerated bridge construction; Socket connection; Precast; Vertical member; Pile; Column; Design; Testing.

Introduction

Accelerated bridge construction (ABC) uses innovative techniques to complete bridge projects in a timely and cost-effective manner. Besides reducing mobility impacts, a number of successful projects have demonstrated that ABC can improve quality of construction, reduce onsite construction, and minimize environmental impacts. Use of Prefabricated Bridge Elements and Systems (PBES) in construction is a common strategy adopted in ABC. Although PBSE has been used in bridge superstructure construction for decades, their use in substructures have been very limited. In recent projects, the Department of Transportations in various states have utilized precast components in the construction of bridge substructures (e.g., bent cap, abutment, pile cap, column, and pile). Use of precast components in substructure is attractive because they can eliminate on-site forming and casting while overcoming challenges associated with the site constraints. When using vertical precast members, they need to be designed with reliable connections to the adjoining members (e.g., column-to-bent cap, column-to-pile cap, pile-to-pile cap, and pile-to-abutment connections). These connections should not only be easy to construct, but also produce dependable structural performance when subjected to the expected serviceability and ultimate loads.

Commercially available grouted splice couplers have been used to establish the connection between precast columns and adjoining elements. Other techniques, involving mechanical bar couplers, grouted ducts, a pocket for embedding reinforcing bars extended from precast member, and a socket for embedding the end of a precast member, and unbonded prestressing tendon, have also shown to be practical either through laboratory evaluation or field applications (Marsh et al. 2011; Culmo 2009). The focus of this study is

on socket connections due to the ease of construction and the ability to provide relatively large installation tolerances, with emphasis on transferring high vertical loads through the connection.

Socket connections for vertical precast members can be constructed using two options: (1) cast adjoining member around the end of the vertical member, or (2) insert the end of vertical member into the preformed socket in the adjoining member and secure the socket using grout closure pour. For the second approach, the preformed socket in the adjoining member can be accomplished using commercially available corrugated steel pipe (CSP) due to its low cost and ready availability in different sizes. In addition to serving as stay-in-place formwork, CSP offers confinement effect to the connection material while its corrugations provide a robust load transfer mechanism (UDOT 2017). The preformed socket, which promotes the use of prefabricated elements for the adjoining members, can be constructed with full or partial penetration (Figure 3.1a). With any construction option, when the vertical precast member is subjected to the design loads, the socket connection should facilitate the transfer of the loads without sustaining any significant sliding. As illustrated in Figure 3.1, the axial strength of fully penetrated connection depends only on the side shear resistance acting along the embedded portion of the vertical member. For a partially penetrated connection (Figure 3.1b), the axial load resistance can be provided by side shear and tipping at the end of vertical member. While relying on both side shear and tipping can be attractive to reduce the required embedment length of the vertical member, this option is not favored herein. This is because the design of such a connection is more challenging due to: (a) the side shear and tipping mechanisms being unlikely to be active simultaneously; and (b) sustaining a tipping mechanism would require design to prevent punching failure caused

by the precast vertical member. Given that sufficient axial resistance can be developed over a short embedment length, it is suggested that both fully and partially penetrated connections be designed relying only on side shear.

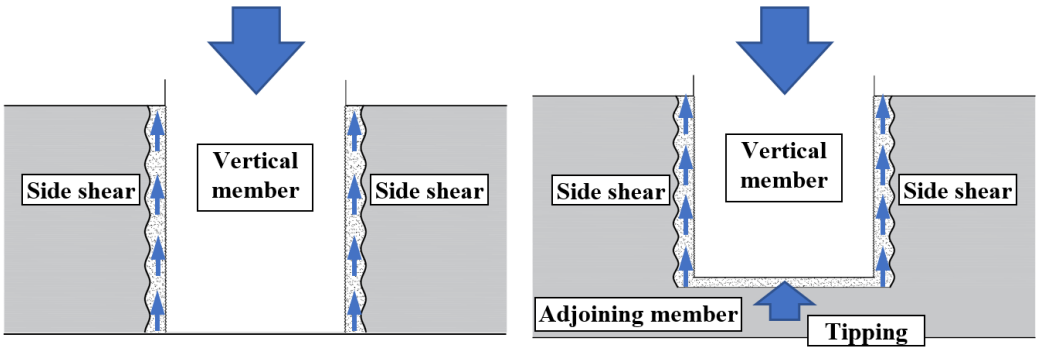

Fully penetrated socket connection (a)

Partially penetrated socket connection (b)

Figure 3.1 *Axial strength of (a) a fully penetrated socket connection and (b) a partially penetrated socket connection*

The side shear strength in a socket connection depends on how the connection is established. The connections with cast-in-place adjoining members exhibited high side shear strength in an experimental study. Haraldsson et al. (2013), who tested the connections constructed by casting spread footings around precast columns. The specimen with an intentionally roughened column surface and a column embedment length of 1.1 times the column diameter of 508-mm (20-in.) subjected to the high axial load. The corresponding axial load ratio was 58% based on the specified properties, but the connection was not failed using a high axial load ratio.

Several experimental studies have also utilized preformed sockets connections for seismic bridge columns, which were designed to form plastic hinges at the member ends, thereby contributing to energy dissipation under seismic load. To ensure sufficient column ductility, seismic columns are typically designed with a low axial load ratio (e.g., 5 to 10%).

Motaref et al. (2011) and Kavianipour et al. (2013), who tested bridge piers with socket connections between a precast column and the precast footing with an embedment length of 1.5 times the column diameter of 370-mm (14.57-in.). The tests showed successful development of plastic hinges with an axial load ratio of 6.3% and 8.8%, respectively. Mehrsoroush and Saiidi (2016) tested a scaled bridge pier having preformed socket connections in a bent cap. The corrugated steel pipes (CSPs) were used to create the sockets and the column embedment length was 1.2 times column diameter of 508-mm (20-in.). This test, which induced a maximum axial load ratio of 5.6%, also showed that the column embedment length into the socket was adequate to fully develop the column plastic hinge. Mohebbi et al. (2017) performed an experimental test on a preformed socket connection with a square column. In this test, with an axial load ratio of 14.4%, the column embedment length of only 1.0 times the column side dimension of 356-mm (14-in.) was used and a full column plastic hinge was successfully formed.

In all of the aforementioned studies with a relatively low axial load ratio, the preformed socket connection remained essentially undamaged while the plastic hinge formed in the column just outside the connection. However, these results cannot be applicable to vertical members subjected to high axial load ratios. Precast piles in seismic and non-seismic regions can be designed to sustain as much as 40% of the axial load capacity while bridge columns in non-seismic regions can be subjected to 25 to 30% of the axial load capacity. In addition, for preformed socket connections that are established using CSP and grout closure pour, no guideline is available to help determining the key connection parameters and side shear strength for design due to lack of investigation that examined the failure modes of socket connections. To address this knowledge gap, an experimental study was conducted to

investigate the failure modes of side shear mechanism in preformed socket connections so that the suitable vertical precast members can be designed to transfer large axial load through socket connections. This paper presents the description of the experimental program, test results, and recommendations established from this study.

Parameters Affecting Side Shear Strength

When a preformed socket is established using CSP and the connection is established using grout, the side shear strength will depend on a number of interface parameters. The parameters that most influence the strength include: (1) corrugation pattern of CSP, (2) surface texture along the embedded length of the precast member, (3) clearance between CSP and the embedded member, and (4) the strength and type of grout used for closure pour. More details about each parameter are presented below.

1. A key feature of CSP is its corrugation, which provides additional load transfer capacity. The corrugation types of standard CSPs include annular corrugation and helical corrugation. To make structural connections with CSP, UDOT (2017) recommends annular corrugation over helical corrugation, because helical corrugation is made to intentionally reduce the roughness to improve flow of substance through the pipe. The corrugation pattern in commercially available CSP varies with the pipe size. A pattern with 68-mm (2.67-in.) pitch and 13-mm (0.50-in.) depth is standard for CSPs with inside diameters ranging from 0.30-m (1-ft) to 2.13-m (7-ft), which are suitable for ABC applications.
2. Bond strength between the grout closure pour and the embedded member is another important property as shear sliding failure can trigger at the interface between them. The primary variable that controls the bond strength is surface texture of the embedded member. Smooth surface with no treatment will have

lower bond strength, increasing the likelihood of shear sliding at this interface. To ensure adequate shear transfer, AASHTO (2017) suggests intentionally roughening the surface of embedded member to an amplitude of approximately 6-mm (0.25-in.). Exposed aggregate finish is a popular texture for achieving the desired degree of roughness; regularized patterns with deeper amplitude (e.g., fluted fins and saw-tooth pattern) have also been commonly used. Different practical methods such as chemical formwork retarder, sandblasting, and bush hammering can be used to expose coarse aggregate. Note that the mechanical methods (i.e., sandblasting and bush hammering) may soften the exposed aggregate (PCI 2007), which will degrade the bond strength at the interface. The regularized patterns can be achieved by casting concrete against formliners that are attached to the inside surface of the formwork.

3. The preformed socket connection is secured by filling the clearance between the CSP and embedded member with grout. The thickness of grout closure pour that corresponds to CSP-to-embedded member clearance may affect the transfer of side shear. Sufficient clearance must be provided to conduct grout closure pour and to account for the cumulative effects of all allowed tolerances. For inserting a vertical precast member, a minimum clearance of 25-mm (1-in.) is required around the perimeter between the embedded member and the socket (PCI 2000). This clearance is also controlled by the available sizes of CSP. Considering the available formwork and the weight limits for transportation, the diameter or side dimension of most bridge vertical precast members are fabricated at 0.15-m (0.5-ft) intervals of up to 1.22-m (4-ft). Table 3.1 presents the inside diameters of the

appropriate commercially available CSPs and the resultant CSP-to- embedded member clearances expected for the bridge precast columns and piles. Note that the clearance herein represents the minimum distance between the crest of inside corrugation of the CSP and the most outer surface of the embedded member. As can be seen in the table, the clearances of 38-mm (1.5-in.) and 76-mm (3-in.) are two likely construction clearances in the preformed socket connections for bridge vertical members.

Table 3.1 *CSP-to-embedded member clearances for vertical precast members*

Diameter of vertical member (m)	**Inside diameter of CSP (m)**	**Resultant clearance (mm)**
0.30	0.38	38
0.46	0.53	38
0.61	0.69	38
0.76	0.91	76
0.91	1.07	76
1.07	1.22	76
1.22	1.37	76

4. For the purpose of establishing a strong socket connection, high-strength grout with the minimum compressive strength of 55.2-MPa (8000-psi) is preferred because the concrete strength of the precast member may be in the range of 34.5 to 48.3-MPa (5000 to 7000-psi). Other desirable properties, such as high-early-strength, fluid consistency, extended working time, and non-shrink, are also required to properly secure the socket connection. High-early-strength (i.e., a compressive strength not less than 27.6-MPa [4000-psi] at 1 day) would facilitate the connection to gain strength quickly, such that curing of grout will not cause any construction delays. The extended working time and fluid consistency provide the possibility to complete large grout pour into tight clearance between

the CSP and the embedded member. Non-shrink feature of the grout will minimize formation of cracks at the interfaces or within the grout itself, which are important for durability of the connection. A scanning of commercial available cementitious grouts has been conducted, and the findings indicated that only limited type of grouts meet all the preceding requirements (Sritharan and Cheng 2016).

Based on the above descriptions, it is apparent that once a specific grout meeting the desirable characteristics and commercially available standard CSPs are chosen, the side shear strength of a preformed socket connection will be determined by the surface texture of the embedded member and CSP-to-embedded member clearance. Therefore, the experimental investigation was conducted with these two variables.

Experimental Program

Testing Matrix

A total of eight specimens were constructed to evaluate the side shear strength in preformed socket connection with different surface texture for the embedded portion of the vertical member and CSP-to-embedded member clearance, as detailed in Table 3.2. Three types of surface textures, including exposed aggregate finish, 13-mm (0.5-in.) deep fluted fins, 19-mm (0.75-in.) deep fluted fins, were tested as they are likely to be used for vertical precast members. For the fluted fin patterns, the fins are routinely made in trapezoid shape, and the fin-to-fin pitches of 38-mm (1.5-in.) and 51-mm (2-in.) are standard for the 13-mm (0.5-in.) and 19-mm (0.75-in.) fin depths, respectively. As a reference unit, a smooth surface specimen was also tested. Two CSP-to-embedded member clearance of 38-mm (1.5-in.) and 76-mm (3-in.) were chosen to be tested. To investigate the influence of loading type, the first

four specimens were tested using monotonic loading, whereas the remaining four were subjected to cyclic loading.

Table 3.2 *Testing matrix*

Test specimen	Surface texture	CSP-to-embedded member clearance (mm)	Loading type
F1G1M	13-mm fluted fin	38	monotonic
F2G1M	19-mm fluted fin	38	monotonic
EG1M	exposed aggregate	38	monotonic
F2G2M	19-mm fluted fin	76	monotonic
EG1C	exposed aggregate	38	cyclic
F1G1C	13-mm fluted fin	38	cyclic
SG1C	Smooth	38	cyclic
F1G2C	13-mm fluted fin	76	cyclic

Details of Test Specimens

The test specimens were designed to reproduce the interface as expected in full-sized preformed socket connections, but the area of the interface region was reduced by utilizing the small-sized embedded members to keep the applied vertical load to be less than 1779-kN (400-kips). Each test specimen consisted of a short precast column segment that was embedded in a preformed socket on a precast foundation representing the adjoining member, as shown in Figure 3.2a. When a compressive force is applied to the top of the column segment, the side shear acting on the connection interface produced the resistance. Hence, the side shear strength could be evaluated by loading the column segment until it experiences a sliding failure with respect to the foundation. An oversized cavity, as illustrated in Figure 3.2b, was formed under the socket in each foundation to allow the column segment to be pushed out freely when the side shear mechanism fails. The reinforcement of the specimens is shown in Figure 3.2c. The concrete strength of the column segments and the foundations were kept to that expected for precast products. The measured 28-day compressive strength of these members was 36.97-MPa (5362 psi), following the ASTM C39 (2017).

During construction of the precast column segments, the surface textures were formed as they are on full-sized precast members. The exposed aggregate finish was achieved by applying chemical retarder to the formwork prior to casting the concrete, followed by power-washing the laitance after hardening of the concrete mass. The fluted fines were created by casting concrete against the polystyrene formliners that were installed inside the formwork. For obtaining the smooth surface, the formwork was used without any treatment. The completed surface textures are shown in Figure 3.2d.

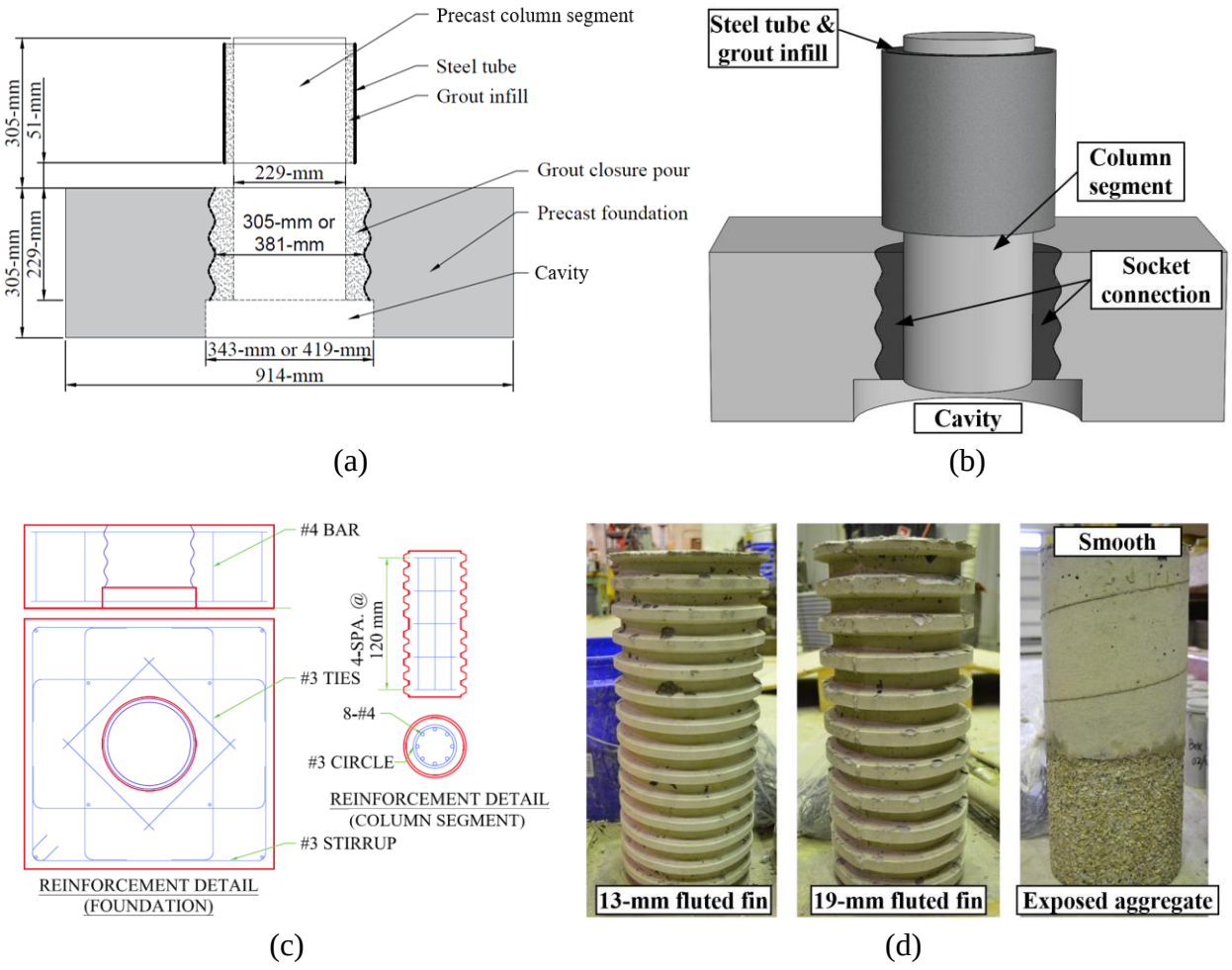

Figure 3.2 *Details of specimens: (a) key dimensions; (b) oversized cavity; (c) reinforcement detail; (d) surface textures of precast column segments*

The socket connection length was chosen to be 229-mm (9-in.), which was equal to the outer dimeter of the column segment. After temporarily supporting the column segments in the sockets that was preformed using CSPs, the connections were established by placing grout in the gaps between CSP and the column segments. The 0.30-m (12-in.) and 0.38-m (15-in.) diameter CSPs with standard corrugation pattern of 68-mm by 13-mm (2.67-in. by 0.50-in.) were used. These CSPs reserved 38-mm (1.5-in.) and 76-mm (3-in.) clearances, respectively, which are two clearances in expected between substructure vertical members and preformed socket connections at full scale. Referring to the specifications for the culvert pipe (AASHTO 2017), the CSPs used for creating preformed sockets met the requirements of AASHTO M 218 (2016). The thickness of CSPs was selected to be 1.63-mm (16 gage), which corresponds to the thickest standard CSP and thus is most likely to be used in practice. Having considered different grouts, one was chosen for securing connections in this study. The selected grout has a specified compressive strength of 27.58-MPa (4000-psi) in 8 hours and a specified compressive strength of 58.61-MPa (8500-psi) at 28 days. It also met the other requirements for closure pour such as fluid consistency, extended working time, and non-shrink characteristic. To prevent the column segments above the foundation from experiencing damage due to high axial compression, they were confined by steel tubes. A 51-mm (2-in.) gap was left between the steel tube and the top of foundation so that the tube will not establish any contact with the top of the foundation block during testing. This approach allowed the axial loads on the column segments to be increased, forcing failure in the connection.

Test Setup and Load Protocol

Figure 3.3a shows the test setup that was used for the experimental investigation. The specimen was supported on two base blocks in order to access the bottom of the column

segment for instrumentation purpose. Using a hydraulic jack that was powered by an electric hydraulic pump, vertical downward forces were applied on the top of the column segment.

A load cell was placed between the jack and the column segment for measuring the applied force. As shown in Figure 3.3b, three sets of the displacement transducers were mounted around the column segment. In each set, the transducers were positioned between the column segment and the foundation to monitor the movement of the column segment and grout with respect to the foundation. In this regard, the relative displacement between the column segment and the foundation (CF displacement), the relative displacement between the column segment and the grout closure pour (CG displacement), and the relative displacement between the grout closure pour and the foundation (GF displacement) were quantified. Note that, for the specimens with 76-mm (3-in.) CSP-to-column segment clearance, two transducers were mounted to measure the vertical deformation of grout (Δ_{grout}). In addition to external instrumentations, the strain gauges were mounted along one longitudinal reinforcing bar in each embedded column segment for capturing force transfer in the connection region.

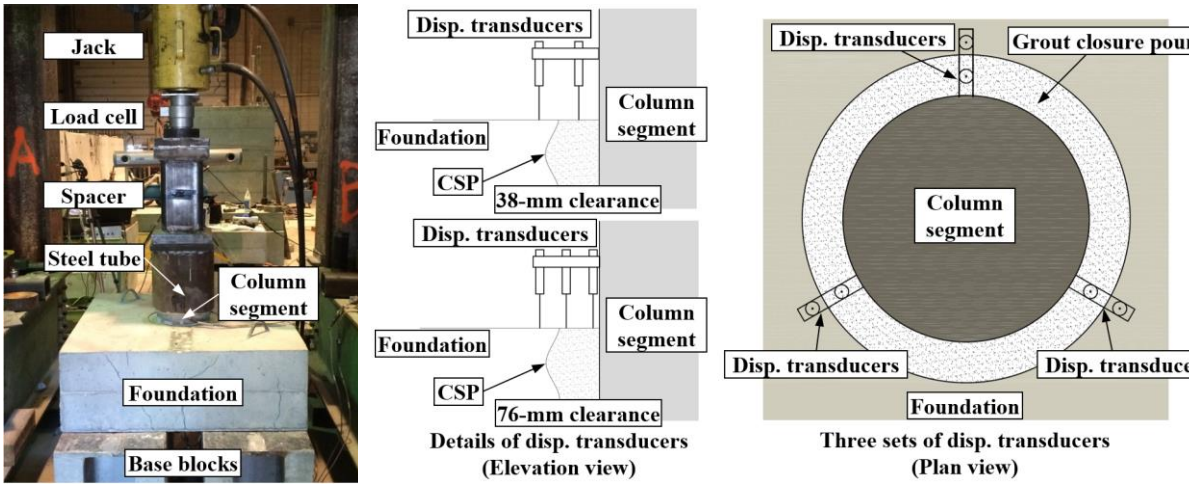

(a) (b)

Figure 3.3 *Test setup: (a) loading device; (b) instrumentations*

The specimens were tested by applying uniaxial compression force to the top of the column segment. For the specimen F1G1M, F2G1M, EG1M, and F2G2M, the loads were applied in a monotonically increasing manner. After the column segment began to slide with respect to the foundation, the displacement was used to control the test until the measured relative vertical displacement between the column segment and the foundation reached a value of at least 5.0-mm (0.195-in.). The remaining four specimens were subjected to a cyclic loading sequence consisted of a force-controlled phase and a displacement-controlled phase. The force-controlled phase was used until it reached 1068-kN (240-kips) at a load step of 178-kN (40-kips). In the displacement-controlled phase, the measured relative displacement between the column segment and the foundation was used as the controlling parameter. The target displacements for this phase were multiples of the relative displacement obtained for the last force-controlled load step. Due to a defect in the load control device, the applied displacements did not exactly reach the targeted values. In cyclic loading sequence, each load step was followed by unloading from a compression to zero force, and reapplying the same displacement two more times.

Experimental Results

During the tests, each specimen began to resist loads in an elastic manner, reached its maximum resistance with some nonlinearity associated with its response, and then exhibited considerable ductility beyond the peak strength. Following the peak strength, some softening in the response was observed.

Failure Modes

Regardless of whether monotonic or cyclic was used, the specimens exhibited two failure modes as shown in Figure 3.4. For the specimens with smooth surface and those with texture of 19-mm (0.75- in.) fluted fins, the sliding failure occurred at the column segment-

to-grout interface, whereas the sliding eventually occurred at the CSP-to-foundation interface for the specimens with exposed aggregate finish and 13-mm (0.5-in.) fluted fins. In case of the specimens with 19-mm (0.75-in.) fluted fins, the failure was due to shearing off the concrete fins. When the failure was at the CSP-to-foundation interface, the sliding of CSP occurred with respect to the surrounding concrete in the foundation, implying shearing in concrete of the foundation.

(a) (b)

Figure 3.4 *Failure modes: (a) column segment-to-grout interface failure; (b) CSP-to-foundation interface failure*

Measured Responses

Figure 3.5 depicts the applied vertical forces as a function of CF displacements, which represents the overall response of each specimen. The CF displacements herein were taken as the average values of the measured displacements from three transducers around the perimeter of the column segment. The monotonically loaded specimens exhibited higher stiffness than their counterparts subjected to cyclic loading. The monotonically loaded specimens reached the peak strength in the range of 1174-kN to 1463-kN (264-kips to 329-kips), while the cyclically loaded specimens resisted as much as 1161-kN to 1370-kN (261-

kips to 308-kips). The one with smooth column segment surface, which was loaded cyclically, failed at 716-kN (161-kips) and exhibited limited ductility. In bridge vertical members, it can be conservatively assumed that the applied loads will not exceed 50% of the axial load capacity. Given that 1161-kN (261-kips) corresponds to 76% of member axial capacity, the side shear in the preformed socket connection with intentionally roughened surface would provide satisfactory axial strength for connecting vertical precast members to adjoining members. As discussed subsequently, when the horizontal dimension of the vertical member increases, the appropriate embedment length should be designed in order for the vertical members to sustain large axial load ratios.

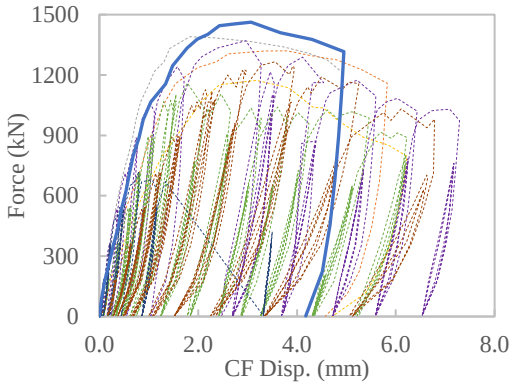

(a) F1G1M

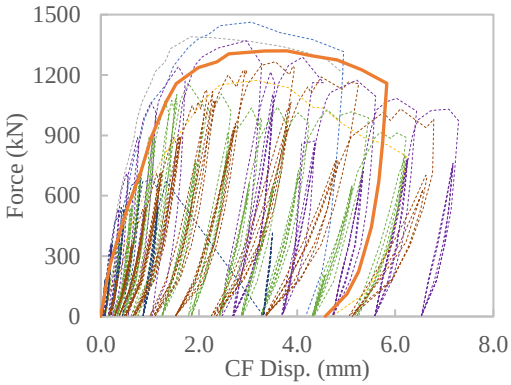

(b) F2G1M

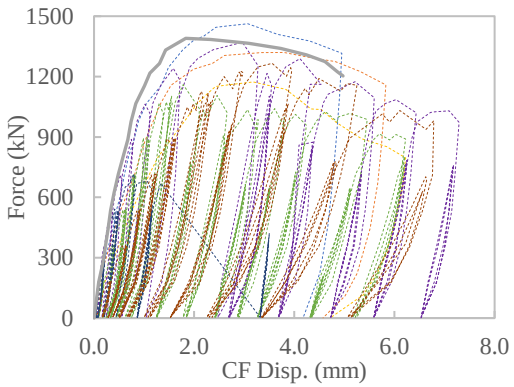

(c) EG1M

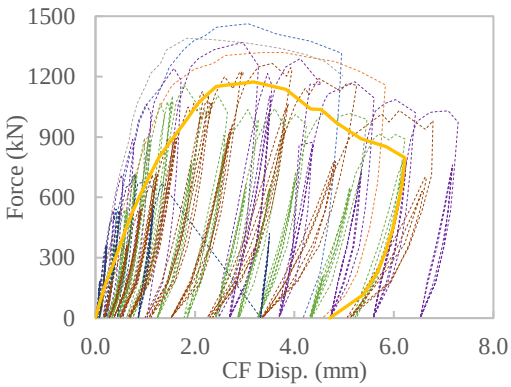

(d) F2G2M

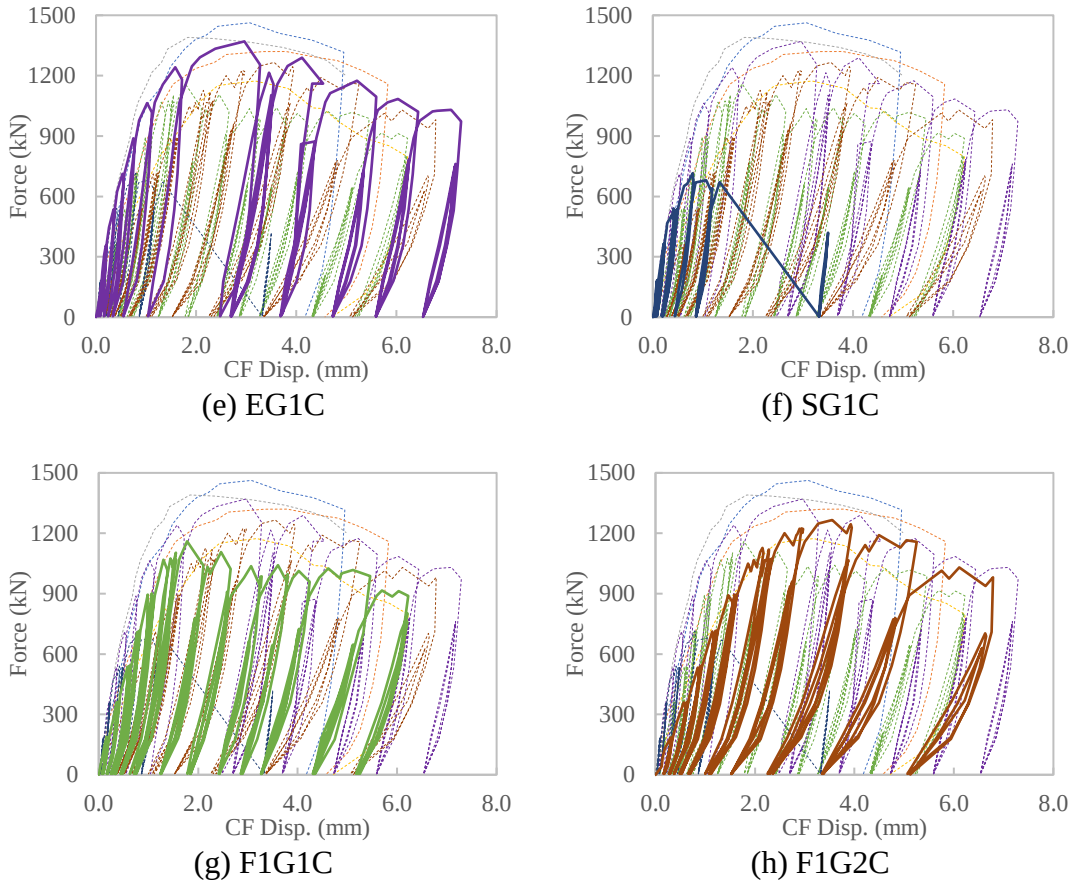

(e) EG1C (f) SG1C

(g) F1G1C (h) F1G2C

Figure 3.5 *Overall responses of specimens*

Overall, the intentionally roughened surface provided adequate bond strength between the grout and the embedded column segment, but the textures with deeper amplitude (i.e., 13-mm [0.5-in.] and 19-mm [0.75- in.] fluted fins) led to softer force-displacement responses. This is because fins that were constructed as integral part of column segment increased the flexibility of the connection in the vertical direction. Longer the fins, more flexible the connection became. In addition, a thicker grout closure pour resulting from wider CSP-to-column segment clearance tended to reduce the shear stiffness of the connections as deformation within the grout closure pour increased.

As illustrated in Figure 3.6, the CF displacements consisted of CG displacements and GF displacements. When a thicker grout closure pour was included, the vertical deformation

of grout (Δ_{grout}) was also quantified. Figure 3.7 describes the connection responses in terms of each component. To reveal the contribution of each component, plots were created with the same scale for the axes. As shown in Figure 3.7a, all specimens exhibited comparable GF displacement responses before reaching the peak strength. Hence, the differences in overall connection responses seen in Figure 3.5 were the result of sliding at the column segment-to-grout interface (CG displacements) and the deformation within the grout closure pour itself (i.e., Δ_{grout}). Figure 3.7b plots the vertical forces versus CG displacements for the specimens with 38-mm (1.5-in.) CSP-to-column segment clearance, but with different column segment surface textures. This plot confirms that the adequate roughness was necessary to successfully develop the bond strength between the grout and the embedded member. However, the textures with deeper amplitude of fins would soften the response at the embedded member-to-grout interface. Figure 3.7c compares the force versus CG displacement responses for the specimens F1G1C and F1G2C, which have the same column segment surface texture but different CSP-to-column segment clearance. Specimen F1G2C with thicker grout closure pour resulting from wider CSP-to-column segment clearance showed a softer overall connection response than Specimen F1G1C, but the two specimens exhibited similar responses at the column segment-to-grout interface. Therefore, given the comparable GF displacement responses, it can be stated that a thicker grout closure pour that induced significant Δ_{grout} would soften the connection response. With reference to the loading type, Figure 3.8 presents a comparison of the specimen responses with the same connection parameters but subjected different loading types (i.e., monotonic vs. cyclic). For the specimens with the exposed aggregate finish (i.e., EG1M and EG1C), no significant cumulative damage was caused by cyclic loading until the applied load was increased to 667-

kN (150-kips), which was approximately 50% of the peak strength. However, the cyclic loading caused increased strength degradation for the specimens with deeper amplitude for the column segment surface texture (i.e., F1G1M and F1G1C).

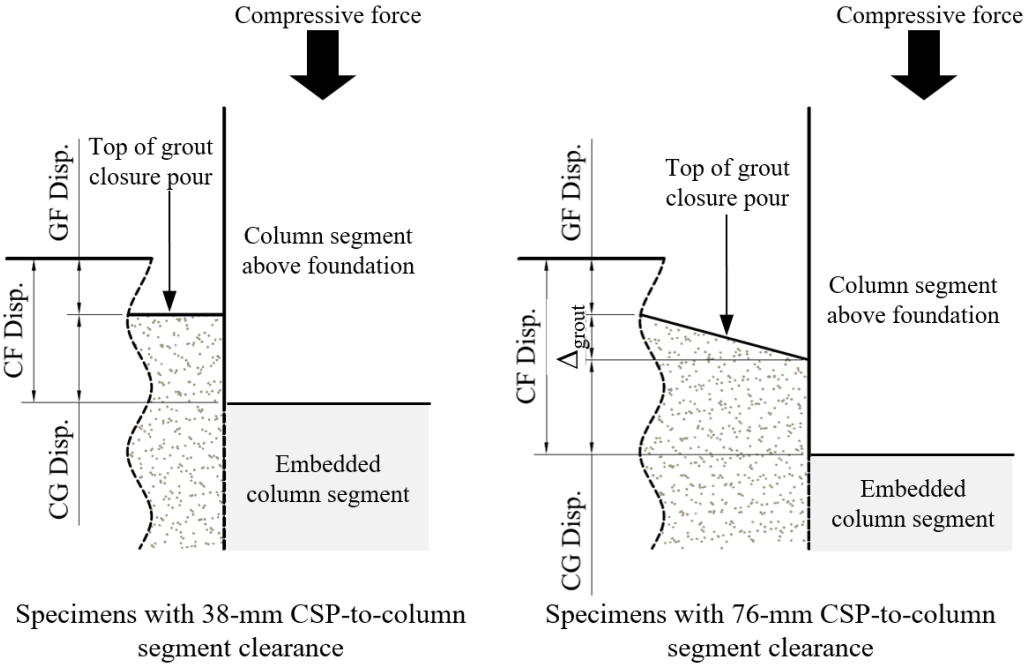

Figure 3.6 *Components of CF Displacement*

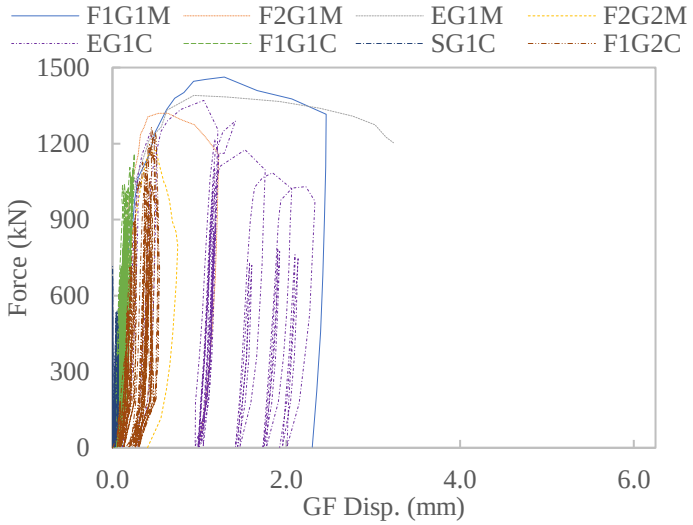

(a)

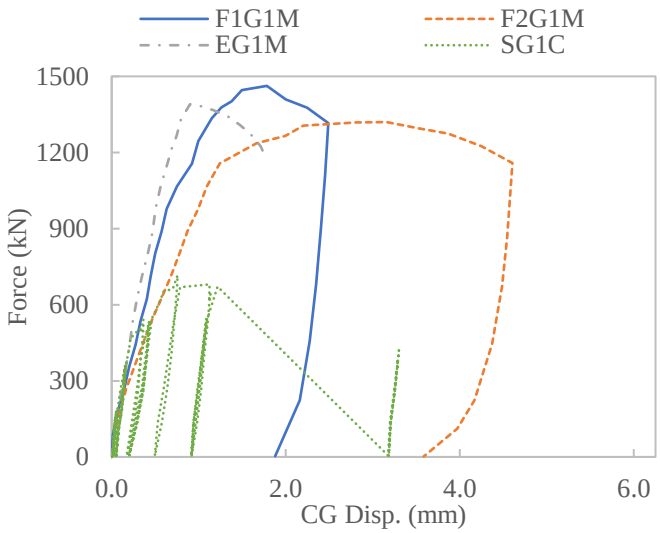

(b)

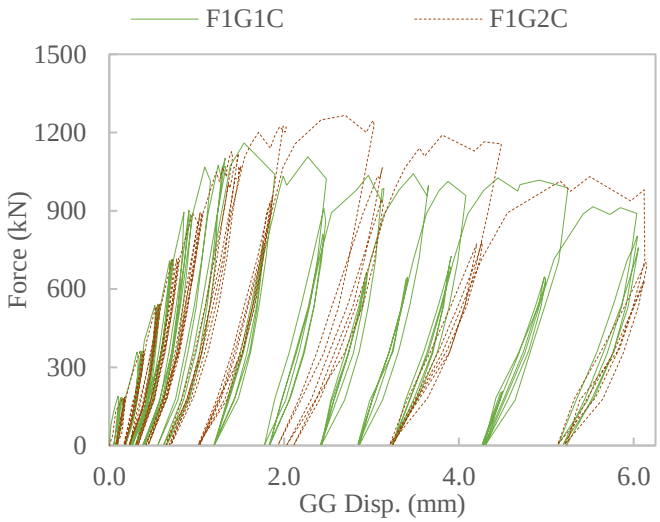

(c)

Figure 3.7 *Comparisons of connection responses: (a) GF disp. responses for all specimens; (b) CG disp. responses for specimens with different column segment surface textures; (c) CG disp. responses for specimens with different CSP-to-column segment clearances*

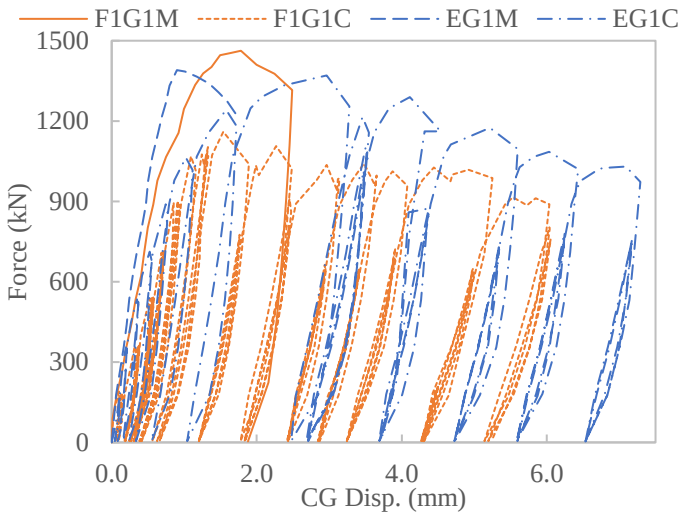

Figure 3.8 *Impact of cyclic loading*

Force Transfer Behavior

The strain values measured along the longitudinal bar in the embedded column segment reflect the transfer of force from the column segment to the foundation through the side shear mechanism. Figure 3.9 presents the normalized embedded column segment longitudinal bar strains as a function of depth ratio under different load levels, in which the strains at the top of the foundation under the applied load of 222-kN (50-kips), 445-kN (100-kips), 667-kN (150-kips), 890-kN (200-kips), and 1112-kN (250-kips) were normalized to 0.2, 0.4, 0.6, 0.8, and 1.0, respectively, for comparison purposes. The depth ratio herein is defined as the depth where the strain was measured to the embedment length of the column segment. A linear response is assumed between two adjacent gauge locations, which implies a constant shear stress along the column embedment length. Based on the observations from these plots, the specimens with same CSP-to-column segment clearance but with different surface textures (F1G1, F2G1, EG1, and SG1) exhibited similar force transfer behavior when subjected to the loads up to 445-kN (100-kips) (Figure 3.9a). When loads were further increased, the force transfer took place mostly in the top half of the connections for the

specimens with column segments having deeper amplitude textures (F1G1 and F2G2) (Figure 3.9b). In other words, when subjected to high loads, the surface textures with deeper amplitude (i.e., fluted fins) were more efficient in transferring the applied force through the side shear mechanism although the corresponding stiffness was earlier found to be softer. As a result, the deep amplitude surface texture may be used to reduce the force transfer length.

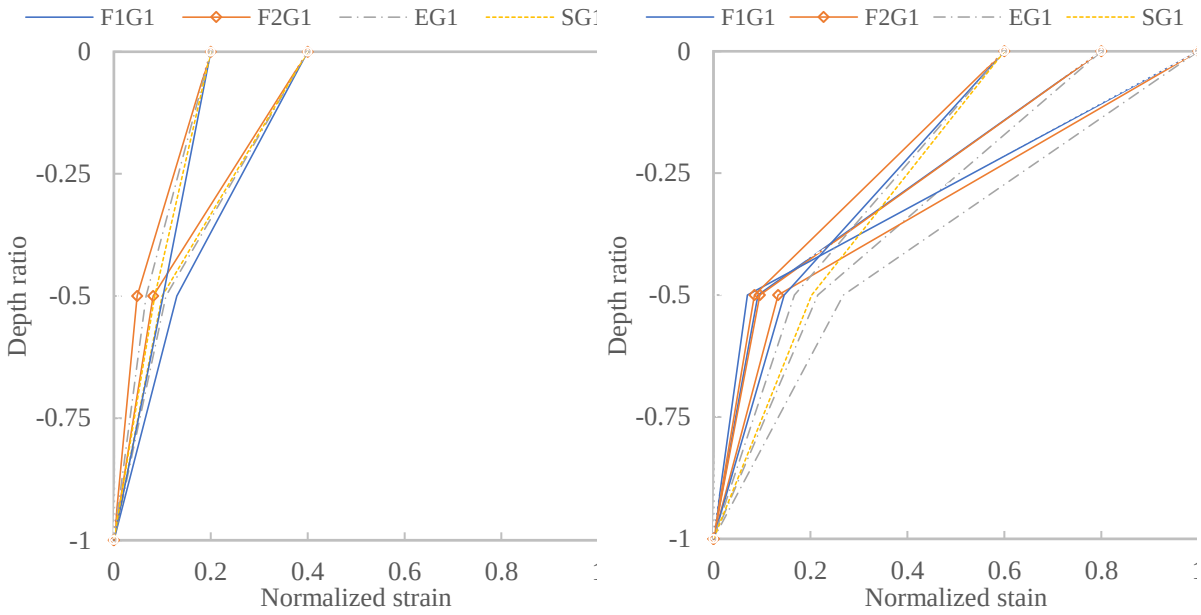

Figure 3.9 *Normalized embedded stub longitudinal bar strains under loads of (a) 222-kN, 445-kN; and (b) 667-kN, 890-kN, 1112-kN*

Discussions

Structural Performance

The structural performances of the specimens presented above facilitated characterization of side shear mechanism and better understanding of force transfer behavior. The socket connections that consisted of embedded members with deeper amplitude surface textures exhibited softer force-displacement relationships compared to the one with exposed aggregate surface, while the surface textures in these connections would transfer the force in

a more efficient manner (i.e., over a shorter depth). The thicker grout closure pour resulting from wider CSP-to-embedded member clearance also reduced the stiffness of the socket connection. The softening was attributed to relatively larger deformations occurring at the column-to-grout interfaces and within the grout closure pour itself, which were caused by the properties of grout. Under the applied loads, the grout exhibited relatively more flexibility than normal concrete due to the lack of hard coarse aggregate and lower modulus. Because of more participation of grout, the connections with deeper amplitude surface texture and wider CSP-to-embedded member clearance showed softer connection responses. However, the deeper amplitude increased the shear resistance, enabling the force to be transferred over a reduced embedment depth. Even though the participation of grout led to relatively larger deformation, the failure did not occur at the grout closure pour but at the stems of concrete fines or foundation concrete surrounding the CSP because the strength of the grout was significantly higher than concrete. The cyclic loading reduced the stiffness on the connections with deeper amplitude surface texture. However, for the connection with exposed aggregate surface, limited effect of cyclic loading was exhibited on the connection response when the applied forces were less than 50% of the peak strength.

Constructability

Based on the experimental investigation presented herein, the preformed socket connection provides great potentials for use in practice due to its ease of construction. The socket can be easily established by CSP that serves as stay-in-place formwork. Through the construction of the specimens, use of chemical formwork retarder was found to be an efficient method to roughen the embedded member surface. The retarder was applied on the formwork up to 3-hours ahead of the concrete pour. After removing the formwork when the concrete was 3-days old, the laitance was easily removed with high-pressure water to expose

the aggregate. The construction process with formliner was also completed with ease. However, the damage on precast fins could possible occur during fabrication and transportation. The experimental study also examined potential time saving measures for the assembly of the socket connection. The process will go smoothly if the right grout is identified for the closure pour. The desirable features for grout include high-early-strength, extended working time, and appropriate fluid consistency.

Design Recommendations

Based on the experimental findings and analyses of data, the following recommendations have been formulated for designing and constructing preformed socket connections that are appropriate for vertical precast members:

- Considering both the structural performance and constructability, the exposed aggregate finish is suggested for preparing the surface of the vertical precast member to be embedded in the preformed socket. This finish can be easily accomplished using chemical formwork retarder or an appropriate formliner that can ensure a similar surface texture.
- The CSP-to-embedded member clearance essentially determines the thickness of grout closure pour. The commercially available CSP sizes result in the clearances of 38-mm (1.5-in.) and 76-mm (3-in.) for most bridge vertical members. These two likely clearances are appropriate for grout closure pours to sustain axial loads in the preformed socket connection. The 76-mm (3-in.) clearance between CSP and embedded member would reduce the stiffness of the connection compared to the 38-mm (1.5-in.) clearance. This could be overcome by stiffening the grout using pea gravel with appropriate permission from the grout supplier.

- The CSPs with standard corrugation pattern is sufficient to preforming a socket in the adjoining member. The minimum 28-days compressive strength of grout established according to ASTM C109 (2016) should be 58.61-MPa (8500-psi) to ensure sufficient strength and stiffness for the connection. In addition, to properly securing the connection, the grout should have the following properties: high early strength, fluid consistency, extended working time, and non-shrink characteristic.
- Failure of a preformed socket connections subjected to an axial load can develop at the embedded member-to-grout interface of at the CSP-to-surrounding concrete interface. Therefore, the shear stress acting on these two interfaces shall be limited when designing the socket connection. For the connections following the above construction recommendations and with concrete attaining a compressive strength no less than 37.92-MPa (5500-psi), the limiting stresses at the embedded member-to-grout interface and the CSP-to-concrete interface may be taken as 6.89-MPa (1000-psi) and 4.83-MPa (700-psi), respectively. Conservatively, these stress limits were determined with the lowest axial load of 1174-kN (264-kips) that was reached by the tested specimens and the assumption that the shear transfer occurs uniformly along the entire length of connection. Therefore, the minimum embedment length in a preformed socket connection required for a precast vertical member subjected primarily to axial loads can be determined as follows:

$$l_{min} = \frac{P}{p_e f_{grout}} \leq \frac{P}{\pi d_{CSP} f_{CSP}} \qquad \text{Equation 3-1}$$

where l_{min} = the minimum embedment length of the precast vertical member; P = the design axial load in the vertical member; p_e = the outer perimeter of embedded vertical member cross-section; d_{CSP} = inside diameter (nominal diameter) of CSP;

f_{grout} = permissible stress for the embedded member-to-grout interface, recommended as 6.89-MPa (1000-psi); f_{CSP} = permissible stress for the CSP-to-surrounding concrete interface, recommended as 4.83-MPa (700-psi).

Conclusions

The use of ABC has been implemented to speed up bridge construction. In recent years, there has been growing interest in using vertical precast members for the substructure, such as columns and piles. Precast vertical members can be embedded in a socket that is preformed in the adjoining member using CSP and high-strength grout. This type of connection has been identified as a viable means to promote the use of precast vertical members. However, there is lack of knowledge regarding the side shear mechanisms that provide resistance against axial load and the corresponding stress limits so that the preformed socket connection can be designed to sustain high axial loads. As a result, an experimental investigation was conducted to evaluate the side shear strength in the preformed socket connection. Eight specimens were constructed with the embedded potion of the member in the socket connection having the following outer surfaces: a smooth finish, exposed aggregate finish, 13-mm (0.5-in.) deep fluted fins, and 19-mm (0.75-in.) deep fluted fins. The connection regions replicated typical socket connections at full scale. The specimens with different connection parameters were tested by subjecting them to monotonic and cyclic axial loading. Based on the findings from the tests and analyses of data, the following conclusions can be drawn:

- All specimens, except the one with smooth column surface, provided significant side shear strength against the axial load applied to the column segments. Hence, the intentionally roughened embedded member surface, as required by AASHTO, is

necessary to develop satisfactory side shear strength to sustain axial loads used in routine design practice. However, surface roughness smaller than an amplitude of 6-mm is adequate, which can be easily achieved by exposing the aggregates.

- The specimens consisted of the column segments with deep amplitude surface textures (i.e., fluted fins) exhibited softer connection responses compared to the one with exposed aggregate surface finish. Thicker grout closure pour resulting from wider CSP-to-column segment clearance also reduced the stiffness of the socket connection.ex
- For the specimens with deeper amplitude column segment surface texture, the force transfer was more efficient when subjecting to high loads due to the increased surface roughness, enabling the load to be resisted over a shorter length.
- Exposed aggregate for embedded member surface preparation, standard CSP, and high-strength grout are recommended for establishing socket connections effectively. For connections established as described in this study, the side stress limitations of 6.89-MPa (1000-psi) and 4.83-MPa (700-psi) suggested, respectively, for the embedded member-to-grout interface and CSP-to-surrounding concrete interface to determine the minimum embedment length of the precast vertical member.

Acknowledgements

This study was supported by Iowa Highway Research Board (IHRB) and Federal Highway Administration State Transportation Innovation Council (STIC). The authors would like to thank the members of the Technical Advisory Committee for their advices and suggestions. The experimental investigation used Rapid Set® UltraFlow® 4000/8 and Flex-

Liner™ formliner in the construction of the test specimens. We appreciate the material contributions from CTS Cement Manufacturing Corp. and Scott System.

Reference

American Association of State Highway and Transportation Officials (AASHTO) (2016). "Standard Specification for Steel Sheet, Zinc-Coated (Galvanized), for Corrugated Steel Pipe", *AASHTO M 218*, Washington, DC.

American Association of State Highway and Transportation Officials (AASHTO) (2017). *LRFD Bridge Design Specifications*, 8th Ed., Washington, DC.

ASTM (2016). "Standard Test Method for Compressive Strength of Hydraulic Cement Mortars (Using 2-in. or [50-mm] Cube Specimens)", *ASTM C109/C109M-16a*, West Conshohocken, PA.

ASTM (2017). "Standard Test Method for Compressive Strength of Cylindrical Concrete Specimens", *ASTM C39/C39M-17b*, West Conshohocken, PA.

California Department of Transportation (Caltrans) (2013). *Seismic Design Criteria*, Version 1.7, Sacramento, CA.

Culmo, M. P. (2009). "Connection details for prefabricated bridge elements and systems." *FHWA-IF-09-010, Federal Highway Administration*, U.S. Department of Transportations, Washington, DC.

Haraldsson, O.S., Janes, T.M., Eberhard, M.O., and Stanton, J.F. (2013). "Seismic resistance of socket connection between footing and precast column", *J. Bridge Eng.*, 18(9), 910-919.

Kavianipour, F. and Saiidi, M.S. (2013). "Experimental and analytical seismic studies of a four-span bridge system with composite piers", CCEER-13-17, Center for Civil Engineering Earthquake research, *Department of Civil and Environmental Engineering, University of Nevada, Reno*, Reno, NV.

Marsh, L. M., Wernli, M., Garrett, B. E., Stanton, J. F., Eberhard, M. O., and Weinert, M. D. (2011). "Application of accelerated bridge construction connections in moderate-to-high seismic regions." *Rep. 698, National Cooperative Highway Research Program (NCHRP)*, Transportation Research Board, Washington, DC.

Mehrsoroush, A. and Saiidi, M.S. (2016). "Cyclic response of precast bridge piers with novel column-base pipe pins and pocket cap beam connections", *J. Bridge Eng.*, 21(4): 04015080.

Mohebbi, A., Saiidi, M.S., and Itani, A. (2017). "Development and seismic evaluation of pier system w/pocket connections, CFRP tendons, and ECC/UHPC columns", CCEER-17-02, Center for Civil Engineering Earthquake research, *Department of Civil and Environmental Engineering, University of Nevada, Reno*, Reno, NV.

Motaref, S., Saiidi, M.S., and Sanders, D. (2011). "Seismic response of precast bridge columns with energy dissipating joints", CCEER-11-01, Center for Civil Engineering Earthquake research, *Department of Civil and Environmental Engineering, University of Nevada, Reno*, Reno, NV.

Precast/Prestressed Concrete Institute (PCI). (2000). "Tolerance Manual for Precast and Prestressed Concrete Construction", MNL 135-00, *Precast/Prestressed Concrete Institute*, Chicago, IL.

Precast/Prestressed Concrete Institute (PCI). (2007). "Architectural Precast Concrete Manual, Section 3.5", *Precast/Prestressed Concrete Institute*, Chicago, IL.

Sritharan, S. and Cheng, Z. (2016). "Accelerated Bridge Construction (ABC) – Substructure: Grout." ⟨http://sri.cce.iastate.edu/ABC-Guidelines/Grout%20New.html⟩ (Sep. 30, 2017)

Utah Department of Transportation (UDOT) (2017). *Structural Design and Detail Manual, UDOT SDDM*, Taylorsville, UT.

CHAPTER 4. AN OUTDOOR TEST OF A PREFABRICATED COLUMN-PILE CAP-PILE SYSTEM UNDER COMBINED VERTICAL AND LATERAL LOADS

A paper prepared for the ASCE Journal of Structural Engineering

Zhao Cheng, S.M.ASCE[1] and Sri Sritharan, Ph.D., M.ASCE[2]

[1]Graduate Research Assistant, Dept. of Civil, Construction, and Environmental Engineering, Iowa State Univ., Ames, IA 50011. E-mail: zcheng@iastate.edu

[2]Wilkinson Chair of Interdisciplinary Engineering, Dept. of Civil, Construction, and Environmental Engineering, Iowa State Univ., Ames, IA 50011 (corresponding author). E-mail: sri@iastate.edu

Abstract

An outdoor test was conducted on a prefabricated column-pile cap-pile system at a cohesive soil site. The half-scale test unit consisted of a precast column, a precast pile cap, and eight steel piles. The components were connected utilizing socket and pocket connections that were preformed in the pile cap with corrugated steel pipes. To evaluate the system performance and the behavior of various connections, the test unit was subjected to combined vertical and lateral loads at the operating conditions as well as at conditions representing extreme events. The test unit remained undamaged under the loads representing the operating conditions, and a plastic hinge was formed in the column under loading condition representing a seismic event. The socket and pocket connections exhibited excellent behavior as they maintained fixity with the formation of a column plastic hinge. The outdoor test demonstrated that up to 40% column top displacement was produced by foundation flexibility at the operating conditions. The description of the outdoor test and key results are included in this paper.

Keywords: Column; Pile cap; Pile; Socket connection; Pocket connection; Soil-Foundation-Structure Interaction (SFSI); Outdoor testing.

Introduction

Prefabricated components for bridges and other structures have several advantages over conventional cast-in-place components as they can be used to repair and build structures faster and better. The use of prefabricated components reduces mobility impacts, enhances work-zone safety, improves construction quality and durability, and minimizes environmental impacts (Culmo 2011). Due to their advantages, prefabricated components have been continuously gaining momentum in construction of bridge columns (ABC-UTC 2018). However, there are few, if any, projects that have utilized prefabricated components to construct the entire column-pile cap-pile systems. An important concern for prefabricated column-pile cap-pile system is the lack of efficient and easily deployable connections between the key prefabricated components. Piles are normally capped with a concrete cap to support a column. If a full prefabricated column-pile cap-pile system is desired, the connection between column and pile cap as well as the connections between pile cap and piles must be able to transfer loads under regular operating conditions dependably and preferably remain elastic when the structure is subjected to extreme events including earthquakes. The seismic design takes advantage of deliberate formation of plastic hinges in preselected locations and protect all the other regions against damage by maintaining elastic response. For typical bridge column-pile cap-pile systems, practices seek to design plastic hinges at the column ends. Therefore, the column connection and pile connections to the pile cap need to sustain high design forces resulting from the formation of column plastic hinges, making their designs more challenging.

Several methods have the potential to establish connections for prefabricated column-pile cap-pile systems. They include: 1) splicing of reinforcements of adjoining prefabricated elements using mechanical couplers (Ameli and Pantelides 2017; Haber et al. 2014); 2)

grouted ducts to embed individual reinforcement extending from one component to another (Restrepo et al. 2011); 3) preformed pockets for embedding a group of reinforcements or the end of a prefabricated member with a large volume closure pour (Restrepo et al. 2011); 4) preformed sockets for embedding the end of members with a small volume closure pour; 5) casting a concrete member surrounding the prefabricated member (Haraldsson et al. 2013), and 6) post-tensioning (Culmo 2009; Marsh et al. 2011). Among these connection types, the socket and pocket connections offer numerous advantages including compatibility with prefabricated components, ample installation tolerance, and simplified construction procedure, making these two types of connections more desirable for field implementations.

The feasibility of using socket connections for prefabricated columns has been investigated in the past. Motaref et al. (2011) and Kavianipour et al. (2013) tested socket connections between precast columns and precast footings. The octagonal shaped sockets were performed in the precast footings and then filled with high strength grout. The column embedment length was 1.5 times column diameter in both studies. The tests showed successful development of column plastic hinges with column axial load ratio of 6.3% and 8.8%, respectively. Mehrsoroush and Saiidi (2016) used corrugated steel pipe (CSP) to create sockets. This study, which applied a maximum axial load ratio of 5.6%, showed that a column embedment length of 1.2 times column diameter was adequate to form plastic hinges in the column. Mohebbi et al. (2017) tested a socket connection for a square column with an axial load ratio of 14.4%. Results revealed that the column embedment length equal to the column side dimension was sufficient to develop the column plastic moment. Cheng and Sritharan (2019) evaluated the side shear strength of socket connections under uniaxial loads. Test results showed that side shear mechanism can provide significant resistance, facilitating

high axial loads to be sustained. The study also provided design limits for side shear stress in socket connections.

The performed pocket connections for steel H-piles were tested under axial load, and the results indicated that the axial strength of the pocket connection was at least as good as that of a comparable cast-in-place connection (Wipf et al. 2009). Shama et al. (2002) evaluated the behavior of a pile-to-cap connection with the pile embedment length of 2.8 times pile depth. In this study, the connection remained essentially undamaged when the combined axial and lateral loads caused fail in the piles. Xiao et al. (2006) demonstrated that, using shallow embedment length of 0.36 times pile depth, the pile-to-cap connection can sustain a significant amount of moment, while localized brittle failure was observed in the connection.

Conceptual Design of a Precast Pile Cap

Addressing the challenges of constructing a prefabricated column-pile cap-pile system, a precast pile cap with preformed column socket and pile pockets (Figure 4.1a) was developed. By embedding a precast column and steel piles into a socket and pockets, respectively, with the use of closure pours, the construction of the column-pile cap-pile system can be completed in a shortened period. The socket and pockets can be accomplished using commercially available CSP due to its low cost and ready availability in different sizes. In addition to serving as stay-in-place formwork, CSP offers confinement effects to the connection material while its corrugations provide a robust load transfer mechanism (UDOT 2017). The column socket is intended to penetrate the pile cap partially for multiple reasons. First, this allows the precast column to be supported on the bottom of the pile cap during assembly. Second, the bottom mat reinforcement of the pile cap can be continuous below the column, which also helps minimizing punching failure of the column through the soffit of the

pile cap. Third, the bottom of the socket connection does not need to be sealed during the closure pour. Finally, given the stress limits suggested by Cheng and Sritharan (2019), the partially penetration is sufficient to transfer column axial force through the side shear mechanism and without increasing the depth of the pile cap, eliminating any significant increase in the weight or cost of the pile cap.

The pile pocket is envisioned to fully penetrate through the pile cap to facilitate closure pours from the top of the pile cap. The upper portion of the pocket is made in the shape of a cone, which ensures satisfactory distribution and quantity of the top pile cap mat reinforcement. A straight CSP option was also considered for the pile pocket, which required cutting of numerous notches to place all the top mat reinforcement, and thus this option was not pursued.

As illustrated in Figure 4.1b, to assemble the column-pile cap-pile system, the following steps are planned: 1) drive steel piles into the ground by employing a template to maintain the piles at the appropriate location; 2) install the friction collars to the piles and place sealing pads made from plywood on top of the friction collars to close the bottom opening of the pile pockets; 3) support the precast pile cap on the friction collars, allowing the piles to be extended into the pile pockets; 4) erect and brace the precast column into the column socket; and 5) fill the column socket and pile pockets with grout and self-consolidating concrete (SCC), respectively. Instead of directly positioning the pile cap on the ground, the use of friction collars allows quick assembly of the system in in all types of ground conditions. Friction collars are designed to carry the weights of pile cap, column, and upper structural components before SCC reaches an adequate strength. Therefore, construction can continue on the day after completing the closure pours, at which point high

early-strength grout would reach the specified compressive strength of 44.8 MPa (6500 psi). After SCC reaches its specified short-term strength (e.g., at the age of 7 days), the friction collars can be removed.

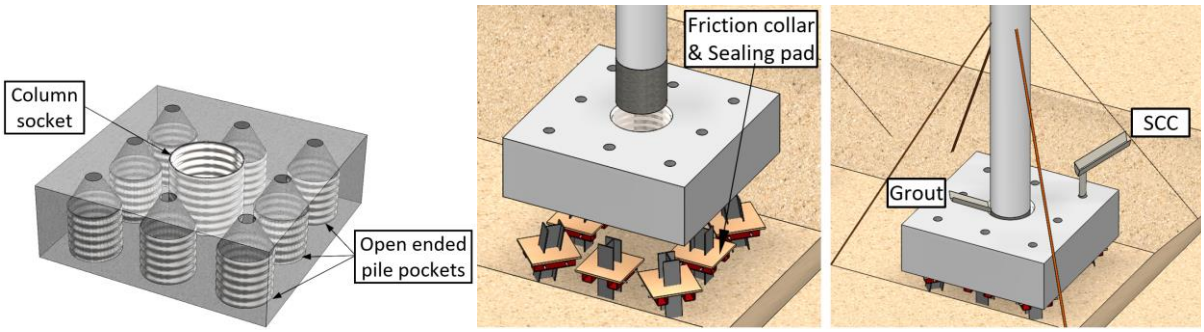

Figure 4.1 *Prefabricated column-pile cap-pile system: (a) precast pile cap and (b) construction process*

Test Plan

An experimental test plan was formulated to investigate the performance of the proposed prefabricated column-pile cap-pile system. The prototype was designed using a recently built, three-span pretensioned prestressed concrete beam bridge in Iowa, with a 27-m (87-ft) midspan and 14-m (46-ft) end span. The pier of the prototype bridge consisted of two precast concrete columns, and eight steel H-piles capped with a precast pile cap supports each column. For the columns, the longitudinal reinforcement ratio was 1.7%, and the transverse reinforcement was designed following the approach of Priestley et al. (1996) to fully develop the column flexural capacity. Battered piles were used at the corners of the pile cap in conjunction with four straight piles. Using this prototype structure, a half-scale column-pile cap-pile system with a single column was planned for the outdoor test.

Site Conditions

The outdoor test was conducted at a cohesive soil site close to the campus of Iowa State University. Subsurface exploration was performed using a cone penetration test (CPT) to the depth of 15 m (50 ft) below the ground, which indicated that soil at the test site mainly consists of stiff clay with a 1.5-m (5-ft) thick sand layer at the depth of 10 m (33 ft). The CPT data obtained at the test site is comparable to that reported in Sritharan et al. (2007). The average tip resistances in the 0-m (0-ft) to 9.3-m (30.5-ft), 9.3-m (30.5-ft) to 10.8-m (35.5-ft), and 10.8-m (35.5-ft) to 15 m (50 ft) depth ranges were 2.4 MPa (25 tsf), 12.5 MPa (130 tsf), and 4.8 MPa (50 tsf), respectively. The water table was at approximately 2.3 m (7.5 ft) below the ground surface at the time of testing.

Details of Test Unit

As noted, the test unit incorporated a column, a pile cap, and eight steel H-piles. The column diameter was scaled to 0.46 m (1.5 ft), and the height of the column was chosen to be 1.83 m (6 ft), resulting in a flexure-critical column with a height-to-depth ratio of 4. The column embedment length was chosen to be equal to the column diameter in the light of the recommendations from previous studies. Under a column axial load ratio of 25%, the side shear stress corresponding to this embedment length would be 1.7 MPa (246 psi), which was significantly lower than the limits proposed by Cheng and Sritharan (2019). Combining with the embedded portion, the total column length was 2.29 m (7.5 ft). According to Cheng and Sritharan (2019), 0.46-m (1.5-ft) length of the column at the end, which was designed to be embedded into the socket, was intentionally roughened. As shown in Figure 4.2a, the column was reinforced with fourteen #16M (#5) longitudinal reinforcing bars and a continuous #10M (#3) reinforcing spiral at a spacing of 76 mm (3 in.), resulting in identical reinforcement ratios to these of the prototype. For applying the vertical and lateral loads, a 1 m (3.5 ft) by 1

m (3.5 ft) by 0.61 m (2 ft) loading block was added to the top of the column. Figure 4.2b shows the pile layout used for the test unit, in which the four corner piles were battered at a 1 horizontal to 6 vertical slope as in the case of the prototype structure. The piles for the test unit were scaled to be U.S. W 6 × 20 beams, and the length of the piles were determined to be 15 m (50 ft) based on the unit friction of 23.4 kN/m (1.6 kip/ft) for firm silty glacial clay and a geotechnical resistance factor of 0.6. The dimensions of the pile cap were 1.83 m (6 ft) by 1.83 m (6 ft) in plan and 0.61 m (2 ft) in depth. The bottom and top reinforcement mats in the pile cap consisted of fourteen and twelve continuous #13M (#4) reinforcing bars in both directions, and the vertical reinforcements were #10M (#3) fully lapped stirrups with 180° hooks at both ends. As shown in Figure 4.2b, a partially penetrated socket and eight fully penetrated pockets were designed for the pile cap. The depth of the column socket was 483 mm (19 in.) to incorporate the 457-mm (18-in.) column embedment length. Following the routine design practices (Iowa DOT, 2018) and previous studies, the pile embedment length of 229 mm (9 in.) was selected, corresponding to 1.5 times the depth of pile. CSPs with a thickness of 1.29 mm (i.e., 16 gauge) for creating column socket and pile pockets met the requirements of AASHTO M 218 (2016). The nominal inside diameter of the column socket CSP was selected to be 553 mm (21 in.), which was the smallest commercially available size fitting the 457-mm (18-in.) diameter column. The 457-mm (18-in.) diameter CSPs were used for pile pockets from considerations of construction tolerances and geometry of the battered piles.

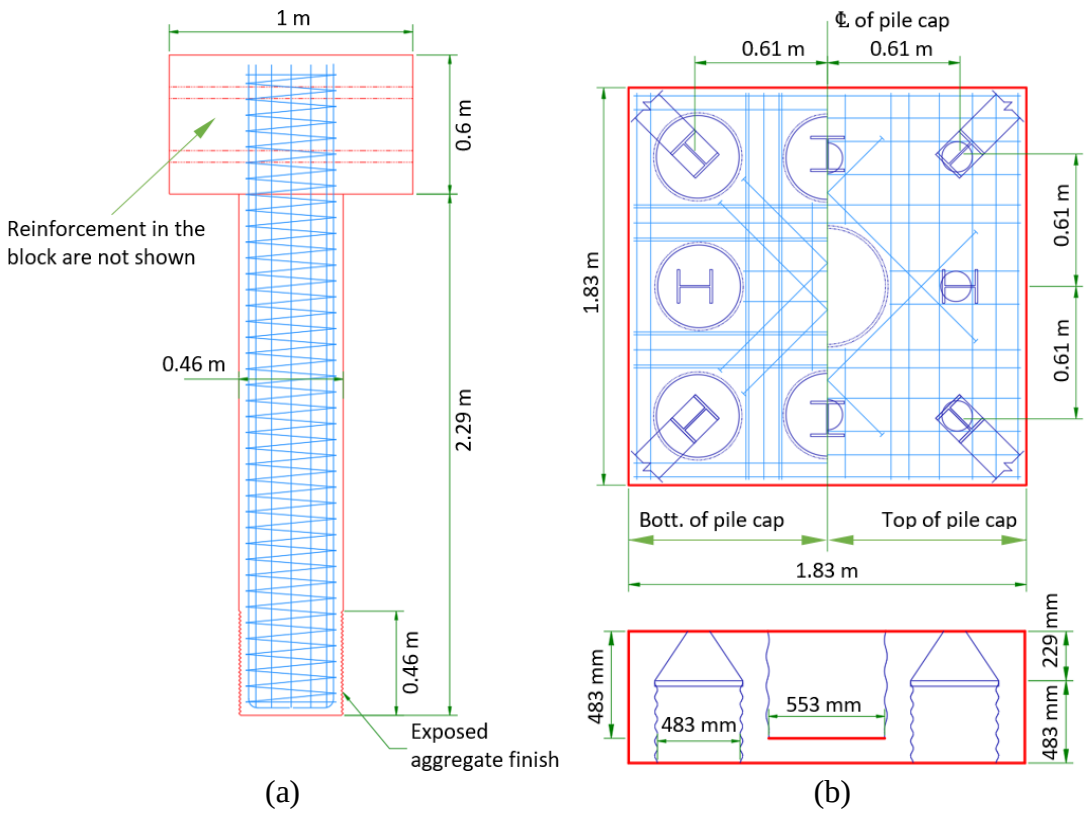

Figure 4.2 *Test unit details: (a) column and (b) pile cap*

Construction

The column and the pile cap were prefabricated at the Structural Engineering Research Laboratory of Iowa State University, transported to the field site, and connected to the driven piles. To achieve the desired surface roughness on the end portion of the column (Figure 4.3a), Altus Series In-Form retarder was applied on the formwork interior surface, followed by power-washing the laitance after hardening of the concrete mass at the age of 3 days. When constructing the pile cap, the pipe diameter reducers were used to create the cone-shaped upper portions of the pile pockets. As seen in Figure 4.3b, the CSP for creating the column socket was suspended from a crossing beam that was clasped to the formwork, and its bottom end was temporarily closed by a round plywood board. The crossing beam and the plywood were removed after the concrete set.

To ensure that the piles were driven at the right location, a template was secured to the ground. Because piles with high slenderness ratio may buckle during driving, each 15-m (50-ft) long pile was made from two 9-m (30-ft) long segments. After the first 9-m (30-ft) pile segments were driven into the ground, the second 9-m (30-ft) top segments were spliced by full penetration groove welds and subsequent driving of piles. Once the designed pile penetration depth was reached, the extra length was cut, such that tip of all piles were at the same horizontal plane. As seen in Figure 4.3c, the friction collars were then attached to the piles. The height of the friction collars were adjusted such that the pile cap would be positioned at 0.3 m (1 ft) above the ground. The gap between the pile cap and ground was to eliminate the passive earth pressure acting on the pile cap and to provide access to the bottom of the pile cap for test observation and instrumentation purposes. The plywood pads with rubber foam strips attached around their perimeters were placed on the friction collars in order to seal the bottom opening of the pile pockets. After positioning the pile cap on the friction collars and erecting the column into the socket, grout and SCC were poured on the same day to secure the column socket and the pile pockets, respectively. To establish a strong and durable connection, grout with the following properties was chosen to fill the column socket: high-strength, non-shrink, fluid consistency, extended working time, and high-early-strength. The grout gained compressive strength of 60.9 MPa (8834 psi) in 24 hours and SCC achieved 31.8-MPa (4613-psi) compressive strength at the age of 7 days, at the point the friction collars and the plywood pads were removed from the test unit. The completed test unit is shown in Figure 4.3d.

(a)

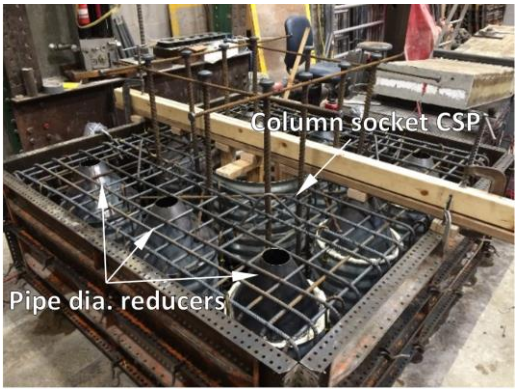

(b)

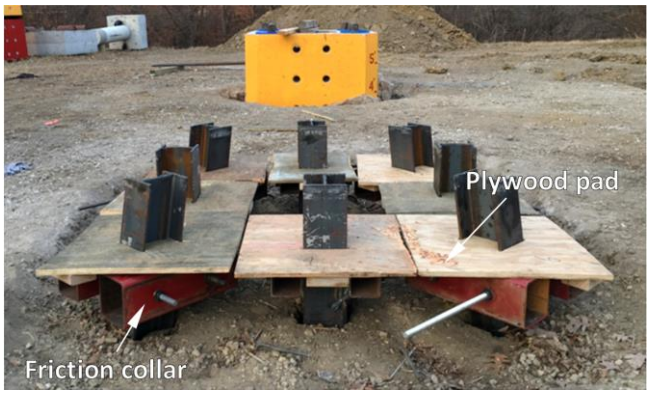

(c)

(d)

Figure 4.3 *Test unit construction: (a) roughened surface of column end, (b) pile cap prior to concrete pour, (c) driven piles, and (d) completed test unit*

Material Properties

The strength of concrete and grout on the day of testing were obtained from uniaxial compression tests on standard 102 mm (4 in.) by 204 mm (8 in.) cylinders and 50-mm (2-in.) cube specimens, respectively. The properties of the reinforcement were established from uniaxial tension tests for each reinforcement type. Table 4.1 lists the material properties of the test unit components, which also include the pile steel properties reported in the mail certificate.

Table 4.1 *Test unit material properties*

Component	Compressive strength (MPa)	Yield strength (MPa)	Tensile strength (MPa)
Column[a]	31.2	N.A.	N.A.
Pile cap[a]	39.9	N.A.	N.A.
SCC for filling the pile pockets[a]	48.7	N.A.	N.A.
Grout for filling the column socket[b]	66.1	N.A.	N.A.
Reinforcing spiral[c]	N.A.	468.8	682.6
Reinforcing bar[c]	N.A.	437.8	690.9
Pile[d]	N.A.	369.5	498.5

[a]Tested as per ASTM C39-18 (2018)

[b]Tested as per ASTM C109-16a (2016)

[c]Tested as per ASTM A370-14 (2014)

[d]Tested as per ASTM A709-15 (2015)

Test Setup and Instrumentation

A reaction frame and a reaction column, as shown in Figure 4.4, were constructed at the test site for applying the vertical and lateral loads to the test unit, respectively. The reaction frame was composed of four U.S. HP 14 × 73 anchor piles driven to 15 m (50 ft) into the ground, a main reaction beam, four hollow hydraulic cylinders powered by an electric pump, and miscellaneous attachments. The hydraulic cylinders pushed the main reaction beam down as they were pressured, thereby generating gravity effects on the column while subjecting the anchor piles to tension. A friction pendulum bearing was installed between the top of the column loading block and the main reaction beam. This bearing was used to transfer the vertical loads from the main reaction beam to the column with minimal friction against lateral load, while allowing translation and rotation of the column. The lateral reaction column was composed of five precast column segments and a 1.8-m (6-ft) diameter, 12-m (40-ft) deep drilled shaft foundation, which were connected together through four post-tensioned rods anchored into the drilled shaft. A double-acting hydraulic actuator controlled

by an electric servo pump was attached between the column loading block and the reaction column. This actuator was used to apply lateral loads to the top of the column.

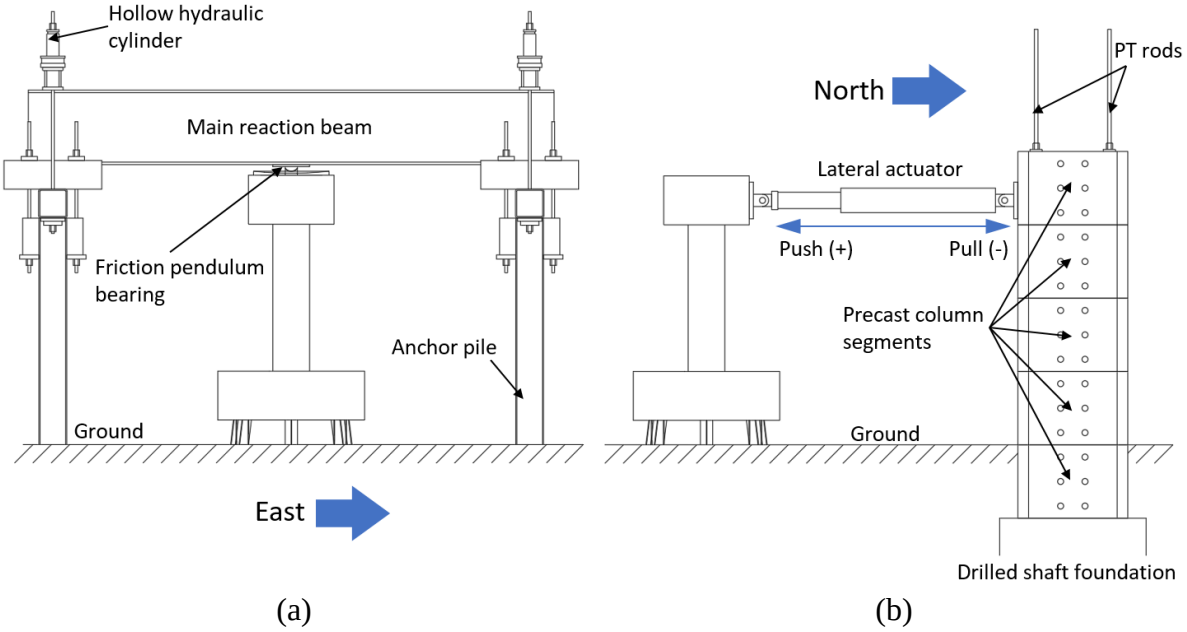

Figure 4.4 *Test setup: (a) vertical reaction frame, and (b) lateral reaction column*

Load Protocol

The outdoor test of the column-pile cap-pile system consisted of two phases. Each phase applied a combination of vertical and lateral load as shown in Figure 4.5. A load combination representing the design loads at the regular operating conditions was applied in Phase I. In this phase, after the application of the cyclic vertical loads, the reversed cyclic lateral loads were applied to the top of the column while the vertical load was maintained. The target vertical load corresponded to a column axial load ratio of 0.25, and the target lateral load was equal to 5% of the targeted vertical load. The target values for both vertical and lateral loads were achieved in five steps with three cycles at each loading step. Phase II test was conducted with a reduced column axial load ratio of 0.1, but evaluated the ability to develop the full flexural capacity with the designed connections. Following the vertical load application, the lateral load that was expected to cause yielding of the column longitudinal

reinforcement was achieved in four steps with three cycles at each load step. Subsequently, the test unit was subjected to a reversed cyclic lateral displacement history. The peak of each step was controlled by the measured displacement at the location where the lateral load was applied, and the displacement was increased in steps such that the displacement ductilities of 1, 1.5, 2, 3, 4, and 6 could be achieved with the lateral displacement of 31.75 mm (1.25 in.) corresponding ductility 1.

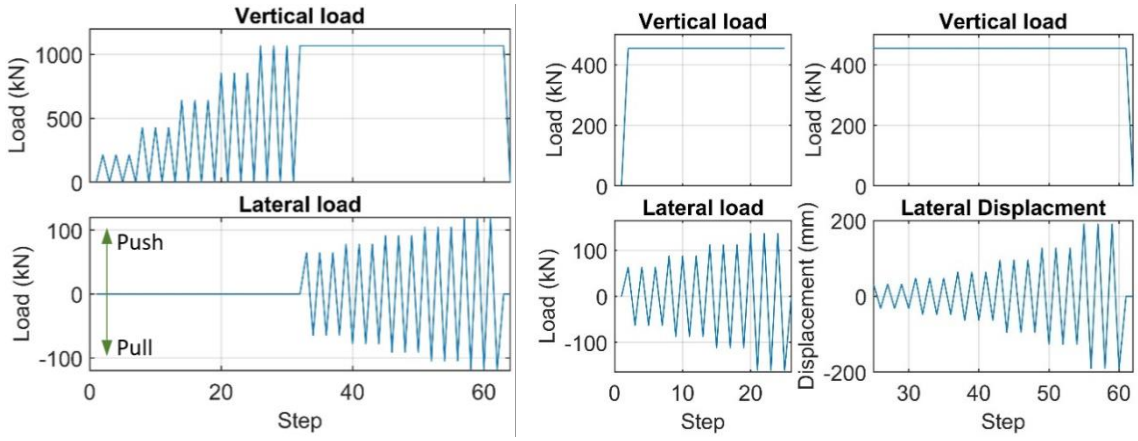

Figure 4.5 *Test protocol for (a) Phase I and (b) Phase II*

Test Outcomes

Observations

After applying the vertical and lateral loads in Phase I, no cracking or any other damage was observed on column, pile cap, piles, or their connections. Response of the test unit during Phase II was also excellent with an eventual formation of a plastic hinge at the base of the column as intended, while the pile cap, piles, and connections remained essentially elastic and undamaged. Flexural cracks began to develop at the column base when the applied lateral load reached 112 kN (25.2 kips). Cracking continued to develop over the lower 914 mm (36 in.) of the column as testing progressed and the column lateral displacement was progressively increased. When the column lateral displacement at the

height of the lateral actuator, hereafter referred to as the column top lateral displacement, reached 48 mm (1.875 in.), the concrete covers on the base of the column began to crushed and spall. The extent of spalling increased during loading cycles of ±63.5 mm (±2.5 in.), and the longitudinal reinforcements and reinforcing spiral in the column were exposed during loading cycles of ±95 mm (±3.75 in.), as shown in Figure 4.6a. During loading cycles to ±127 mm (±5 in.), column concrete damage extended to the core concrete, and a longitudinal reinforcement buckled between two adjacent spirals near the base. When the column was pushed to 191-mm (7.5-in.) lateral displacement, the longitudinal reinforcement that buckled in the previous load step fractured in tension. As the column was subjected to cyclic displacement of ±191 mm (±7.5 in.), multiple column longitudinal reinforcements fractured, and a significant portion of the core concrete was crushed. The condition of the column base at the end of Phase II after removal of loose concrete is shown in Figure 4.6b. A cracking appeared in the column connection at the grout-to-CSP interface during loading cycles to ± 32 mm (±1.25 in.). During subsequent large displacement cycles in Phase II, the top 19-mm (0.75-in.) layer of the grout experienced crushing (Figure 4.6c), but the connection maintained its integrity and continued to sustain the vertical and lateral load applied to the column.

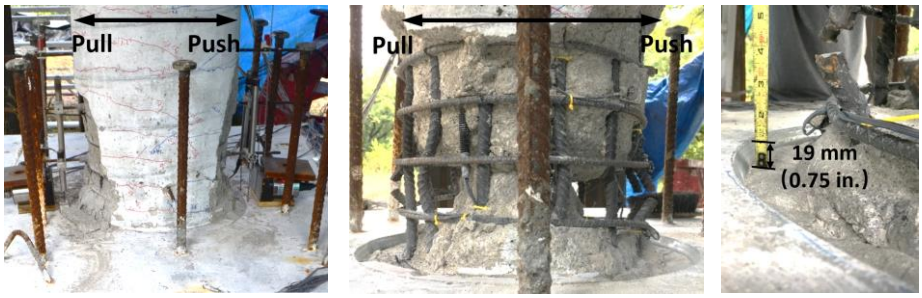

(a) (b) (c)

Figure 4.6 *Test Observations: (a) damage in column, (b) column base at the end of Phase II, and (c) grout spalling*

System Response

Figure 4.7 presents the measured vertical load as a function of the column top lateral displacement with respect to the pile cap. Due to the concave shape of the pendulum bearing base, the vertical load increased as the column was laterally displaced with respect to the main reaction beam. To avoid overloading the test unit during Phase II, the vertical load was intentionally adjusted twice when the column top displacement reached -64 mm (2.5 in.) and -95 mm (3.75 in.). The presence of vertical load caused some lateral resistance at the top of the column due to friction in the pendulum bearing. Therefore, the lateral load transferred to the column, which will be referred as the column lateral resistance, was not equal to the load applied by the actuator and had to be determined by other means as detailed below.

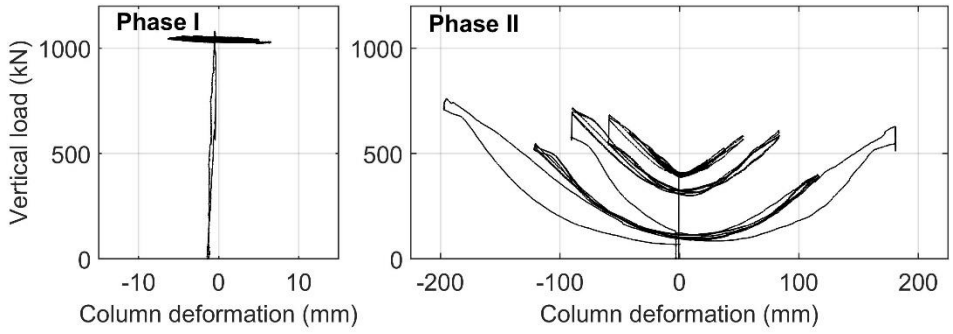

Figure 4.7 *Vertical load versus column top lateral displacement*

The moment of an uncracked column section located at 1.22 m (48 in.) above the column base (i.e., the reference section) was estimated using the theoretical moment-curvature relationships obtained for different axial forces and as-built column section properties. Given the curvature at the reference section that was obtained from the strains measured in the two extreme column longitudinal reinforcements, the moment at the reference section was estimated from the moment-curvature verses axial force plot shown in Figure 4.8. Note that the column did not experience any cracking at this level and that the

moment estimated at the reference section included the component resulting from the *P-Δ* effect. Therefore, as illustrated by Figure 4.8, the column lateral resistance was calculated as follows:

$$F = \frac{M - P\Delta_1}{h_1} \qquad \text{Equation 4-1}$$

where F = column lateral resistance; M = moment estimated at the reference section; P = vertical load; Δ_1 and Δ_2 = eccentricities of the vertical load measured at the reference section and the column base; h_1 and h_2 = distances from where the lateral load was applied to the reference section and the column base.

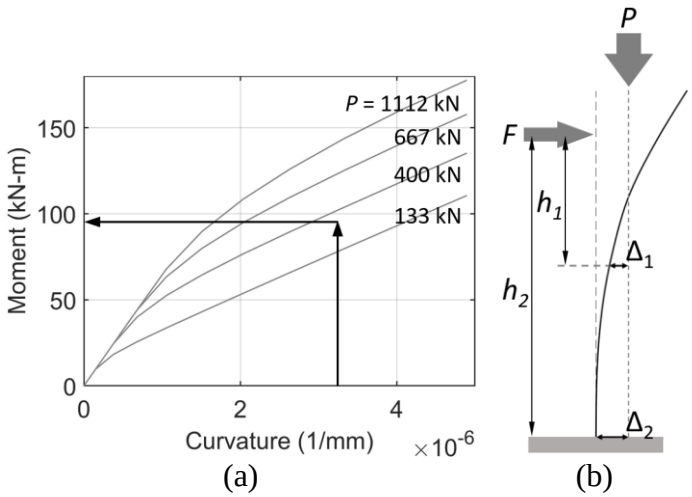

Figure 4.8 *(a) Calculation of moment at the reference section and (b) calculation of column lateral resistance*

Figure 4.9 presents the moment component at the column base resulting from the estimated column lateral resistance (Fh_2) and the component resulting from the vertical load ($P\Delta_2$), representing the column lateral response. The theoretical moment-deformation responses for the column subjected to 1068-kN (240-kips) and 556-kN (125-kips) axial forces were calculated as per Priestley et al. (1996), which are also included in Figure 4.9 for Phase I and Phase II testing, respectively. The good agreement between the calculated and

theoretical responses confirmed the sufficient accuracy of the estimated lateral load resisted by the column. The column remained elastic during Phase I testing, but experienced stable nonlinear response with dependable hysteresis loops during Phase II testing. The response remained essentially elastic up to the column lateral deformation of up to ±25 mm (±0.98 in.), beyond which inelastic behavior dominated the response with a slight positive slope. The maximum moments reached in the push and pull directions were 282 kN-m (2496 k-in.) and -275 kN-m (2434 k-in.), which were estimated at the column displacement of 84 mm (3.31 in.) and -58 mm (-2.30 in.), respectively. The first drop of the column base moment occurred when the column displacement reached 116 mm (4.57 in.) due to the damage that occurred to the core concrete and buckling of a longitudinal reinforcement. As the column was displaced to 181 mm (7.13 in.) in the push direction, one column longitudinal reinforcement fractured in the plastic hinge region, causing a further drop in moment resistance. As more reinforcements fractured when the column was pulled to the deformation of -191 mm (-7.5 in.), significant strength degradation occurred.

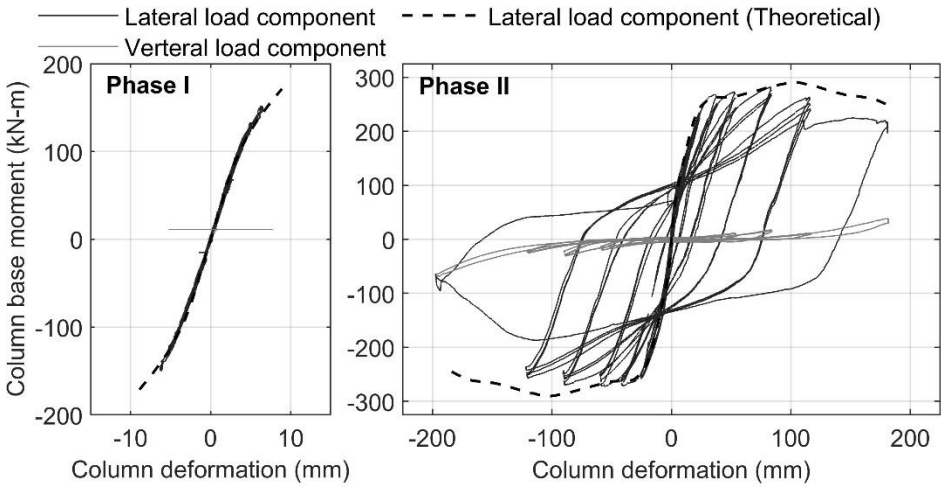

Figure 4.9 *Column base moments versus column lateral displacement*

To illustrate the foundation flexibility, Figure 4.10 shows the column lateral load versus the pile cap lateral displacement response, which indicated essentially elastic response in both phases of testing. The maximum displacements that the pile cap reached in the push and pull directions were 4.3 mm (0.17 in.) and -4.8 mm (-0.19 in.), respectively. The response exhibited some nonlinearity during Phase II due to the formation of permanent gaps between the piles and surrounding soil.

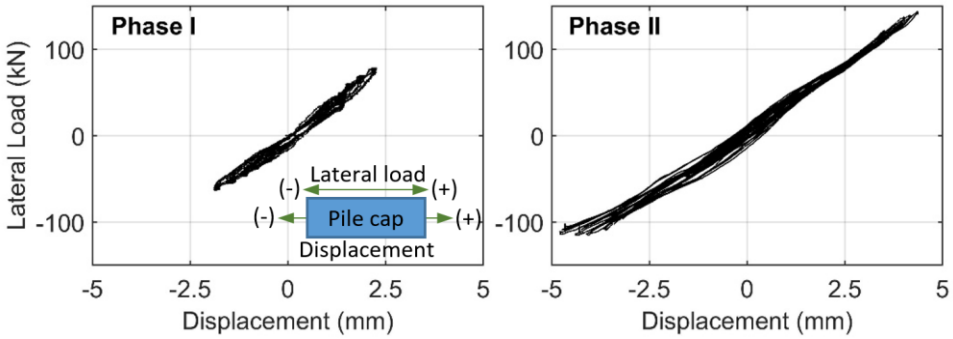

Figure 4.10 *Column lateral load-pile cap displacement response*

Connection Performance

The strains along the two extreme column longitudinal reinforcements (i.e., Rebar 1 on the south side and Rebar 4 on the north side) were instrumented with strain gauges. Figure 4.11a and Figure 4.11b present the strain profiles obtained for these two bars for the push (positive load) and pull cycles (negative load) during Phase I and Phase II testing. Some of the gauges became malfunctioned during Phase II. In Phase I, the recorded strains were less than 45% of the yielding stain, conforming the elastic column response. Within the connection, the strain penetration was seen, but the magnitude of strains abruptly decreased to a fraction of that at the top of the pile cap. The reading became negligible within the lower 152-mm (6-in.) region of the embedded column end. During Phase II testing, the tensile strains in the column reinforcements significantly increased compared to those in Phase I, as

the column lateral loads increased and the vertical load decreased. Prior to the column lateral loads reaching 81 kN (18.1 kips) and 58 kN (13.1 kips) in the push and pull directions, the strains along the reinforcements remained approximately linear with the magnitudes remaining below the yielding value. As the load increased, the extreme column longitudinal reinforcing bars experienced yielding over the 610-mm (24-in.) region above the top of the pile cap, with the largest strain being recorded near the column to pile cap interface. Reinforcement yielding also penetrated up to 152 mm (6 in.) into the connection, but the strains within the connection decreased abruptly. Down from 305 mm (12 in.) below the top of the pile cap, the strains maintained below 50% of the yield strain.

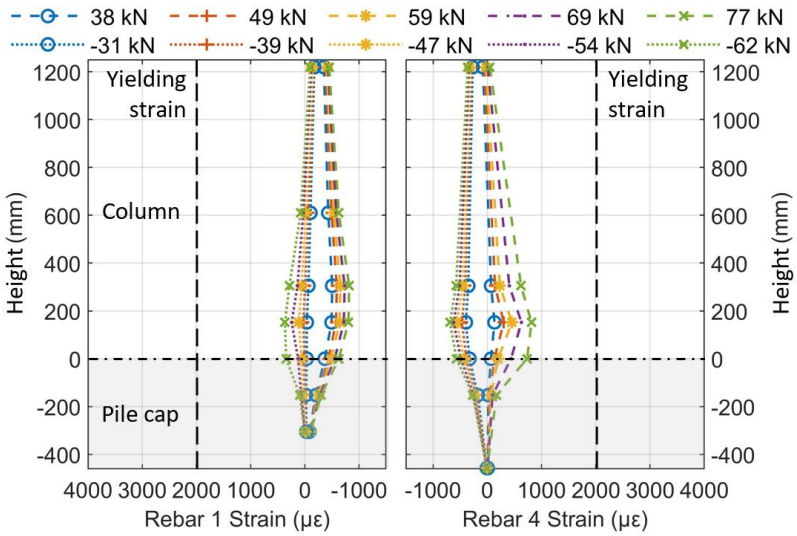

(a)

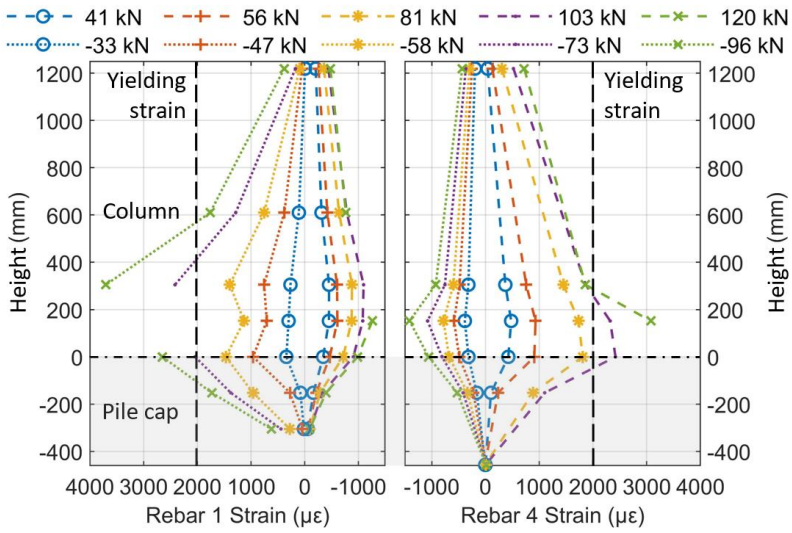

(b)

Figure 4.11 *Strain profiles along two extreme column longitudinal reinforcements for (a) Phase I and (b) Phase II*

The strain profiles at the north sides of the CSP that created the column socket are shown in Figure 4.12. With the largest reading of 170 με, the strains in the CSP remained far below its specified yielding strain of 1138 με for the duration of Phase I and Phase II. The strains on the north side of the CSP consistently varied with the application of the lateral loads. Generally, the gauges captured compressive strains for the push cycles and tensile strains for the pull cycles. Few exceptions occurred when relatively large pull loads (e.g., 73-kN and 96-kN loads in Phase II) were applied.

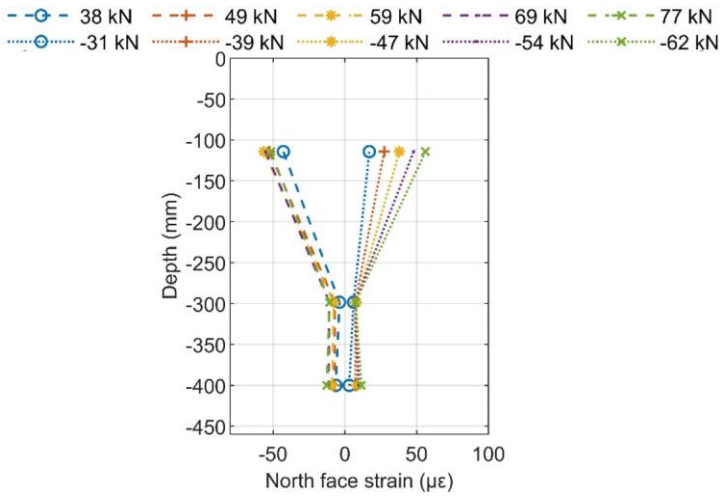

(a)

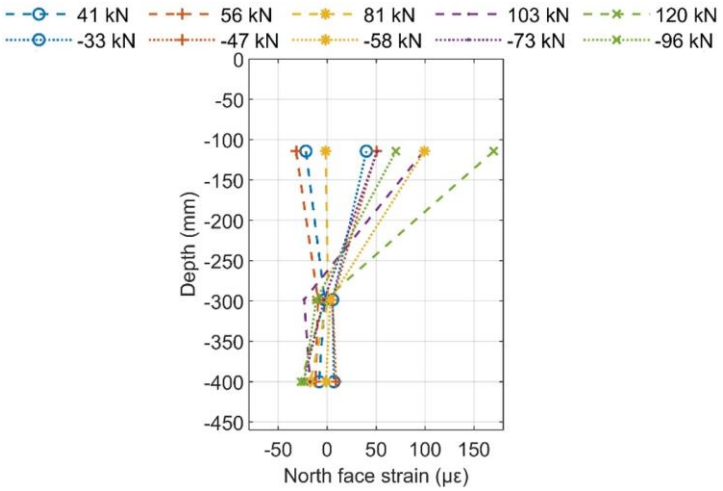

(b)

Figure 4.12 *Strain profiles of column socket CSP for (a) Phase I and (b) Phase II*

For the duration of Phase I and Phase II, the measured pile penetrations and rotations with respect to the pile cap were negligible. Figure 4.13a and Figure 4.13b present the profiles of the strains along the embedded ends of the southwest pile, west pile, and south pile in Phase I and Phase II, respectively, in which the strains at the pile tops were taken as zero. During Phase I and Phase II, the measured strains did not exceed 18% of the yielding value. In Phase I, piles remained in compression, indicating that the gravity load effects were still predominate. The tensile strains were recorded on the southwest and south piles in Phase II. The magnitude of

the strains varied depending on the magnitude of the lateral load. As the lateral load produced more effect on the extreme piles, the strain variations for the southwest and south piles were greater than that of the west pile. The strains of the two piles at mid-depth of the embedded portion were approximately half of those at the pile cap bottom regardless of the magnitude of the lateral loads, resulting in the roughly linear strain profiles. The strains of the CSPs that created the pockets for connecting the southwest, south, and west piles were also monitored, but the measured values were negligible for the duration of Phase I and Phase II.

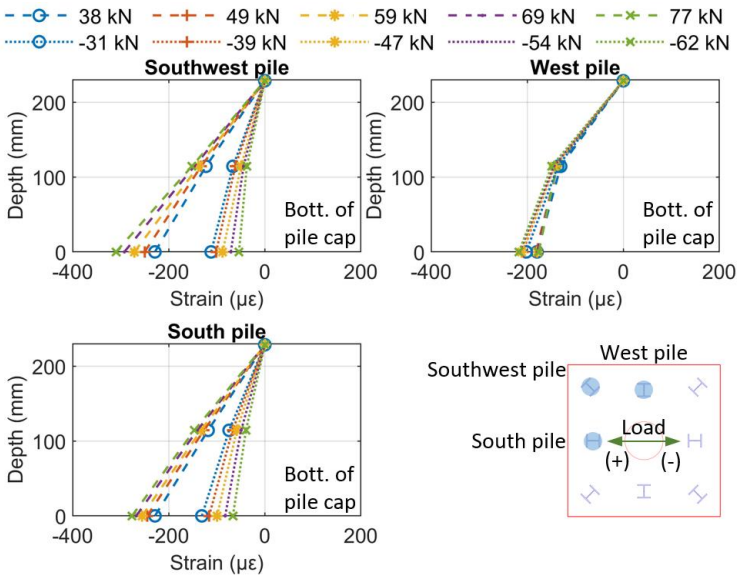

(a)

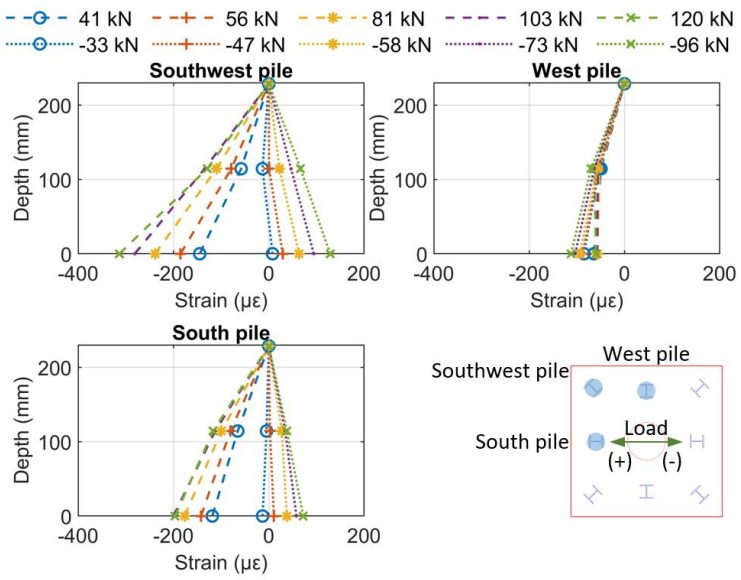

(b)

Figure 4.13 *Strain profiles of embedded piles for (a) Phase I and (b) Phase II*

Discussion

Column Socket Connection and Pile Pocket Connections

Visual observations indicated that, except slight spalling of the grout closure pour in the column socket toward the end of Phase II test, the connections remained mostly damage-free when the column flexural capacity was fully developed. The strain profiles below the top of the pile cap reflect the force transfer in the connection. In Phase I, as a high axial load acted in the column, the strain profiles above the pile cap top shifted to the compressive side, whereas the shifting abruptly decreased within the connection. Additionally, the strains became negligible in the bottom third of the connection regardless of the application of the lateral loads. This phenomenon demonstrated that the socket connection transferred the axial compressive force over a short length, as evidenced by Cheng and Sritharan (2019). Even with small lateral load applied in Phase I test, the force transfer took place mostly in the top two thirds of the connection. The shifting of the strain profiles was barely visible in Phase II because the applied vertical load dropped to the 40% of that in Phase I. When the applied

lateral load developed the column plastic capacity, the strains measured at where right below the top of the pile cap exceeded the yielding value, but abruptly decreased and were negligible at the end of the column, suggesting that the embedment length of the socket connection sufficiently transferred the combined axial force and moment. The force transfer capacity of the socket connection was also demonstrated by the measured behavior of the column CSP (Figure 4.12). The strain profiles suggested that the force transfer took place mostly in the top two thirds of the connection, as the strains in the bottom third of the column CSP were negligible. Given the captured force transfer behavior and the low magnitude of the strain in the column CSP, the embedment length equal to one times the column diameter was required for the column socket connection subjected to combined axial and lateral forces, but the thickness of the CSP could likely be reduced without compromising the connection performance.

No damage was observed in the pile pocket connections, proving the connection fixity. The force transfer capacity of the pocket connection was reflected by the approximately linear strain profiles along the embedded ends of the piles (Figure 4.13). By embedding the piles 229 mm (9 in.) (i.e., 1.5 times the pile section depth) into the pockets, the connections transferred pile compressive and tensile forces to the pile cap, evidencing the sufficiency of the pile embedment length.

Foundation Flexibility

For the column-pile cap-pile system, it is important to recognize the foundation flexibility, which can be quantified using the measured pile cap response. The lateral load-translation response shown in Figure 4.10 demonstrate that, as the design required, the foundation remained linearly elastic and damage-free when the column flexural capacity was fully developed at the end of Phase II. The effect of foundation flexibility on the system

response was examined in terms of column top lateral displacement. As illustrated in Figure 4.14a, the lateral displacement at the top of the column consisted of three distinctive components, namely the column deformation with respect to the pile cap and those due to pile cap lateral translation and pile cap rotation. Figure 4.14b presents the proportions of each component to the column top displacement for different lateral loads in Phase I and Phase II. In Phase I, about 40% of column top displacement was induced by the foundation flexibility, and this proportion remained approximately constant regardless of the magnitude of lateral load. Furthermore, the components due to pile cap translation and rotation were approximately the same. As the lateral load increased in Phase II with the plastic capacity of the column was developed, the contribution of the pile cap became small due to the foundation response remaining essentially elastic. The combined proportion of the pile cap translation and rotation components was 10% of the column top lateral displacement when the effective lateral load reached its maximum value of 139 kN (32.3 kips). Given the notable contribution of the pile cap translation and rotation towards the column top lateral displacement, it is important to account for the foundation flexibility when estimating the column yield and ultimate displacement. Note that the test was conducted in stiff clay and therefore larger contribution from foundation flexibility should be expected in softer soils.

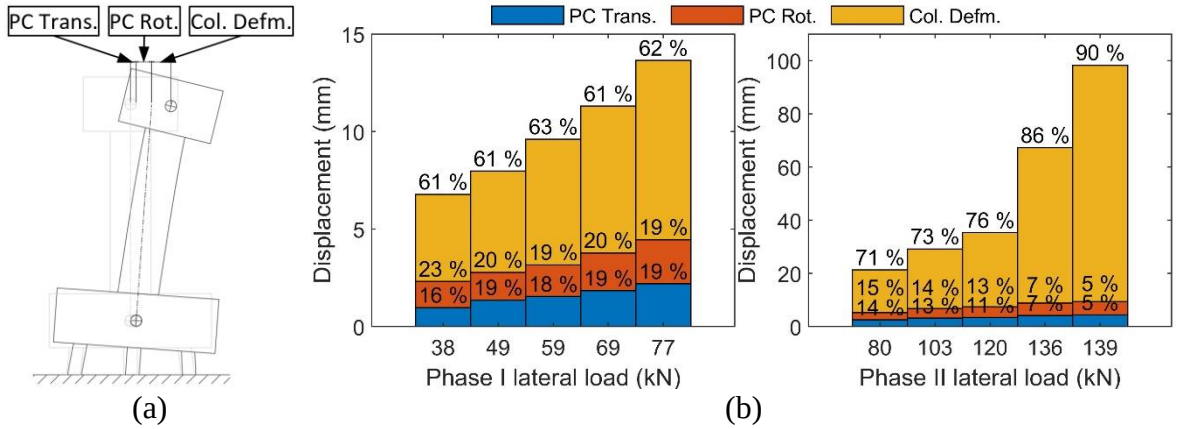

(a) (b)

Figure 4.14 *(a) Components of column top displacement and (b) their proportions for Phase I and Phase II*

Energy Dissipation

The area of the effective lateral load-displacement loop and equivalent viscous damping are shown in Figure 4.15a and Figure 4.15b, respectively. An excellent hysteresis response was obtained from the test unit. The area of the hysteretic loop increased almost linearly as the displacement ductility increased. The equivalent viscous damping of the system increased from 2.3% for the first cycle at displacement ductility of 1 to 31% for the first cycle at displacement ductility of 6. The difference in the equivalent damping was negligible between Cycle 1, 2, and 3.

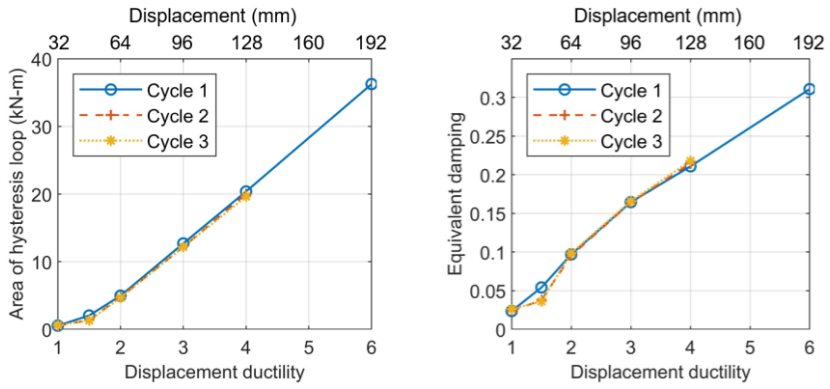

(a) (b)

Figure 4.15 *(a) Area of hysteresis loops and (b) equivalent viscous damping*

Constructability

Based on the experimental works presented herein, the precast pile cap with column socket and pile pockets provides great potential for use in routine practices due to its ease of construction. The socket and pockets can be easily established by commercially available CSP served as stay-in-place formwork. Chemical formwork retarder was found to be an efficient method to achieve the desirable surface roughness at the end of the column. The use of friction collars allows quick assembly of the system in all types of ground conditions and facilitates better control on erection tolerances. The closure pour for the column socket went smoothly which was due to the following desirable features of the grout: high-early-strength, extended working time, and appropriated fluid consistency.

Conclusions

In recent years, there has been interested in using prefabricated components in bridge construction. The preformed socket and pockets connections have been identified as a viable means to connect prefabricated components. The prefabricated column-pile cap-pile system was developed utilizing the socket and pocket connections that are created in the precast pile cap using commercially available CSPs. To investigate the performance of the prefabricated column-pile cap-pile system as well as the connection behavior, an outdoor test was conducted at a cohesive soil site. The unique features of the test included the following: 1) incorporation of foundation flexibility, 2) use of steel H-piles to design a foundation supporting a column that could resist seismic loads, 3) inclusion of battered piles, and 4) use of axial load in an outdoor lateral load test.

Under the combination of vertical and lateral loads acting on the column top, the column plastic capacity was developed near the column base, but no damage was observed in

the pile cap, piles, or in any of the connections. Based on the test results, the following conclusions can be drawn:

- The test unit exhibited stable energy dissipation capacity as the plastic hinge was fully developed in the column, and the pile cap and connections remained undamaged throughout the test. This proved that the performance of the prefabricated column-pile cap-pile system was excellent and is believed to be at least as good as, if not better than, that of a conventional cast-in-place system. For the column socket connection, the embedment length equal to one times the column diameter is sufficient to allow a plastic hinge to be developed in the column. The pile embedment length of 1.5 times the depth of pile is also sufficient to maintain the fixity of the pile pocket connection.
- Foundation flexibility produced a significant effect on the system response. About 40% of column top displacement was due to the foundation flexibility prior to the development in elastic strain in the column. As the damage progressed in the column, the foundation flexibility caused less effect to the total column top lateral displacement, while it still accounted for an important component when the effective lateral load reached its maximum.
- The constructability advantages of the prefabricated column-pile cap-pile system are that it is quick and simple to build. The precast column and precast pile cap with no projected reinforcement are easy to build and transport and are unlikely to be damaged during construction. Given the friction collar and grout with desirable characteristics (including high-early-strength, extended working time, and appropriated fluid consistency), the assembly of a column-pile cap-pile system can be completed within one day.

Acknowledgements

This study was supported by the Iowa Highway Research Board (IHRB) and the Federal Highway Administration State Transportation Innovation Council (STIC). The authors would like to thank the members of the Technical Advisory Committee for their advice and suggestions.

References

AASHTO (American Association of State Highway and Transportation Officials). (2016). "Standard specification for steel sheet, zinc-coated (galvanized), for corrugated steel pipe", *Rep. No. AASHTO M 218*, Washington, DC.

ABC-UTC (Accelerated Bridge Construction University Transportation Center) (2019). "*Accelerated Bridge Construction University Transportation Center:* ABC Project Database." ⟨https://abc-utc.fiu.edu/resources/project-research-databases/⟩.

Ameli, M. J., and Pantelides, C. P. (2016). "Seismic analysis of precast concrete bridge columns connected with grouted splice sleeve connectors", *J. Structural Eng.*, 143(2), 04016176.

ASCE (America Society of Civil Engineers) (2017). "2017 Infrastructure Report Card: Bridges." ⟨https://www.infrastructurereportcard.org/cat-item/bridges/⟩.

ASTM (2018). "Standard Test Method for Compressive Strength of Cylindrical Concrete Specimens", *ASTM C39/C39M-18*, West Conshohocken, PA.

ASTM (2016). "Standard Test Method for Compressive Strength of Hydraulic Cement Mortars (Using 2-in. or [50-mm] Cube Specimens)", *ASTM C109/C109M-16a*, West Conshohocken, PA.

ASTM (2014). "Standard Test Methods and Definitions for Mechanical Testing of Steel Products", *ASTM A370/A370M-14*, West Conshohocken, PA.

ASTM (2013). "Standard Test Methods for Tension Testing of Metallic Materials", *ASTM E8/E8M-13*, West Conshohocken, PA.

Cheng, Z. and Sritharan, S. (2019). "Side shear strength of preformed socket connections suitable for vertical precast members", *J. Bridge Eng.*, 24(5), 04019025.

Culmo, M. P. (2011). "Accelerated Bridge Construction- Experiences in Design, Fabrication and Erection of Prefabricated Bridge Elements and Systems." *FHWA-HIF-12-013, Federal Highway Administration*, U.S. Department of Transportations, Washington, DC.

Culmo, M. P. (2009). "Connections Details for Prefabricated Bridge Elements and Systems." *FHWA-IF-09-010, Federal Highway Administration*, U.S. Department of Transportations, Washington, DC.

Haber, Z. B., Saiidi, M. S., and Sanders, D. H. (2014). "Seismic performance of precast columns with mechanically spliced column-footing connections", *ACI Structural Journal*, 111(3), 639-650.

Haraldsson, O.S., Janes, T.M., Eberhard, M.O., and Stanton, J.F. (2013). "Seismic resistance of socket connection between footing and precast column", *J. Bridge Eng.*, 18(9), 910-919.

Iowa DOT (Iowa Department of Transporatation) (2018). *LRFD Bridge Design Manual*, Ames, IA.

Kavianipour, F. and Saiidi, M.S. (2013). "Experimental and analytical seismic studies of a four-span bridge system with composite piers", CCEER-13-17, Center for Civil Engineering Earthquake research, *Department of Civil and Environmental Engineering, University of Nevada, Reno*, Reno, NV.

Marsh, L. M., Wernli, M., Garrett, B. E., Stanton, J. F., Eberhard, M. O., and Weinert, M. D. (2011). "Application of accelerated bridge construction connections in moderate-to-high seismic regions." *Rep. 698, National Cooperative Highway Research Program (NCHRP)*, Transportation Research Board, Washington, DC.

Mehrsoroush, A. and Saiidi, M.S. (2016). "Cyclic response of precast bridge piers with novel column-base pipe pins and pocket cap beam connections", *J. Bridge Eng.*, 21(4): 04015080.

Mohebbi, A., Saiidi, M.S., and Itani, A. (2017). "Development and seismic evaluation of pier system w/pocket connections, CFRP tendons, and ECC/UHPC columns", CCEER-17-02, Center for Civil Engineering Earthquake research, *Department of Civil and Environmental Engineering, University of Nevada, Reno*, Reno, NV.

Motaref, S., Saiidi, M.S., and Sanders, D. (2011). "Seismic response of precast bridge columns with energy dissipating joints", CCEER-11-01, Center for Civil Engineering Earthquake research, *Department of Civil and Environmental Engineering, University of Nevada, Reno*, Reno, NV.

Priestley, M.J.N., Seible, F., and Calvi, G.M. (1996). *Seismic Design and Retrofit of Bridges*, John Wiley & Sons, New York, USA.

Restrepo, J. I., Tobolski, M. J., and Matsumoto, E. E. (2011). "Development of a precast bent cap system for seismic regions." *Rep. 681, National Cooperative Highway Research Program (NCHRP)*, Transportation Research Board, Washington, DC.

Shama, A. A., Marder, J. B., and Aref, A. J. (2002). "Seismic performance and retrofit of steel pile to concrete cap connections." *ACI Struct. J.*, 99(1), 51–61.

Sritharan, S., Suleiman, M.T., and White, D.J. (2007). "Effects of Seasonal Freezing on Bridge Column-Foundation-Soil Interaction and Their Implications", *Earthquake Spectra*, 23(1), 199-222.

UDOT (Utah Department of Transportation) (2017). *Structural Design and Detail Manual, UDOT SDDM*, Taylorsville, UT.

Wipf, T. J., Klaiber, F. W., Hockerman, S., Bowers, R. P., and Becker, M. (2009). "Precast concrete elements for accelerated bridge construction: laboratory testing of precast substructure components, Boone County bridge", IHRB Project TR-561, Center for Transportation Research and Education, *Iowa State University*, Ames, IA.

Xiao, Y., Wu, H., Yaprak, T. T., Martin, G. R., and Mander, J. B. (2006). "Experimental studies on seismic behavior of steel pile-to-pile-cap connections", *J. Bridge Eng.*, 11(2), 151-159.

CHAPTER 5. BEHAVIOR OF A PILE GROUP UNDER COMBINED VERTICAL AND LATERAL LOADS

A paper prepared for Journal of Geotechnical and Geoenvironmental Engineering

Zhao Cheng, S.M.ASCE[1]; Sri Sritharan, Ph.D., M.ASCE[2]; and Jeramy C. Ashlock, Ph.D., A.M.ASCE[3]

[1]Graduate Research Assistant, Dep. of Civil, Construction, and Environmental Engineering, Iowa State Univ., Ames, IA 50011. E-mail: zcheng@iastate.edu

[2]Wilkinson Chair of Interdisciplinary Engineering, Dept. of Civil, Construction, and Environmental Engineering, Iowa State Univ., Ames, IA 50011 (corresponding author). E-mail: sri@iastate.edu

[3]Richard L. Handy Associate Professor of Geotechnical Engineering, Dept. of Civil, Construction, and Environmental Engineering, Iowa State Univ., Ames, IA 50011. E-mail: jashlock@iastate.edu

Abstract

A large-scale load test was conducted on a pile group at a stiff clay site. The pile group consisted of eight steel H-piles, with a battered pile at each corner. To evaluate a new Accelerated Bridge Construction foundation design concept, a precast pile cap was connected to the piles by embedding the pile heads into preformed pockets. The pile group was tested under different combinations of vertical and lateral loads. The magnitude of the loads as well as the height of the lateral loads were varied to produce different overturning moment-to-lateral load ratios. The pile group exhibited significant resistance to the combined vertical and lateral loads, and the battered piles behaved differently from the vertical piles, as expected. A numerical model with nonlinear springs representing soil resistance was developed to further investigate the battered pile behavior. Good agreement was achieved between the measured and computed pile group behavior. The analytical results showed that

the battered piles were subjected to larger axial forces but smaller bending moments than the vertical piles.

Keywords: Pile group; Battered pile; Precast pile cap; Pocket connection; Load test; Vertical load; Lateral load; Numerical model; Accelerated Bridge Construction (ABC).

Introduction

Piles are most often used in groups and capped by a pile cap to support superstructures. In addition to vertical loads transferred from the superstructures, pile groups are often simultaneously subjected to lateral loads caused by soil pressures, earthquakes, high winds, vessel and vehicular collisions, ice impacts, etc. In many cases, lateral loads are applied on a structural component above the pile cap and transferred to the pile group through the pile cap. As a result, an accompanying overturning moment is induced if a fixed connection is used between the structure and pile cap. However, because of the high cost and logistical difficulty of conducting load tests on pile groups, relatively few large-scale load tests are available that show the behavior of pile groups under combined vertical and lateral loads. McCabe and Lehane (2006) performed a vertical load test on a group of five precast concrete piles in soft clayey silt. Brown et al. (1987), Rollins et al. (1998), and Rollins et al. (2005) tested 3 × 3 pile groups, in which the piles were laterally loaded using a load frame that employed moment-free connections to each pile. Rollins and Sparks (2002), Mokwa and Duncan (2001), and Richards et al. (2011) conducted lateral load tests on pile groups capped by concrete pile caps. These pile-group tests were conducted under either vertical load or lateral load, and thus did not fully represent the lateral loading conditions for actual pile groups, as the vertical structural load was missing. In addition, the tests directly applied the lateral loads to the pile caps rather than through structural columns, which neglects the accompanying overturning moments acting on the pile cap.

To improve the understanding of pile group behavior under more realistic loading conditions, a large-scale pile group consisting of eight steel H-piles was tested under combined vertical and lateral loads in a natural soil profile in this study. As precast components have been widely implemented in recent years (Culmo 2011), a precast pile cap was used, which was connected to the piles by embedding the pile heads into preformed pockets. Along with static vertical loads, cyclic lateral loads were applied at the different heights above the pile cap to induce various combinations of vertical load, lateral load, and overturning moment on the pile cap.

In addition to the behavior of the pile group, another focus of this experimental study was the behavior of the battered piles in the pile group. Battered piles have been used for many decades to resist lateral loads from soil pressures, winds, and impacts. They transmit the applied lateral loads partly through axial force, thereby providing higher lateral stiffness than vertical piles of the same size. However, due to their poor performance in past earthquakes, battered piles are currently not recommended for resisting seismic lateral loads (Lund 2003). The primary causes for historical poor seismic performance of battered piles include inadequate strength of the piles and improper design of the pile connections (Giannakou et al. 2010). These deficiencies tend to be the direct consequences of the design assumption that the pile connections were pinned and thus transferred only axial and lateral force but zero moment. However, even though the piles were embedded a short distance into the pile cap to intentionally create a pinned condition, the pile connections developed considerable moment resistance and failed in a brittle manner (Xiao et al. 2006). With this understanding of the causes of poor performance, it was suggested that for withstanding large lateral loads, design of battered piles should be based on the fixed-head assumption, and both

the battered piles and their connections to the pile cap need to provide sufficient strength (Kavazanjian 2006).

H-piles with deep embedment into pile caps have exhibited potential for use as battered piles subjected to seismic lateral loads (Shama et al. 2002), but their performance needs to be evaluated in the field. To address these concerns, the four corner piles in the pile group in this study were battered to examine their performance experimentally through the large-scale load test. This paper presents the primary results of the pile group test. The behavior of the tested pile group, especially the battered pile behavior, was also investigated through numerical analyses. This paper also outlines the development of the numerical model and compares the numerical and experimental results.

Pile Group Test

Geotechnical Site Conditions

The previous Spangler Geotechnical Laboratory site at Iowa State University was chosen for the pile group test. The subsurface was characterized using the standard penetration test (SPT) and cone penetration test (CPT), which were terminated at a depth of 15 m (50 ft) below the ground surface. The soil profile determined from the in situ tests is shown in Figure 5.1. It primarily consists of stiff clays, with a 1.5-m (5-ft) thick sand layer at a depth of approximately 11 m (35 ft). During the time of testing, the ground water table was at a depth of approximately 2.3 m (7.5 ft).

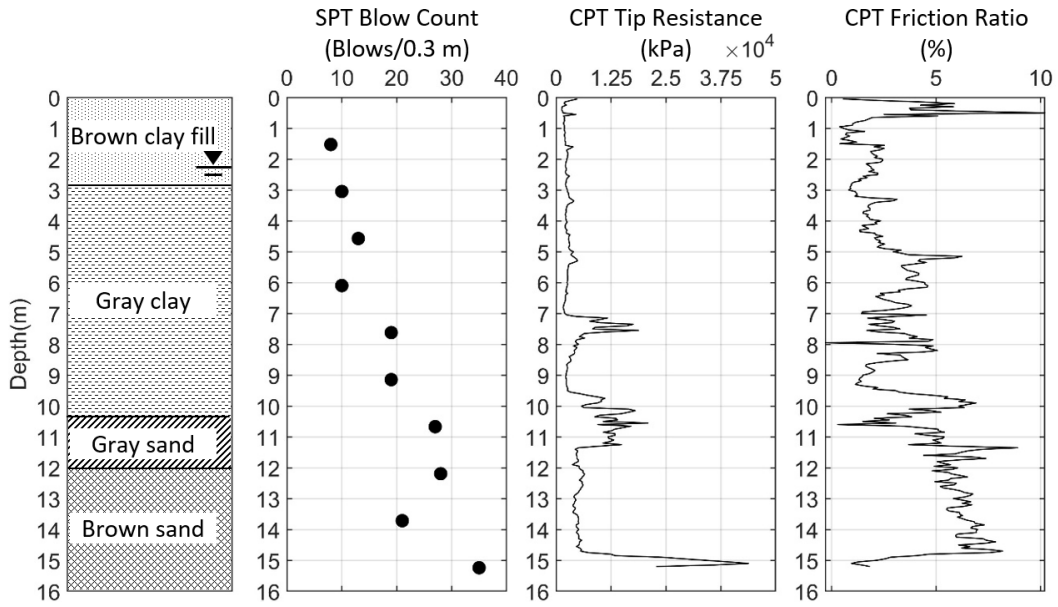

Figure 5.1 *Soil profile along with SPT and CPT data from the test site*

Pile Group Layout

The pile group consisted of eight steel piles, which were capped by a precast pile cap supporting a precast column with a loading block on its top. Another loading block was cast on top of the pile cap for applying lateral loads close to the pile cap. The piles were U.S. W 6 × 20 beams and were driven to a depth of 15 m (50 ft) below the ground surface. The pile steel conformed to ASTM A992 Grade 50 specifications. According to the mill test report, the yield strength of the piles was 370 MPa (53.5 ksi) based on the 0.2% offset criteria, and the ultimate strength was 499 MPa (77.3 ksi). As shown in Figure 5.2a, the piles were arranged in a 3-2-3 pattern, and the four corner piles (i.e., Piles A1, A3, C1, and C3) were battered at a slope of 1 horizontal to 6 vertical. The nominal center-to-center spacing between the piles at the height of the pile cap base was 0.61 m (2 ft). Because piles with a high slenderness ratio may buckle during driving, each 15-m (50-ft) pile was constructed starting from two 9-m (30-ft) long segments. After the first 9-m (30-ft) long segments were driven into the ground, the second 9-m (30-ft) segments were spliced by full penetration groove

welds and subsequently driven. Once the designed pile penetration depth was reached, the extra length was cut at 0.53m (1.75 ft) above the ground. Plugging of the top layer of soil was observed during driving of the piles, developing plugging holes inside the flanges of each pile to an average depth of roughly 0.61 m (2 ft).

The precast pile cap was 1.83 m (6 ft) by 1.83 m (6 ft) in plan and 0.61 m (2 ft) thick. As seen in Figure 5.2b, eight fully penetrated pockets were preformed on the pile cap for connecting the cap to the piles. The pockets were created using corrugated steel pipes, which were topped by steel cones to ensure satisfactory distribution and spacing of the mat reinforcement at the top of the pile cap. Considering the construction tolerances and geometry of the battered piles, the nominal inside diameter of the corrugated steel pipes was selected to be 457 mm (18 in.). Following routine design practices (Iowa DOT 2018) and findings from previous studies (Shama et al. 2002; Xiao et al. 2006), a pile embedment length of 229 mm (9 in.) was selected, corresponding to 1.5 times the depth of the pile's cross-section. After placing the pile heads into the pockets, the bottom openings of the pockets were sealed, and the pockets were then filled with self-consolidating concrete to establish the pile-to-pile cap connections. The pile cap was positioned at 0.30 m (1 ft) above the ground to eliminate contact pressures acting on the pile cap, and to provide access to the bottom of the pile cap for test observation and instrumentation purposes. More details about the precast pile cap and pocket connection can be found in Cheng and Sritharan (2019).

The precast column was inserted into the socket that was preformed in the precast pile cap, and the surrounding void was filled with high strength grout. The loading block formed on top of the column allowed the lateral load to be applied at a height of 2.13 m (7 ft) above the top of the pile cap in test Phases I and II. The second loading block cast above the pile

cap and surrounding the column base was used for applying lateral loads at 0.30 m (1 ft) above the top of the pile cap in test Phases III–VI, as seen in Figure 5.2c.

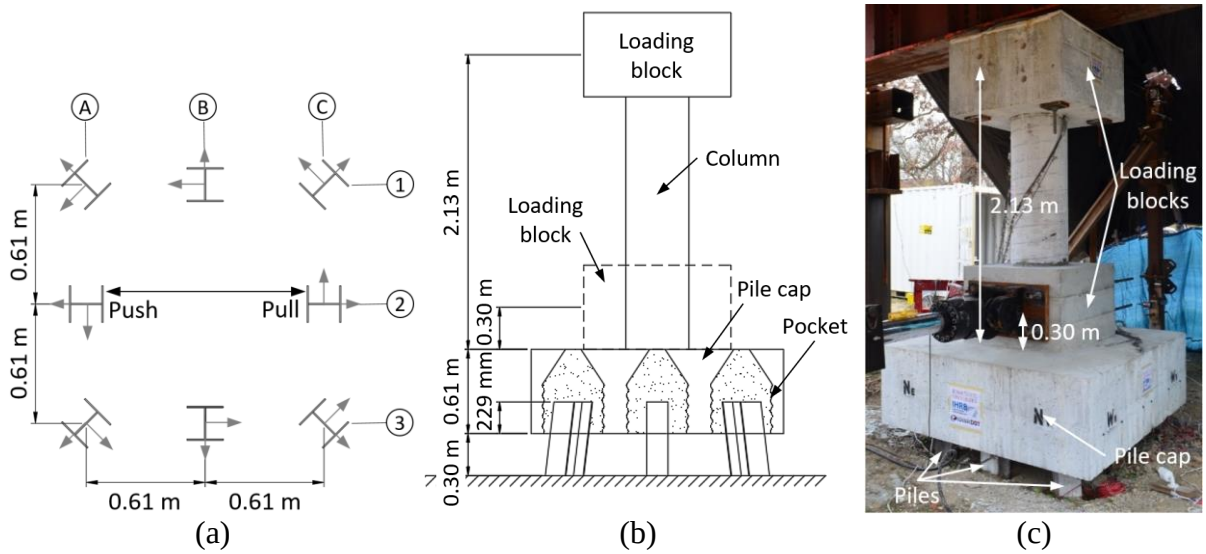

Figure 5.2 *Pile group layout: (a) pile configuration; (b) pile cap, column, and loading blocks; (c) photograph of the pile cap and loading blocks*

Test Setup

A reaction frame and a reaction column were constructed at the test site for applying vertical and lateral loads to the pile group, respectively. The reaction frame was anchored by four U.S. HP 14 × 73 steel piles driven to 15 m (50 ft) below the ground. As shown in Figure 5.3a, four hollow hydraulic cylinders in the reaction frame pushed the main reaction beam down, thereby applying vertical loads to the test piles while subjecting the anchor piles to tension. A friction pendulum bearing was installed between the reaction beam and the column loading block. This bearing was used to transfer vertical load, while allowing translation and rotation of the pile cap. The lateral reaction column consisted of five precast concrete segments and a 1.8-m (6-ft) diameter, 12-m (40-ft) deep drilled shaft foundation, which were connected using four post-tensioned rods anchored into the drilled shaft. A double-acting hydraulic actuator was attached between the reaction column and loading

block. As seen in Figure 5.3b, the actuator was positioned at two different heights for applying the lateral load at either 2.13 m (7 ft) or 0.30 m (1 ft) above the top of the pile cap in the different test phases.

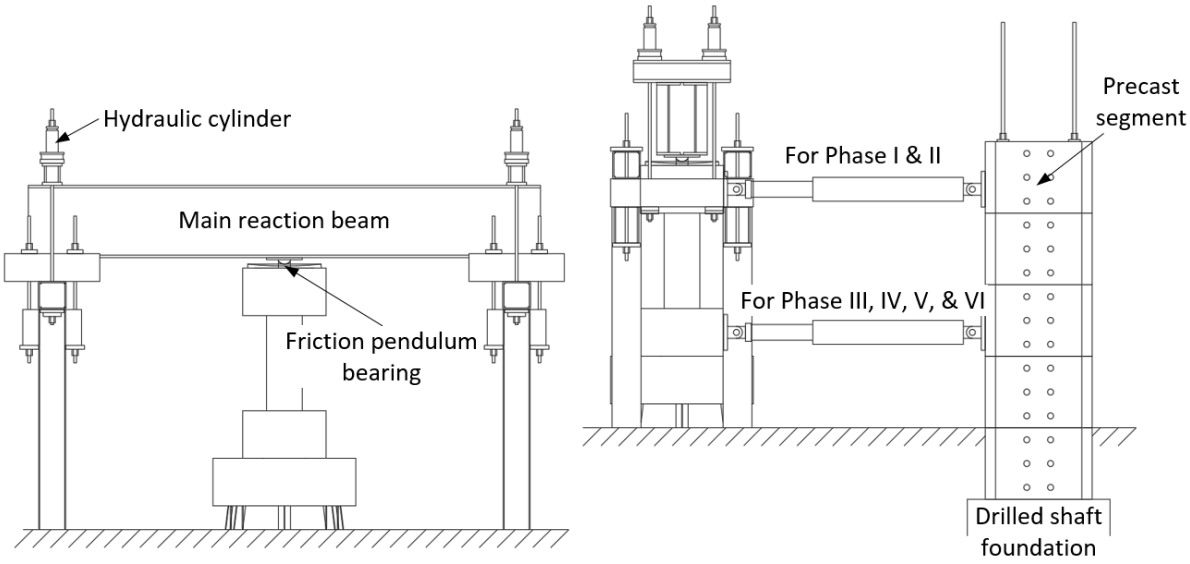

Figure 5.3 *Test setup: (a) reaction frame; (b) reaction column*

Load Protocol

The pile group test consisted of six phases to examine the pile group response under different combinations of vertical and lateral loads. As detailed in Figure 5.4, in each phase, following the application of a constant vertical load, the push (positive) and pull (negative) loads were applied cyclically in the horizontal direction. In each phase, the positive and negative lateral loads were gradually increased in multiple levels up to the target maximum amplitude, with three full cycles at each loading level. The peak load was held constant for about 5 min. in the first cycle of each loading level. In some levels, this load-holding period was longer to enable inspecting of the pile group and documenting of observations.

For Phase I and Phase II, the vertical load was targeted at 1,112 kN (250 kip) and 445 kN (100 kip), respectively. The target maximum lateral load of Phase I was equal to 5% of

the vertical load, and the lateral load in Phase II was gradually increased until a plastic hinge formed in the column. As previously noted, the lateral load of the first two phases acted at 2.13 m (7 ft) above the top of the pile cap to produce a high overturning moment-to-lateral load ratio. In the subsequent phases, the lateral load was lowered to 0.30 m (1 ft) above the top of the pile cap to reduce the moment-to-load ratio. For Phase III, the target vertical load was 1,112 kN (250 kip), and the target maximum lateral load was ±623 kN (±140 kip). For Phase IV, the target vertical load was reduced to 445 kN (100 kip), and the target maximum lateral load was 979 kN (220 kip). However, the applied negative lateral load was limited by the actuator capacity and therefore only achieved an amplitude of -667 kN (150 kip). Phase V and Phase VI were conducted to test the pile group under extreme loading conditions. The target vertical load for Phase V was 1,112 kN (250 kip), and was reduced to 0 kN (0 kip) in Phase VI. The maximum applied lateral loads for Phase V and Phase VI were 1,001 kN (225 kip) and -667 kN (-150 kip), respectively.

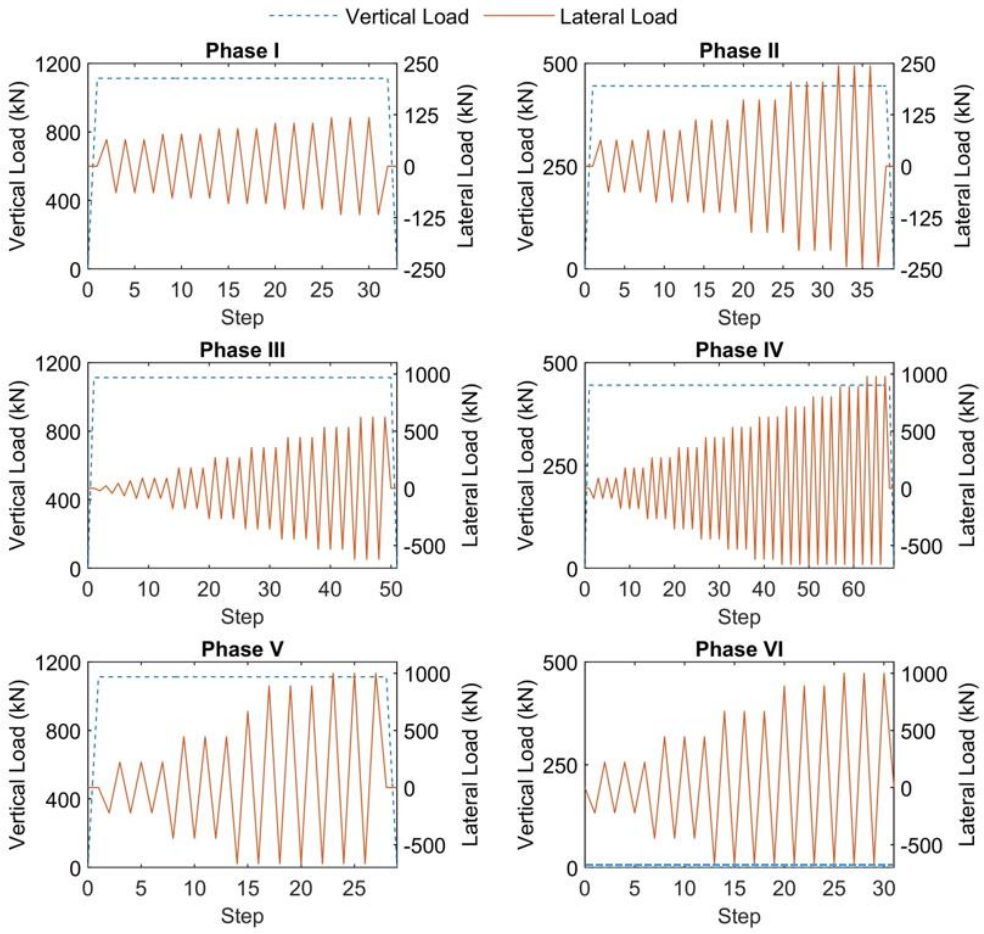

Figure 5.4 *Load protocol for test Phases I through VI*

Test Observations

For the duration of Phase I and II, no damage was observed on the piles, pile cap, or their connections. During Phase III, when the lateral loads reached 623 kN (140 kip) in positive and negative directions, cracks appeared in the connections of the two straight Piles A2 and C2 in succession, but no damage occurred in the other pile-to-pile cap connections. The crack adjacent to Pile A2 expanded as the positive lateral loads exceeded 712 kN (160 kip) during Phase IV (Figure 5.5a). Under the maximum lateral load applied during Phase IV, yielding was visible on the flanges of Pile B1 and B3 (Figure 5.5b), and two battered Piles C1 and C3 slightly pulled out from the pile cap. The high vertical load of Phase V

induced additional compression in the piles, thereby impeding the progression of tensile damage in the pile-to-cap connections. Under the combination of the zero vertical load and 1,001-kN (225-kip) lateral load in Phase VI, the connections of battered Piles C1 and C3 failed in tension (Figure 5.5c), one flange of Pile A1 and A3 buckled (Figure 5.5d), and rotation of Pile B1 and B3 was visible (Figure 5.5e). The formation of gaps between the piles and cohesive soil initiated from Phase II, and the gap width continually grew as the pile group was subjected to cyclic loads in subsequent phases. As shown in Figure 5.5f, the maximum permanent gap at the end of Phase VI was approximately 152 mm (6 in.).

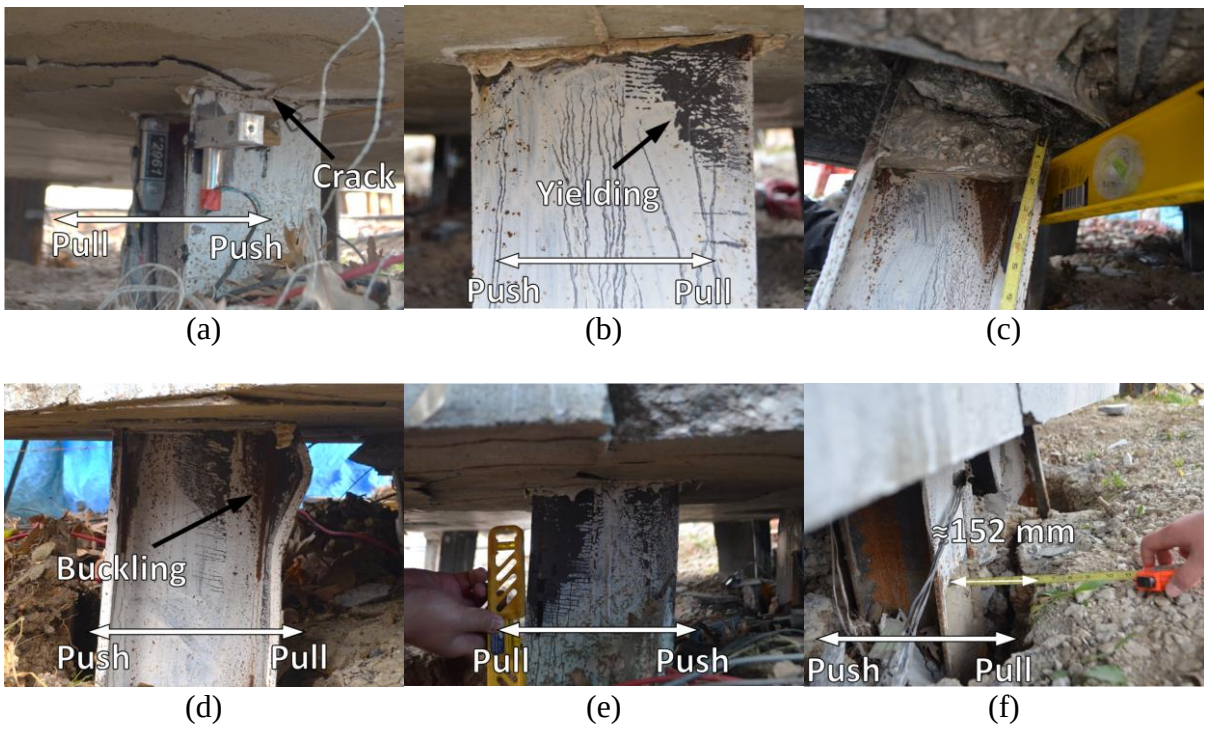

(a) (b) (c)

(d) (e) (f)

Figure 5.5 *Observations: (a) crack in the connection to pile A2; (b) yielding of pile B3; (c) pull out of pile C3; (d) buckling of pile A3; (e) rotation of pile B1; (f) gap next to pile C2*

Load-Displacement Response

The load-displacement responses for the pile group during the different test phases are shown in Figure 5.6, which contains the lateral load transferred to the pile cap versus the

displacements measured at the mid-depth of the pile cap. For ease of comparison, the plots are presented with the same scales for both axes. The load-displacement response remained linearly elastic for the duration of Phase I and II. The backbone of the response for Phase III was approximately linear, whereas the responses during individual loading cycles exhibited slight nonlinearities. This phenomenon was due to the formation of permanent gaps between the piles and cohesive soil. When the pile group first reached a given displacement, the applied lateral load was resisted by the pile stiffness and soil pressure. As the load on the pile group was cycled, gaps developed next to the piles. For pile displacements less than the width of the gap, the resistance is only due to the pile stiffness. As the piles approached the previous maximum displacement, the piles engaged the soil which progressively provided additional resistance, causing the observed increase in the stiffness of the load-displacement response of the pile group.

For Phase IV, the response under negative load was similar to that for the last loading step of Phase III, but the displacement slightly increased due to progressive plastic failure of the soil as the load on the pile group was cycled at the same negative load level. When the positive lateral load of Phase IV exceeded 551 kN (124 kip), the slope of the response backbone gradually decreased, which was mainly associated with yielding of the piles and damage in the pile-to-pile cap connections. Creep under constant load occurred during the load-hold periods of the positive loading levels of 810 kN (182 kip), 890 kN (200 kip), and 916 kN (206 kip) for Phase IV.

During Phase V, as the high vertical load induced additional compression in the piles, no further significant damage was observed, and the hysteresis responses for the three cycles of each loading level were stable. An exception was the last loading step, in which soil creep

occurred during the load-holding period. As evidenced by the tensile failure of the pile connections and buckling of the piles documented at the end of test, the reduction of vertical load in Phase VI triggered failure of the pile group, causing the continuous increase of lateral displacement under a sustained lateral load of 1,001 kN (225 kip).

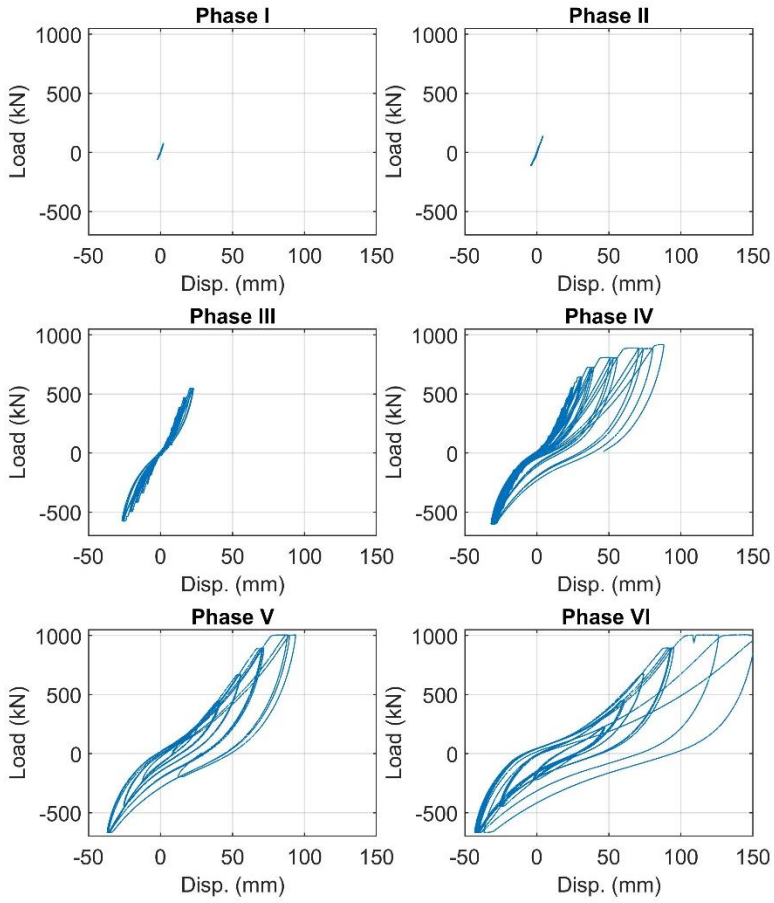

Figure 5.6 *Measured lateral load-displacement responses for pile group*

Moment-Rotation Response

The lateral load applied above the pile cap produced overturning moments acting on the pile cap in all loading phases of the test. The relationships between the overturning moment and pile cap rotation are presented in Figure 5.7. For the duration of Phase I, the moment-rotation response remained linearly elastic. As the gap formed between the piles and soil during Phase II, the moment-rotation response exhibited some nonlinearity but remained

elastic. Following the first two phases, the height of lateral load was lowered from 2.13 m (7 ft) to 0.30 m (1 ft) above the top of the pile cap. As a result, the overturning moment-to-lateral load ratios for the subsequent phases were significantly lower than those for Phases I and II, causing noticeable reductions in the slopes of the moment-rotation responses.

During Phase III, the moment-rotation response exhibited increasing amounts of nonlinearity as the pile-to-soil gaps expanded. Subsequent to the moment reaching 265 kN-m (2,345 kip-in.) in Phase IV, the slope of the moment-rotation response backbone decreased, and the hysteresis loop widened. This degradation was associated with damage occurring in the piles and pile-to-pile cap connections, especially pull-out of the battered Piles C1 and C3. For Phase V, the nonlinearity of the moment-rotation response became more pronounced as the gaps around the piles continually grew. The high vertical load of this phase impeded the progression of tensile damage in the pile connections, and thus maintained a stable hysteretic response. With the vertical load reduced to zero in Phase VI, tension failure of the connections caused the significant deterioration in the moment-rotation response.

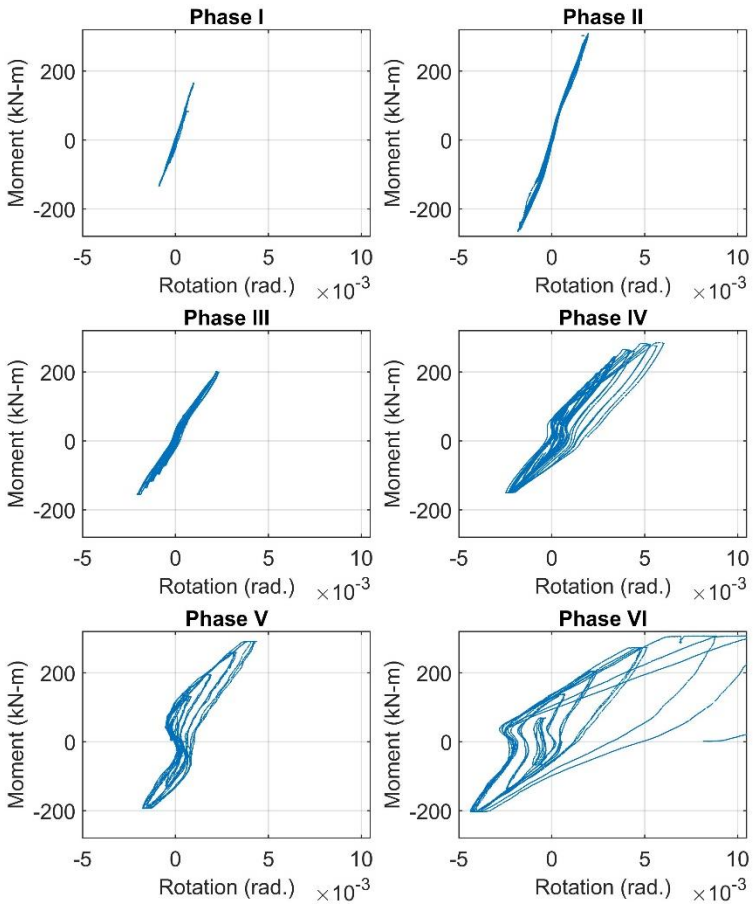

Figure 5.7 *Measured moment-rotation responses for pile group*

Analysis Approach

Numerical Model

The behavior of the pile group was further investigated analytically using a three-dimensional numerical model developed using the computer software SAP 2000. For the numerical model, the concrete material properties were defined following the Mander unconfined concrete model (Mander et al. 1984) with a compressive strength of 39.9 MPa (5.79 ksi), corresponding to the measured concrete strength for the precast pile cap. The steel stress-strain curve was formulated following the detailed model suggested by Lee et al. (2015) with a yield strength of 370 MPa (53.5 ksi) and ultimate strength of 499 MPa (77.3 ksi). As shown in Figure 5.8a, the loading blocks and the column were modeled with rigid

beams to simplify the model. The pile cap was modeled using elastic concrete shell elements with a thickness of 0.61 m (2 ft), and its geometry was reproduced by the rigid links assigned on the top and bottom of the shell elements. Each steel pile was represented by an elastic beam-column element with two concentrated fiber hinges capturing inelastic damage in the pile and the pile-to-pile cap connection. Based on a nonlinear analysis of the single pile subjected to lateral load, the hinges were assigned at the top of the pile and at 1.1 m (3.75 ft) below the ground surface, where the maximum bending moment occurred. The response of the hinges was characterized by integrating the stress-strain relation of uniaxial steel fibers on the pile section (Figure 5.8b) over a hinge length that was taken to be 0.5 times the depth of the pile's cross-section.

To represent the combined effects of pile yielding and connection damage at the top of the piles, various models were evaluated for defining the hysteresis behavior of individual fibers of the top hinge. Based on the results, the pivot model (Dowell et al. 1998) with the following parameters was selected, as it best matched the measured response: $\alpha_1 = 2$, $\alpha_2 = 2$, $\beta_1 = 0.5$, $\beta_2 = 0.5$, and $\eta = 0$. The fibers for the in-ground hinges were defined following a kinematic hysteresis model for capturing only the nonlinear behavior of the steel piles. Zero-length uniaxial nonlinear springs were assigned for connecting the piles to the pile cap. The purpose of these springs was to model pull-out of the piles from the pile cap, for which their force-displacement relation as well as hysteresis response were defined as shown in Figure 5.8c, where A = area of pile section, D = depth of pile section, E = modulus of elasticity of pile steel, and f_y = yield strength of pile steel.

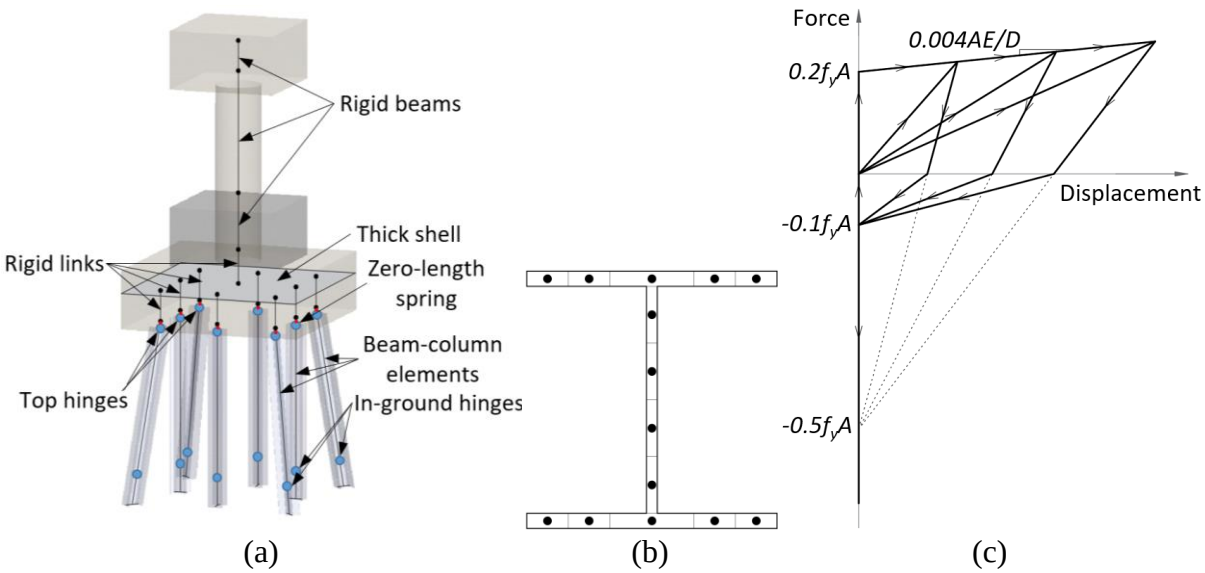

Figure 5.8 *Model of pile group: (a) schematic of the model; (b) fiber layout for concentrated hinge; (c) behavior of zero-length spring*

The soil profile used for the analysis was idealized into six layers. For each layer, the soil properties were determined from correlations to the CPT data measured at the test site (Mayne 2007). Table 5.1 summarizes the soil properties for the different layers. The soil around the piles was modeled as a set of springs having prescribed *p-y* and *t-z* curves. The *p-y* curves represent the lateral soil resistance as a nonlinear function of pile lateral displacement, and the *t-z* curves characterize the nonlinear relation of soil vertical resistance to the pile vertical displacement. Given the various soil types and conditions of the soil layers, different empirical formulations were employed to establish the *p-y* and *t-z* curves at the different depths. The sources for the *p-y* and *t-z* formulations used are listed in Table 5.1.

In order to capture the formation of the gaps between the piles and cohesive soil when the piles were subjected to cyclic loads, compression-only *p-y* springs with the Takeda hysteresis model (Takeda et al. 1970) were assigned on four sides of the pile elements, as illustrated in Figure 5.9. The *t-z* springs were defined to provide both compressive and tensile

resistances and follow the Takeda hysteresis model. For the four battered piles at the corners of the group, the outside and inside *p-y* springs were modified using the soil resistance modifying factors of 1.20 and 0.86, respectively, as suggested by Reese (1958), to account for the effects of pile batter. To account for the effects of the holes caused by pile plugging during driving, as well as group effects and the uncertainty of the idealized soil resistance prescribed by empirical formulations, a *p*-multiplier of 0.25 was applied to the *p-y* springs representing the top 0.61-m (2-ft) of the soil profile, and the *t-z* springs were adjusted by a *t*-multiplier of 0.9 and a *z*-multiplier of 2.75. The multiplier values were determined through a trial and error procedure, by performing repeated analyses with different multipliers until a reasonable agreement was obtained between the measured and computed pile group response.

Table 5.1 *Soil Properties, p-y Curves, and t-z Curves Used for Numerical Analyses*

Depth below ground		**Effective unit weight (kN/m^3)**	**Undrained Cohesion (kPa)**	**Friction angle (degrees)**	***p-y* curve type**	***t-z* curve type**
Top (m)	**Bottom (m)**					
0	2.29	17.28	47.9	—	Stiff clay w/o free water (Welch and Reese 1972)	Driven pile in clay (API 2002)
2.29	7.01	8.26	186.7	—	Stiff clay with free water (Reese et al. 1975)	Driven pile in clay (API 2002)
7.01	7.62	10.62	651.2	—	Stiff clay with free water (Reese et al. 1975)	Driven pile in clay (API 2002)
7.62	10.06	8.26	244.2	—	Stiff clay with free water (Reese et al. 1975)	Driven pile in clay (API 2002)
10.06	11.58	11.40	—	36	Sand (Reese et al. 1974)	Driven pile in sand (API 2002)
11.58	16.76	10.62	306.4	—	Stiff clay with free water (Reese et al. 1975)	Driven pile in clay (API 2002)

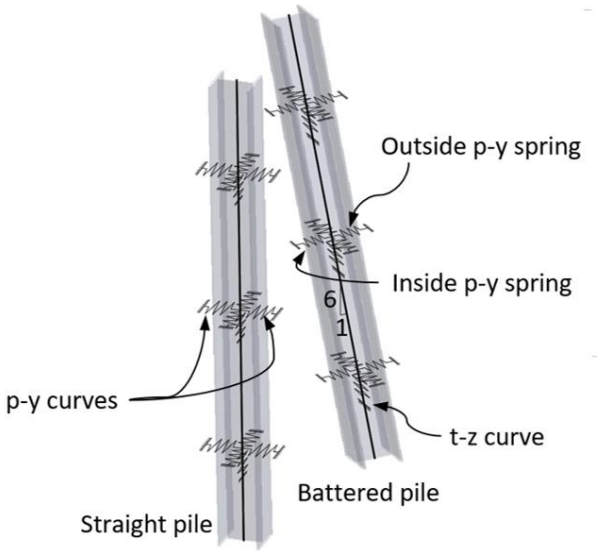

Figure 5.9 *Nonlinear springs representing soil resistances*

Model Validation

The pile group load-displacement and moment-rotation responses computed using the numerical model are compared to the measured responses in Figure 5.10a and Figure 5.10b, respectively. These comparisons show that the numerical model satisfactorily captures both stiffness and hysteresis characteristics of the pile group under the different combinations of vertical and lateral loads. The errors in terms of displacement and rotation were attributed to the effects of creep, which were not taken into account for the soil nonlinear springs. Furthermore, the measured and computed axial forces and bending moments at the heads of Piles A2, A3, and B1 for the duration of the Phase II test are presented in Figure 5.11a and Figure 5.11b as a function of the overturning moment acting on the top of the pile cap. The results show a reasonably good agreement in light of the simplifications adopted.

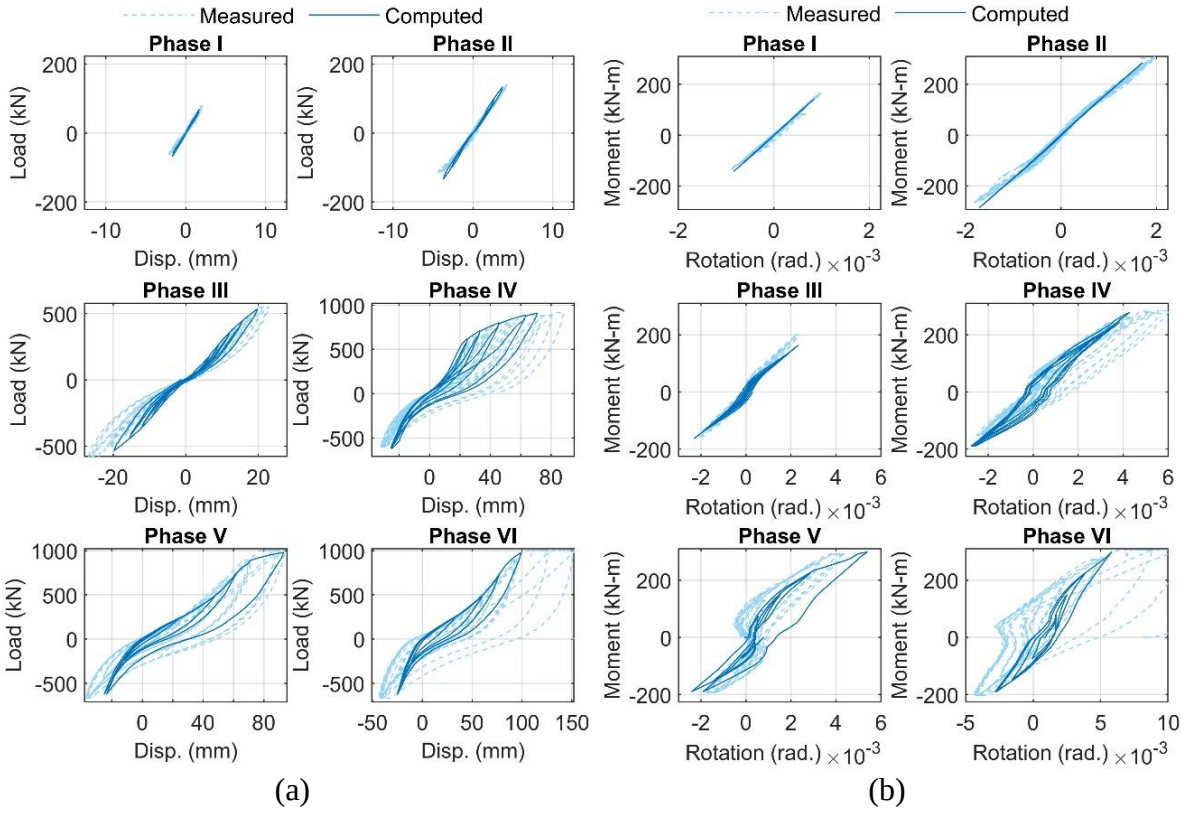

Figure 5.10 *Comparison of measured and computed (a) load-displacement and (b) moment-rotation responses*

Figure 5.12 shows the computed pull-out of Piles C1 and C2 during Phase IV as a function of overturning moment. These computed responses indicate that the vertical Pile C2 experienced no pull-out during Phase IV, whereas the battered Pile C1 began pulling out from the pile cap when the applied overturning moment reached 173 kN-m (1,531 kip-in.), and it pulled out by approximately 5.4 mm (0.21 in.) under the maximum overturning moment in Phase IV. This computed pull-out behavior correlates well with that observed during the pile group test. Because of the good match between measured and computed responses at both global and local levels, the numerical model was considered satisfactory for capturing the pile group response and soil-foundation-structure interaction in this study.

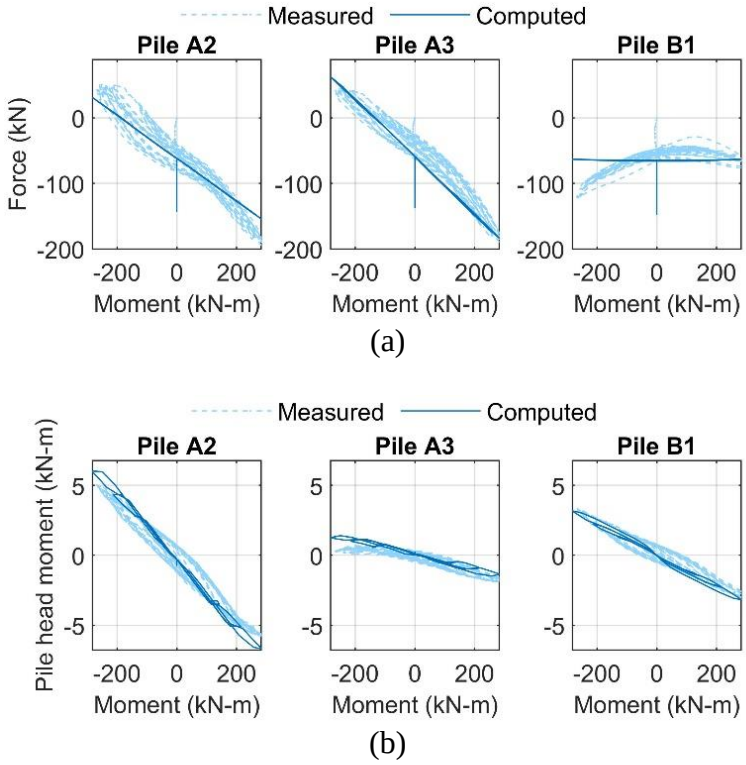

Figure 5.11 *Comparison of measured and computed (a) axial force and (b) bending moment at pile heads for Phase II*

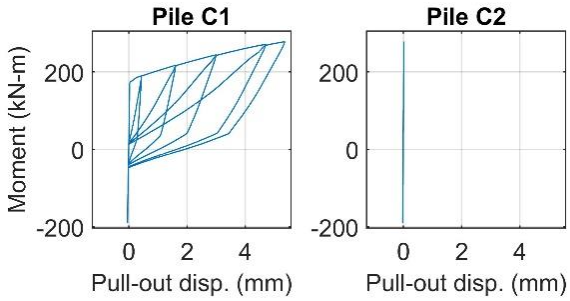

Figure 5.12 *Computed pull-out of pile C1 and C2 for Phase IV*

Behavior of Battered Piles

The available data from the pile group test was inadequate to fully characterize the behavior of battered piles. Therefore, the verified numerical model, supplemented by the observations from the pile group test, was used to investigate the battered pile behavior. Table 5.2 summarizes the computed axial force and bending moment at the head of Piles A1, A2,

C1, and C2 under the different load combinations, in which the bending moment represents the resultant in the loading-direction (i.e., push and pull direction) as defined in Figure 5.2. Generally, for piles in the same row (e.g., Piles A1 and A2, or Piles C1 and C2), the lateral load induced larger axial forces and smaller bending moments in the battered piles compared to the vertical piles, and the magnitude of these effects depended greatly on the height of the lateral load. In the vertical-load-only condition, the vertical piles were subjected to higher axial forces than the battered piles because the vertical piles have a higher stiffness in the vertical direction. For Phase I and II with the lateral load applied at 2.13 m (7 ft) above the top of the pile cap, a large overturning moment was produced by relatively small lateral load. The overturning moments acting on the pile cap were primarily resisted by vertical reactions of the piles, thus, additional compressive forces were induced in Pile A1 and A2, but Pile C1 and C2 was subjected to less axial compressive forces than those in the vertical-load-only condition. The lateral force distributed to the individual piles was small, causing that the bending moments at the pile heads were negligible compared to the pile yield moment of 75 kN-m (668 kip-in.) in the strong-axis direction. The battered piles transmitted the lateral loads partly through axial force, and the vertical piles resisted the lateral load mainly through bending stiffness. Therefore, the bending moment in the vertical piles were higher than those in the battered piles, and the battered piles were subjected to higher axial forces.

Table 5.2 *Pile Head Axial Forces and Bending Moments*

Test phase	Vertical load (kN)	Lateral load[a] (kN)	Overturning moment (kN-m)	Axial force[b] (kN)				Bending moment (kN-m)			
				A1	A2	C1	C2	A1	A2	C1	C2
Vertical load only	1112	—	—	141	145	141	145	—	—	—	—
	445	—	—	59	62	59	62	—	—	—	—
Phase I[c]	1112	67	142	200	192	78	98	0.2	4.0	0.8	2.1
Phase II[c]	445	133	285	185	155	-64	-32	1.4	6.7	1.3	6.0
Phase III[d]	1112	534	163	415	269	-173	23	40	57	40	57
Phase IV[d]	445	912	278	575	186	-385	-182	56	89	57	90
Phase V[d]	1112	979	298	603	307	-370	85	55	88	57	95
Phase VI[d]	0	979	298	517	110	-417	-277	54	89	53	90

[a]Positive value indicates push load as defined in Figure 5.2.
[b]Positive value indicates compressive force and negative value indicates tensile force.
[c]Lateral load is applied at 2.13 m above the top of the pile cap.
[d]Lateral load is applied at 0.30 m above the top of the pile cap

For Phases III to VI with the lateral load applied at 0.30 m (1 ft) above the pile cap, larger lateral loads were applied in order to produce overturning moments comparable to those of Phases I and II. Therefore, the piles were subjected to considerable bending moments because of the large lateral loads. The vertical piles experienced larger moments than the battered piles, as evidenced by the observations that the cracks first appeared in the connections to vertical Piles A2 and C2. In contrast, the axial forces in the battered piles were considerably larger than those in the vertical piles because the battered piles transmitted the applied lateral loads to axial force. In Phase IV, the lateral load induced a tensile force in the battered Pile C1 that was almost double the force in the vertical Pile C2, causing the observed pull out of the battered piles in the pile group test. The high vertical load in Phase V imposed greater compressive forces on the piles. A comparison between the pile head axial forces for Phase IV and V revealed that the battered piles were less sensitive to the vertical load than the vertical piles because the vertical piles provided more resistance to the vertical load than the battered piles. When the pile group is only subjected to lateral load during Phase VI, the compressive axial force in the battered Pile A1 was roughly 4.7 times the axial force in the vertical Pile A2, showing that the effects of pile batter became more prominent.

Conclusions

A large-scale pile group test was conducted at a stiff clay site with combined vertical and cyclic lateral loads. The pile group consisted of eight steel H-piles capped by a precast pile cap. Four piles at the corners of the group were battered at a 1 horizontal to 6 vertical slope. The precast pile cap was connected to the piles by embedding the pile heads into the pockets that were preformed using corrugated steel pipes. For the different phases of the load test, the magnitudes of the vertical and lateral loads were varied, and the lateral loads were applied at two different heights to produce various overturning moment-to-lateral load ratios. A

numerical model was developed to better understand the behavior of the test pile group. Based on the results of the experiments and numerical analyses, the following conclusions can be drawn:

- The pile group exhibited significant resistance to the combined vertical and lateral loads. Under the load combinations with high pile cap overturning moment-to-lateral load ratios, the bending moments at the pile heads were negligible, and the applied loads were primarily resisted by the vertical reactions provided by the piles. When the overturning moment-to-lateral load ratio was reduced, considerable bending moments were also developed at the pile heads.
- The precast pile cap exhibited satisfactory performance and remained essentially undamaged under the different combinations of vertical and lateral loads. Sufficient pile-to-pile cap connections were established by embedding the pile heads into the preformed pockets. With the embedment length of 1.5 times the cross-section depth of the piles, the connections developed considerable resistance to the axial forces and bending moments imposed on the piles. Under the extreme lateral loads, the piles pullout due to the significant tensile forces, and the connections were damaged in a ductile manner.
- The numerical model adequately captured the behavior of the tested pile group. The nonlinear response of the piles and pile-to-pile cap connections was accounted for using concentrated hinges and zero-length springs assigned to the pile elements. The soil resistances were represented by nonlinear springs characterized by *p-y* and *t-z* curves. These nonlinear curves developed from

empirical formulations were adjusted using multipliers to account for the effects of the pile batter, plugging holes surrounding the piles, and pile group interaction.

Acknowledgements

This study was supported by the Iowa Highway Research Board (IHRB) and the Federal Highway Administration State Transportation Innovation Council (STIC). The authors would like to thank the member of the Technical Advisory Committee for their advice and suggestions.

References

API (2002). "Recommended practice for planning, designing and constructing fixed offshore platforms-working stress design." *RP 2A-WSD*, American Petroleum Institute.

Brown, D. A., Resse, L. C., and O'Neill, M. W. (1987). "Cyclic lateral loading of a large-scale pile group." *J. Geotech. Engrg.*, 113(11), 1326–1343.

Cheng, Z., and Sritharan, S. (2019). "An outdoor test of a prefabricated column-pile cap-pile system under combined vertical and lateral loads." Prepared for *J. Struct. Engrg.*.

Culmo, M. P. (2011). "Accelerated Bridge Construction- Experiences in Design, Fabrication and Erection of Prefabricated Bridge Elements and Systems." *FHWA-HIF-12-013*, Federal Highway Administration, U.S. Department of Transportations, Washington, DC.

Dowell, R. K., Seible, F., and Wilson, E. L. (1998). "Pivot hysteresis model for reinforced concrete members." *ACI Struct. J.*, 95(5), 607– 617.

Giannakou, A., Gerolymos, N., Gazetas, G., Tazoh, T., and Anastasopoulos, I. (2010). "Seismic behavior of batter piles: elastic response." *J. Geotech. Geoenviron. Eng.*, 136(9), 1187-1199.

Iowa DOT (Iowa Department of Transporatation) (2018). *LRFD Bridge Design Manual*, Ames, IA.

Kavazanjian, E. (2006). "A driven-pile advantage: Batter piles." *Piledriver*, Q4, 21–25.

Le Val Lund. (2003). "El Salvador earthquakes of January 13 and February 13, 2001: Lifeline performance." *Monograph ASCE*, C. Sepponen, ed., Technical Council on Lifeline Earthquake Engineering, No. 24.

Lee, J., Engelhardt, M. D., and Choi, B. J. (2015). "Constitutive model for ASTM A992 steel at elevated temperature." *International Journal of Steel Structures*, 15(3), 733-741.

Mander, J. B., Priestley, M. J. N. and Park R. (1984). "Theoretical stress strain model for confined concrete." *J. Struct. Eng.*, 114(3). 1804-1826.

Mayne, P.W. (2007). "Cone penetration testing." *NCHRP Synthesis 368*, National Cooperative Highway Research Program, Transportation Research Board, Washington, D.C.

McCabe, B. A., and Lehane, B. M. (2006). "Behavior of axially loaded pile groups driven in clayey silt." *J. Geotech. Geoenviron. Eng.*, 132(3), 401-410.

Mokwa, R. L. and Duncan, J. M. (2001). "Experimental evaluation of lateral-load resistance of pile caps." *J. Geotech. Geoenviron. Eng.*, 127(2), 185-192.

Reese, L. C. (1958). Discussion of "Soil modulus for laterally loaded piles." By Bramlette McClelland & John A. Fotch, Jr. *Proceedings*, ASCE (1081), *Transactions*, ASCE 123, 1071-1074.

Reese, L. C., Cox, W. R., and Koop, F. D. (1974). "Analysis of laterally loaded piles in sand." *Proceedings of the VI Annual Offshore Technology Conference*, Houston, Texas, 2(OTC 2080), 473-485.

Reese, L. C., Cox, W. R., and Koop, F. D. (1975). "Field testing of laterally loaded piles in stiff clay." *Proceedings of the VII Annual Offshore Technology Conference*, Houston, Texas, 2(OTC 22312), 672-690.

Richards, P. W., Rollins, K. M., and Stenlund, T. E. (2011). "Experimental testing of pile-to-cap connections for embedded pipe piles." *J. Bridge Eng.*, 16(2), 286-294.

Rollins, K. M., Peterson, K. T., and Weaver, T. J. (1998). "Lateral load behavior of full-scale pile group in clay." *J. Geotech. Geoenviron. Eng.*, 124(6), 468–478.

Rollins, K. M. and Sparks, A. (2002). "Lateral resistance of full-scale pile cap with gravel backfill." *J. Geotech. Geoenviron. Eng.*, 128(9), 711-723.

Rollins, K. M., Lane, J. D., & Gerber, T. M. (2005). "Measured and computed lateral response of a pile group in sand." *J. Geotech. Geoenviron. Eng.*, 131(1), 103-114.

Shama, A. A., Marder, J. B., and Aref, A. J. (2002). "Seismic performance and retrofit of steel pile to concrete cap connections." *ACI Struct. J.*, 99(1), 51–61.

Takeda, T., Sozen, M. A., and Nielsen, N. N. (1970). "Reinforced concrete response to simulated earthquakes." *Journal of the Structural Division*, 96(12). 2557-2573.

Welch, R. C. and Reese L. C. (1972). "Laterally loaded behavior of drilled shafts." *Research Report 3-5-65-89*, Center for Highway Research, University of Texas, Austin.

Xiao, Y., Wu, H., Yaprak, T. T., Martin, G. R., and Mander, J. B. (2006). "Experimental studies on seismic behavior of steel pile-to-pile-cap connections", *J. Bridge Eng.*, 11(2), 151-159.

CHAPTER 6. CONTROLLED ROCKING PILE FOUNDATION (CRPF) SYSTEM WITH REPLACEABLE BAR FUSES FOR SEISMIC RESILIENCE

A paper prepared for the Engineering Structures

Zhao Cheng, S.M.ASCE[1] and Sri Sritharan, Ph.D., M.ASCE[2]

[1]Graduate Research Assistant, Dept. of Civil, Construction, and Environmental Engineering, Iowa State Univ., Ames, IA 50011. E-mail: zcheng@iastate.edu

[2]Wilkinson Chair of Interdisciplinary Engineering, Dept. of Civil, Construction, and Environmental Engineering, Iowa State Univ., Ames, IA 50011 (corresponding author). E-mail: sri@iastate.edu

Abstract

This paper presents the controlled rocking pile foundation (CRPF) system and numerically investigates its seismic response. The CRPF system allows the pile cap to rock on the pile foundation and dissipates seismic energy through the inelastic deformations of the replaceable bar fuses connecting the pile cap and piles. Following the conceptual design of the CRPF system, two analytical models were developed for a bridge pier utilizing the CRPF system and a pier designed to develop a plastic hinge in its column. Both the two models were subjected to the static cyclic loads, dynamic free vibrations, and earthquake ground motions. The results indicated that, after experiencing a severe earthquake, the conventionally designed bridge pier sustained substantial damages in the column and exhibited significant residual displacement. In contrast, the pier with the CRPF system showed negligible residual displacement and maintained elastic behavior except the bar fuses as expected. The damaged fuses can be rapidly replaced to recover the bridge seismic resistance after the earthquake. Therefore, the CRPF system offers the feasibility to achieve

the desired seismic performance objectives including immediately openings after an earthquake, shorter repair times, and lower repair costs.

Keywords: Bridges; Seismic design; Precast; Pile foundation; Controlled rocking; Repairable; Seismic resilience.

Introduction

Conventional bridge seismic design relies on the formation of ductile plastic hinges in preselected locations to dissipate seismic energy and protect bridges from collapse. Although bridges designed in this manner are generally considered to provide adequate safety, they often sustain excessive damages and exhibit considerable residual drifts following major seismic events. Damaged bridges can disrupt traffic, necessitate time-consuming inspections, and may be difficult and financially prohibitive to repair. Addressing these issues, new design strategies and technologies are required to achieve additional seismic performance objectives such as mitigating economic losses, maintaining bridge functionality, and improving reparability.

Structures with rocking mechanisms offer the potential to achieve the aforementioned seismic performance objectives. Even experiencing large nonlinear deformation for the duration of shaking, rocking structures can suffer less damage and recenter after high-intensity earthquake ground motions. Housner (1963), Meek (1975), Chopra and Yim (1985), Acikgoz and DeJong (2012), and Kalliontzis et al. (2016) investigated the fundamental rocking dynamics of rigid and flexible structures. In light of their findings, numerous efforts have been made to develop rocking structures. Priestley et al. (1999), Restrepo and Rahman (2007), and Sritharan et al. (2015) developed unbonded posttensioned precast rocking walls with additional hysteretic energy dissipaters, in which the prestressing tendons at the center of the wall panels provide the restoring force to recenter the systems. The concept of

posttensioning has been extended to bridge columns (Hewes and Priestley 2002; Chou and Chen 2006; Restrepo et al. 2011). Precast columns with internal unbonded prestressing tendons were designed to rock at their end joints, and additional hysteretic energy dissipaters were provided through internal partially debonded longitudinal bars made of high-performance steel or shape-memory alloy crossing the joints (Wang et al. 2008; Ou et al. 2010; Roh and Reinhorn 2010) or external attached links (Marriott et al. 2009; Guo et al. 2015).

Utilizing the weight of superstructures as the recentering force, bridges with columns supported on shallow foundations would mobilize rocking behavior at their footings. Mergos and Kawashima (2005) and Deng et al. (2012) numerically studied the seismic response of bridges with rocking shallow foundations using the nonlinear Winkler-foundation model. Saidi et al. (2002), Espinoza and Mahin (2008), and Antonellis et al. (2015) conducted shake table tests to study the response of bridge columns supported on rocking shallow foundations. These studies reveal the merits of the rocking shallow foundation (e.g., recentering capacity, significant energy dissipation, well-defined moment capacity, etc.), but the concerns of this type of system include relatively low bearing capacity, the potential settlement and residual rotation due to the permanent deformation of underlying soils, and the difficulty of repairing after an earthquake (Gajan and Kutter 2008; Allmond and Kutter 2014). Several studies demonstrated that the foundations supported on the unattached piles (i.e., no tension is transferred from the pile caps to the piles) can obtain the beneficial rocking mechanisms with less concern regarding the soil conditions. Allmond and Kutter (2012; 2013) conducted centrifuge tests to explore the behavior of the rocking foundation on unattached piles. Antonellis and Panagiotou (2014) numerically analyzed the bridges with rocking pile

foundations subjected to earthquake ground motions. Guan et al. (2018) tested a large-scale pile foundation model allowing rocking of the pile cap, evidencing the feasibility of rocking pile foundation.

In order to complement the rocking systems and facilitate their uniform application in bridges, a new controlled rocking pile foundation (CRPF) system was developed. The CRPF system extends the concept of rocking pile foundation and uses replaceable bar fuses connecting the piles to the pile cap. When subjected to a strong earthquake ground motion, the fuses dissipate seismic energy by undergoing inelastic deformations, and the system is capable of preventing major structural damage and eliminating residual drifts through rocking on top of the piles. Following an earthquake event, bridges can immediately open to normal use as the structural components transferring service loads experience little or no damage, and the seismic resistances of the bridges can be rapidly recovered by replacing the fuses. Moreover, the CRPF system is suitable for implementing prefabricated technologies, thus offering additional benefits such as reduced onsite construction time, minimized mobility and environmental impacts, improved product quality, and more (Culmo 2011).

Rocking Mechanism of the CRPF System

Figure 6.1 illustrates the rocking mechanisms of the CRPF system during a loading cycle in terms of lateral load (F) versus the column drift (Δ) as well as the axial force of the fuse (F_f) versus the fuse elongation (Δ_f). For the duration of loading, the CRPF system first experiences a small elastic deformation. As the lateral load achieves the decompression force (F_d), the axial forces on the piles that are underneath the one side of the pile cap are decompressed (Figure 6.1a). The pile cap starts to uplift from the decompressed piles and rotate about the piles on the opposite side. Consequently, the fuses fastened between the pile cap and the decompressed piles are stretched in tension, which would remain elastic until the

force in the fuses reaches it yield value ($F_{f,y}$) (Figure 6.1b). For increasing uplift, the fuses undergo plastic deformation and dissipate energy. The yielding of the fuses causes the softening of the system lateral load response, thus the column experiences a large drifts without a significant increase in lateral load (Figure 6.1c). During the unloading, the uplift of the pile cap decreases leading to compressive yielding in the fuses (Figure 6.1d). The superstructure weight (W) eventually recenters the system. As the pile cap sets back to the piles, the fuses reach zero displacement and develop residual compressive stresses (Figure 6.1e).

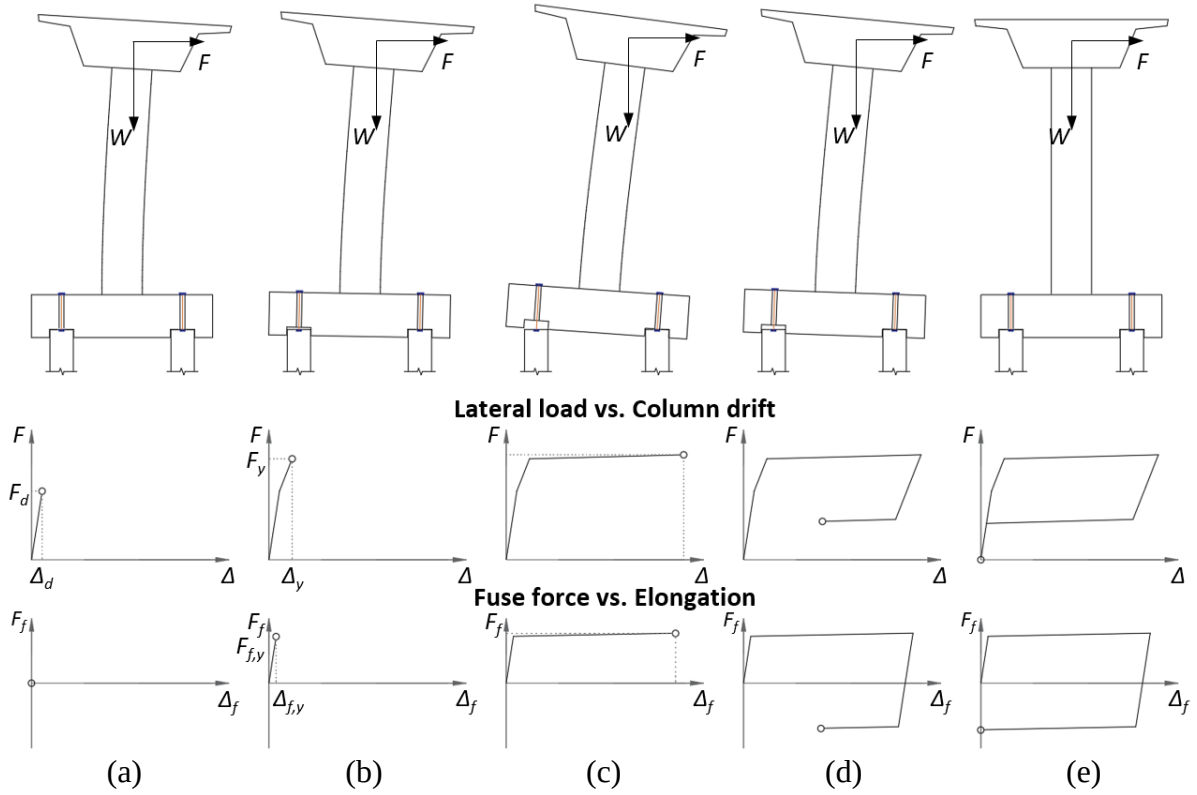

Figure 6.1 *Rocking mechanism of the CRPF system: (a) decompression; (b) fuse tensile yielding; (c) fuse plastic elongation; (d) fuse compressive yielding; and (e) recentering*

Conceptual Design of the CRPF System

A CRPF system consists of bored or driven piles, a precast pile cap supported on the piles, and bar fuses connecting the piles and pile cap. Shallow sockets are preformed on the bottom of the precast pile cap, and the piles are placed into these sockets to transfer lateral forces. For ease of installation and replacement, the fuses are fastened using the threads at their ends. In order to anchor the threaded splicing couplers fastening the fuses and create the pile head with the shape and position precisely fitting the preformed sockets, a cast-in-place (CIP) concrete pile head is needed for each pile. Figure 6.2 illustrates the possible details of the pile head for different types of piles. Among all these details, the steel tube serves as the stay-in-place formwork and provides confinement to protect the pile head from local damage. The bored piles need to extend longitudinal reinforcements into the pile head (Figure 6.2a). If the steel H-piles are used, a slot is cut on the web of the pile to allow the splicing coupler being placed. The tensile force from the coupler is transferred to the pile through the shear studs welded on the pile (Figure 6.2b) or by directly welding the coupler to the pile using the mending plates (Figure 6.2c). The slots are also needed for the steel pipe piles to provide access to weld the shear studs at the inside of the pipe, which are for transferring the tensile force to the pile. The sealing pad prevents the concrete from filling into the pile (Figure 6.2d). For the concrete driven piles (Figure 6.2e), the splicing couplers can be anchored in the hole reserved on the pile top. To ensure full contact between the pile head and pile cap and achieve fast construction, the pile cap is put in place right after pouring the concrete into the steel tube. Prior to the concrete reaching the sufficient strength, the weight of the pile cap can be temporarily carried by: (1) the extended pile reinforcements braced by spiral reinforcement that is securely fastened (or welded) to the extended reinforcements; (2) the

top of the steel H-pile; (3) the top of the steel pipe pile; or (4) the supporting bolts embedded or screwed in the reserved holes on the concrete pile, depending on the type of piles.

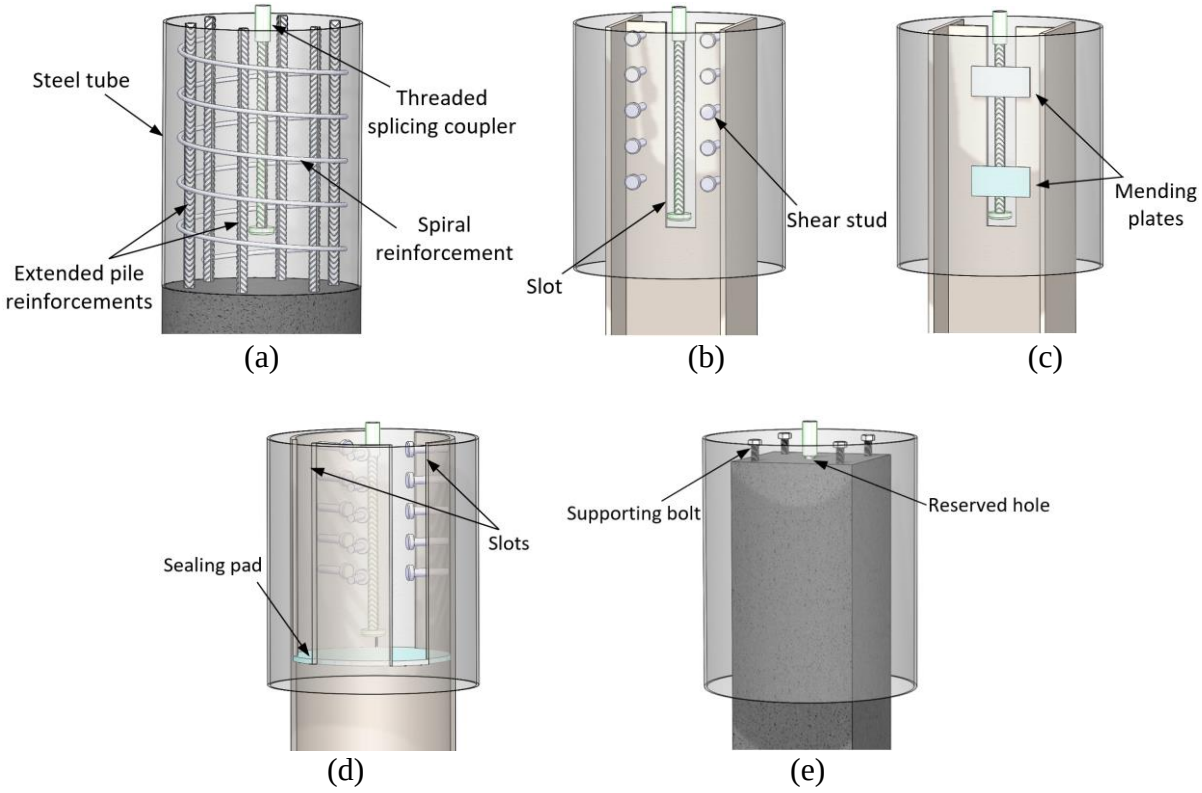

Figure 6.2 *Pile head details for (a) bored pile; (b) steel H-pile with shear studs; (c) steel H-pile with wielded mending plates; (d) steel pipe pile; (e) driven concrete pile*

The bar fuses pass through the vertical voids that are created in the precast pile cap and screwed into the threaded splicing couplers embedded in the pile heads. To allow the fuses yield in tension and compression, the "pinned" connections are required to fasten the fuse to the pile cap. Figure 6.3 shows two possible connection details, namely the threaded pipe connection and plate nut connection. The threaded pipe connection embeds a pipe with external and internal threads on top of the void. The external threads ensure that the pipe is sufficiently anchored in the pile cap, and the internal threads are for fastening the threaded insert. The top of the fuse passes through the plain hole in the center of the threaded insert

and is fastened to the insert by two nuts on the top and bottom of the threaded insert. The protecting cap on top of the void keeps the pipe, insert, and nuts free of corrosion. Alternatively, the plate nut connection screws a plate nut to the fuse. A cap plate is bolted to the pile cap using the threaded rods embedded in the pile cap. The plate nut bears on the pile cap, and the cap plate compresses the plate nut, thereby fastening the top of the fuse to the pile cap. Both two connections are detachable, which allows easy replacement of the fuses following a major earthquake. In case of extraordinarily required long fuses, the pile cap can be made with bumps (Figure 6.4) to accommodate the fuses without any significant increase in the thickness of the pile cap.

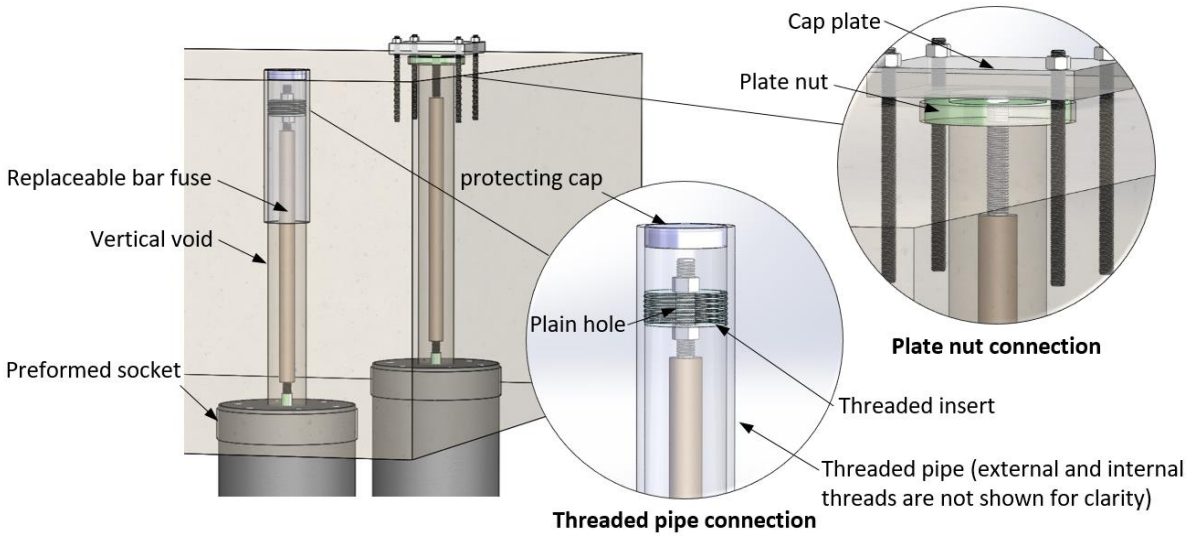

Figure 6.3 *Connections fastening fuse to pile cap*

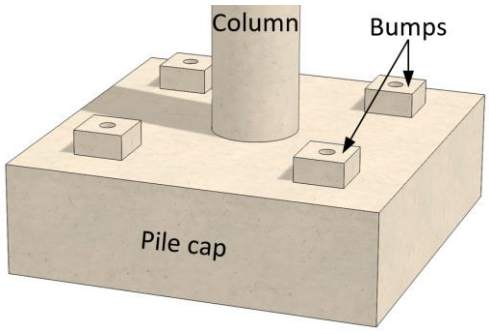

Figure 6.4 *Pile cap with bumps*

Fuses used within the CRPF system are made of mild steel bars with the fuse region manufactured to a reduced cross-section area. The CRPF system dissipates seismic energy mainly through the yielding of the fuses in tension and compression. After evaluating different types of fuses, the groove type buckling-resisting bar fuse (White 2014) is identified to be appropriate for the CRPF system. This type of fuse features a mild steel bar with a number of grooves milled along its length, a steel confining tube placed over the grooved bar, and the end connection regions manufactured with threads (Figure 6.5a). The loading tests conducted by White (2014) demonstrate the energy dissipation capability of the groove type bar fuse when subjected to cyclic tension-compression forces. As a result, the force-elongation response of the fuse is found to follow the kinematic hardening rule and can be characterized as shown in Figure 6.5b, where A_f = area of the fuse region of the mild steel bar, F_f = force in the bar fuse, f_y = yield strength of bar steel, f_u = tensile strength of bar steel, L_f = length of the fuse region of the mild steel bar, ε_y = yield strain of bar steel, ε_u = ultimate strain capacity of bar steel, and Δ_f = elongation of the bar fuse. For mild steel used as energy dissipation component, the PRESSS design handbook (Pampanin et al. 2010) specifies the design strain limit of 5%, strain limits of $0.7\varepsilon_u$ for the Ultimate Limit State (ULS), and $0.9\varepsilon_u$ for the Maximum Credible Earthquake (MCE).

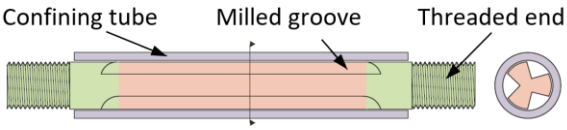

(a)

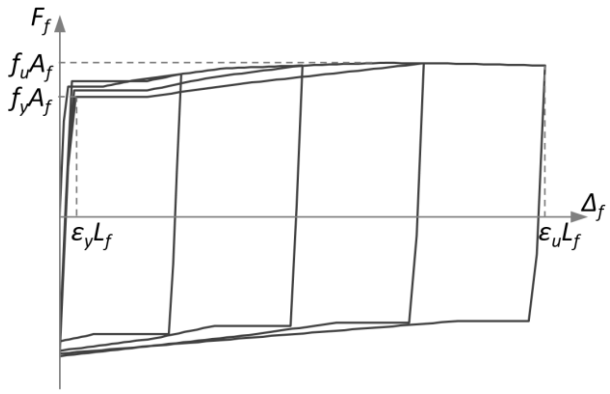

(b)

Figure 6.5 *(a) Configuration (White 2014) and (b) force-elongation response of grooved type bar fuse*

Seismic Response of the CRPF System

The seismic response of the CRPF system was studied through the numerical approach. The structures analyzed were a single column bridge pier supported on the CRPF system (CRPF pier) and a bridge pier with a similar geometry to the CRPF pier but designed to form a flexural plastic hinge at the column base (PH pier). The three-dimensional (3D) numerical models of the CRPF and PH piers were developed and subjected to the static cyclic loads, dynamic free vibrations, and earthquake ground motions, respectively. The response of the CRPF pier was compared with that of the PH pier.

Description of the PH and CRPF Piers

The PH and CRPF piers were hypothetically located at a cohesive soil site with an average undrained shear strength of 96 KPa (2000 psf), which can be classified as competent soil according to Caltrans Seismic Design Criteria (SDC) (2019). All components of the piers were designed for concrete with a specified compressive strength of 28 MPa (4 ksi) and A706M (A706) reinforcing steel with a specified yield strength of 420 MPa (60 ksi). The bar fuses in the CRPF pier were made of A572M (A572) steel bars with a specified yield

strength of 345 MPa (50 ksi). Figure 6.6 shows the key dimensions adopted for the PH and CRPF piers. Both piers consisted of an 11.0-m (36-ft) tall circular column simply supporting the superstructure with a weight of 4381 kN (985 kips). The column diameter was 1.8 m (6 ft), resulting in an axial load ratio of 6%. For the PH pier, the column was reinforced with fifty-six #36M (#11) longitudinal reinforcing bars and a #19M (#6) reinforcing spiral at spacing of 102 mm (4 in.). The PH pier was supported on a 6.1-m (20-ft) by 6.1-m (20-ft) by 1.5-m (5-ft) pile cap with nine 22.9-m (75-ft) deep, 0.9-m (3-ft) diameter bored piles. The reinforcing steel in each pile consisted of sixteen #25M (#8) longitudinal reinforcing bars and #13M (#4) reinforcing hoops at spacing of 152 mm (6 in.). All the column-to-pile cap and pile cap-to-pile connections were designed to be fixed, and they were proportioned so the joint principle stresses met the Caltrans SDC (2019) criteria for the moment resisting connection.

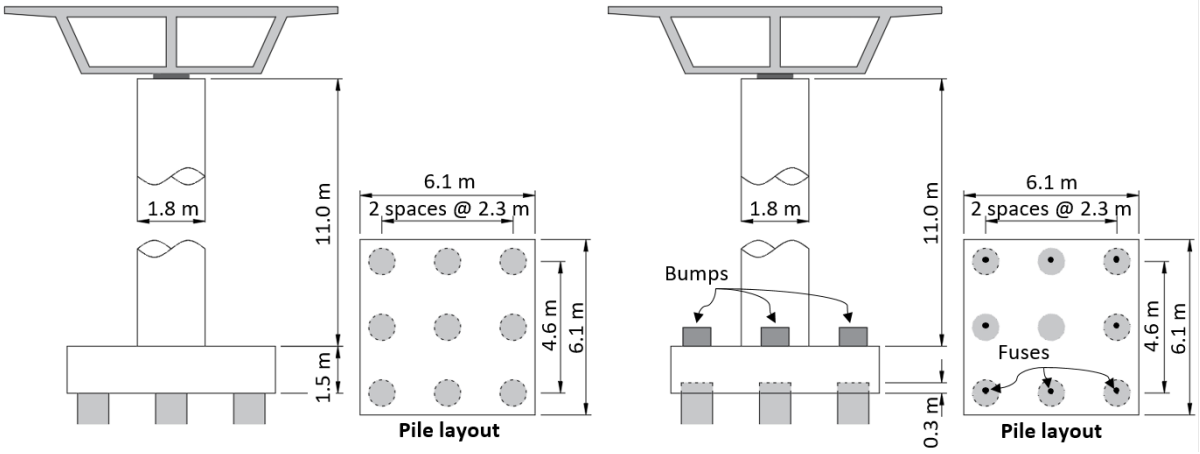

Figure 6.6 *Key dimensions of (a) the PH pier and (b) the CRPF pier*

In order to achieve comparable response with the PH pier, the CRPF pier was designed to provide an elastic lateral force capacity of no less than 1890 kN (425 kips) and be capable of reaching a 5% column drift ratio. As illustrated in Figure 6.7a, for the CRPF

pier, the lateral force decompressing the pile axial forces, F_d, can be approximated as follows:

$$F_d = \frac{\frac{P}{N}\sum N_i d_i}{L + D_{pc}} \quad \text{Equation 6-1}$$

where P = total axial load on the pile group, N = total number of piles in the pile group, N_i = the number of piles in the i^{th} row, d_i = the distance from the i^{th} row to the exterior row, L = column height, and D_{pc} = depth of the pile cap.

Given that the CRPF pier was supported on the pile foundation with a geometry similar to that of the PH pier (Figure 6.6b), the decompression force was computed to be equal to 1170 kN (263 kips). The bar fuses provided additional resistance to allow the CRPF pier to reach the target lateral force capacity. As illustrated in Figure 6.7b, the required fuse area for each pile, A_f, can be determined by the following equation:

$$A_f = \frac{(F_y - F_d)(L + D_{pc})}{f_{ye}\sum n_i d_i} \quad \text{Equation 6-2}$$

where F_y = target lateral force capacity and n_i = the number of fuses in the i^{th} row.

For using the single fuse on each pile except the one directly underneath the column, the resulting fuse area was calculated to be 1516 mm^2 (2.35 in.^{2}), which was provided by a 57-mm (2.25-in.) diameter steel bar with four grooves milled along the length.

Drift of the CRPF pier was conservatively assumed to result from uplift of the pile cap with respect to the piles (Figure 6.7b), even though the column would experience a small elastic deformation. Therefore, to achieve sufficient elongation to accomplish the target drift ratio, the required length of the bar fuse, L_f, can be determined as follows:

$$L_f = \frac{d_p \theta}{0.7\varepsilon_u} \quad \text{Equation 6-3}$$

where θ = target drift ratio and d_p = distance between the exterior rows.

Assuming that the ultimate strain capacity of the fuse bar steel was 0.17, the resulting required length of the bar fuse was computed to be 1.9 m (6.3 ft). Consequently, the CRPF pier utilized eight bar fuses with a 2.0-m (6.5-ft) long fuse region, and the pile cap was made with the 0.9-m (3-ft) tall bumps to accommodate the fuses. Given that the pile cap uplift with respect to the piles was 0.23 m (0.75 ft) for 5% drift ratio, the piles protruded 0.3 m (1 ft) into the pile cap, which also provided sufficient bearing area to transfer lateral forces from the pile cap to the piles. The column in the CRPF pier was reinforced with seventy-two #43M (#14) longitudinal reinforcing bars and a #19M (#6) reinforcing spiral at a spacing of 102 mm (4 in.) to ensure its elasticity.

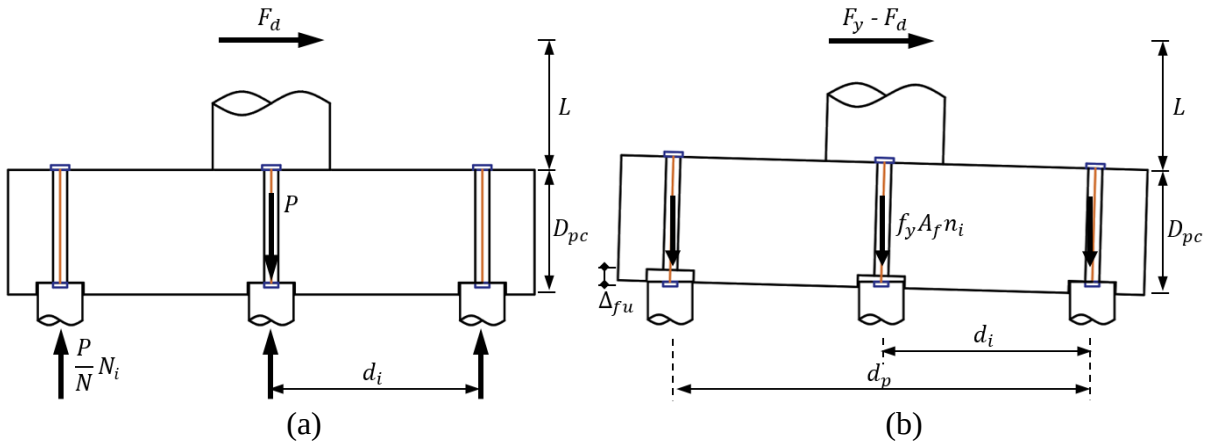

Figure 6.7 *Design of the CRPF pier: (a) decompression force and (b) area and length of the bar fuses*

Numerical Model

The analyses were conducted using the computer software SAP 2000. Figure 6.8 illustrates the 3D numerical models for the PH and CRPF piers. In the models, the superstructure was represented by a concentrated mass, which was connected to the pier column using a rigid link. For the PH pier, the column was modeled as an elastic beam-

column element with the effective moments of inertia approximated based on Caltrans SDC (2019). The nonlinear behavior of the column was captured using a concentrated fiber hinge assigned at 699 mm (27.5 in.) above the base of the column (i.e., the center of the plastic hinge). To define the hinge, the expected material properties according to Caltrans SDC (2019) were used, and the concrete and reinforcing steel were modeled following Mander et al. (1984) and Caltrans SDC (2019), respectively. The moment-rotation response of the hinge was characterized by integrating the stress-strain relation of the uniaxial fibers on the column section over a 1397 mm (55 in.) long plastic hinge, which was determined as per Caltrans SDC (2019). The pile cap was modeled using the elastic thick shell elements with a thickness of 1.5 m (5 ft), and its geometry was reproduced by rigid links assigned on top and bottom of the shell elements. The piles were represented by elastic beam-column elements, and the lateral and vertical soil resistances to the piles were simulated by a set of nonlinear springs prescribed by the *p-y* and *t-z* curves, respectively. Given the soil properties and conditions, the *p-y* and *t-z* curves were established according to the empirical formulations proposed for stiff clay without free water (Welch and Reese 1972; API 2002). In order to capture the formation of gaps between the piles and cohesive soil when the piles are subjected to cyclic load, compression-only *p-y* springs with the Takeda hysteresis model were assigned on four sides of the pile elements. The *t-z* springs were defined to provide both compressive and tensile resistance. The column, pile cap, and piles of the PH pier were modeled as fixed to each other.

For the CRPF pier, the column was modeled using an elastic beam-column element and fixed to the pile cap shell elements. The geometry of the pile cap and its bumps were reproduced by the rigid links, similar to the PH pier model. The piles of the CRPF pier and

the surrounding soil were modeled to be identical to that of the PH pier model. To allow the pile cap to uplift with respect to the piles while transferring the lateral force to the piles, the zero-length gap elements, which were rigid for compression but had zero tensile strength, were assigned between the pile beam-column element and the rigid link representing the pile cap thickness (Figure 6.8). The bar fuses in the CRPF pier were modeled using the uniaxial nonlinear links. These links were assigned connecting the pile cap rigid links to the pile beam-column elements, and their force-elongation response was defined according to the model as shown in Figure 6.5. In light of the findings from Kalliontzis and Sritharan (2018), the mass and stiffness proportionate Rayleigh damping was used for both models with 5% and 7% damping ratios in the first and third modes, which were the most predominant translational components in the lateral and vertical directions.

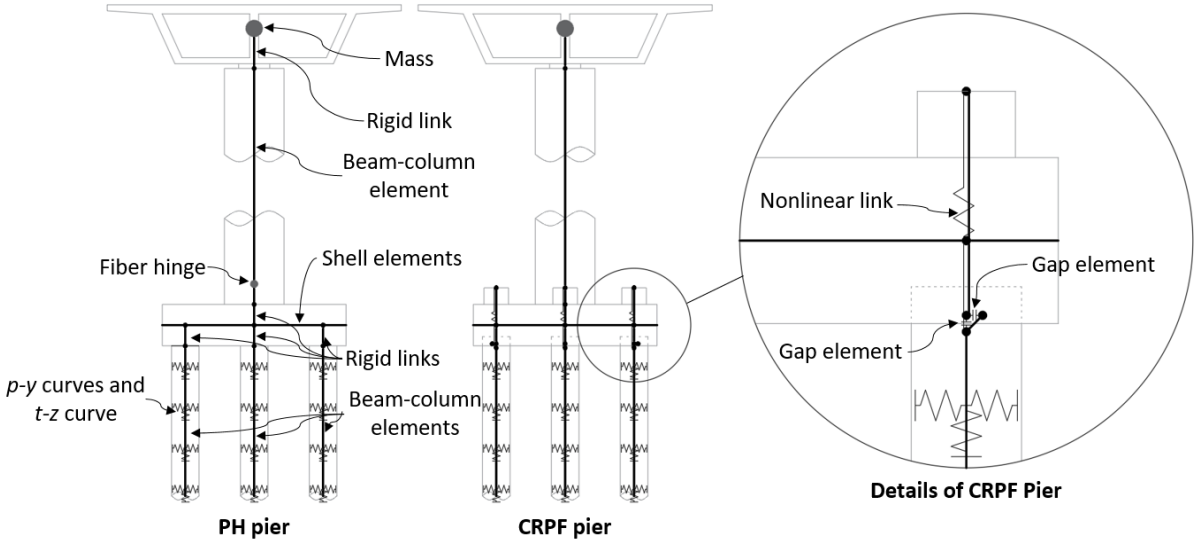

Figure 6.8 *Schematic of the numerical models*

Response to Static Cyclic Loads

Figure 6.9a shows the force-displacement responses of the CRPF and PH piers to the static cyclic loads. For the CRPF pier, the pile cap uplifts with respect to the two exterior piles (i.e., the left and right piles) and the pile underneath the column (i.e., the middle pile),

and the force in the bar fuses connecting to the two exterior piles were plotted as a function of column displacement in Figure 6.9b and Figure 6.9c, respectively. Under the cyclic loads, the CRPF pier rocked symmetrically on the top of the piles as expected. The pile decompression took place at a lateral load of 1086 kN (244 kips). With the pile cap uplifted from the piles, the bar fuses were subjected to tension, thereby producing additional resistance to the lateral force. After the fuse yielded at a lateral load of 2010 kN (452 kips), inelastic behavior dominated the response of the CRPF pier with a slight positive slope. When the lateral force was reversed, the pile cap set back to the piles, and the elongated bar fuses were compressed and yielded in compression. The bar fuses eventually fractured at a displacement of 1.07 m (42.1 in.), corresponding to a column drift ratio of 8.6%. The superstructure weight provided the necessary restoring force to recenter the pier when the applied lateral force was removed. Except the bar fuses, none of the components in the CRPF pier experienced the force exceeding its elastic limit. Thus, even experienced a large displacement, the pier maintained fully operational performance, and its seismic resistance can be rapidly recovered by only replacing the bar fuses. In contrast, the PH pier formed a plastic hinge in the column. Its damage levels corresponding to the different displacements (Figure 6.9a) were estimated as per Hose and Seible (1999). This revealed that, although the PH pier ensured the life safety when subjected to the large displacements, it sustained significant damages and residual displacement, which required weeks to months closure for repairing or even longer for replacement (Marsh and Stringer 2013). Figure 6.9d compares the equivalent viscous damping for the CRPF and PH piers. As expected, the PH pier dissipated more energy for a given displacement. Staring from a displacement of 0.25 m (9.8 in.) (i.e., a column drift ratio of 2%), the equivalent damping of the CRPF pier was more than

10% and reached approximately 20% before the bar fuses fractured. It is worth noting that the damping ratio of the CRPF pier can be increased or decreased by adjusting the pile group layout and dimensions of the bar fuses.

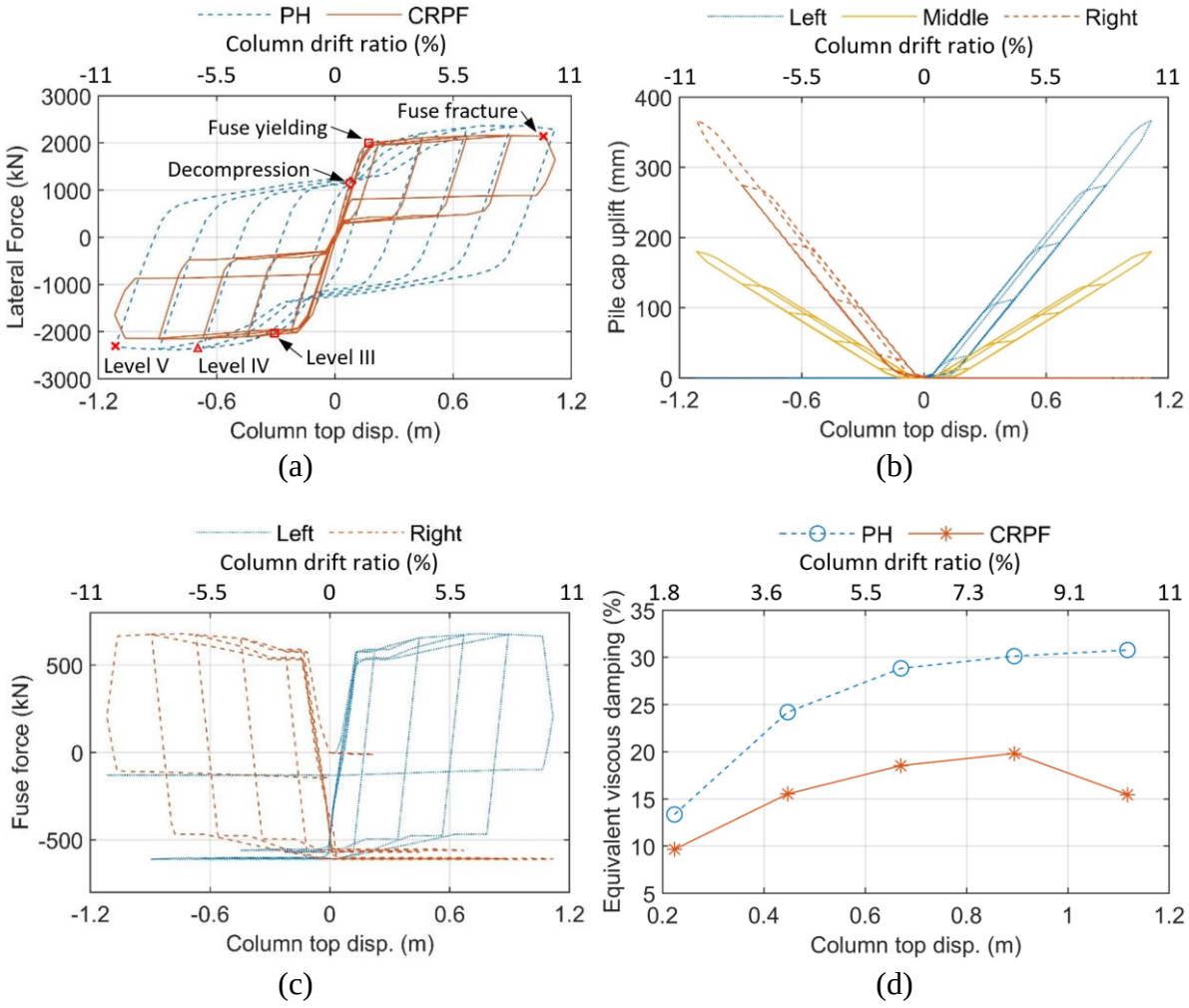

Figure 6.9 *Responses to static cyclic loads: (a) force-displacement behavior; (b) pile cap uplift in the CRPF pier; (c) change in fuse force; and (d) equivalent viscous damping ratio*

Figure 6.10a and Figure 6.10b depict the force-displacement responses at the head of the exterior piles in the lateral and axial directions. When subjected to the cyclic loads, the displacements of the piles in both the CRPF and PH piers were limited, confirming that the design of the pile group was satisfactory. Compared with the moment-resisting connections

between the piles and pile cap for the PH pile, the pinned connections used in the CRPF pier reduced the lateral stiffness of the piles. When the CRPF pier rocked on the top of the pile group, only the piles in the exterior row transferred the applied loads, thus the piles in the CRPF pier experienced higher lateral forces than those of the PH pier. The bar fuses in the CRPF pier transferred tensile forces to the piles, while their yield strength limited the tensile force acting on the pile to be less than 679 kN (153 kips), regardless of the magnitude of the applied lateral force.

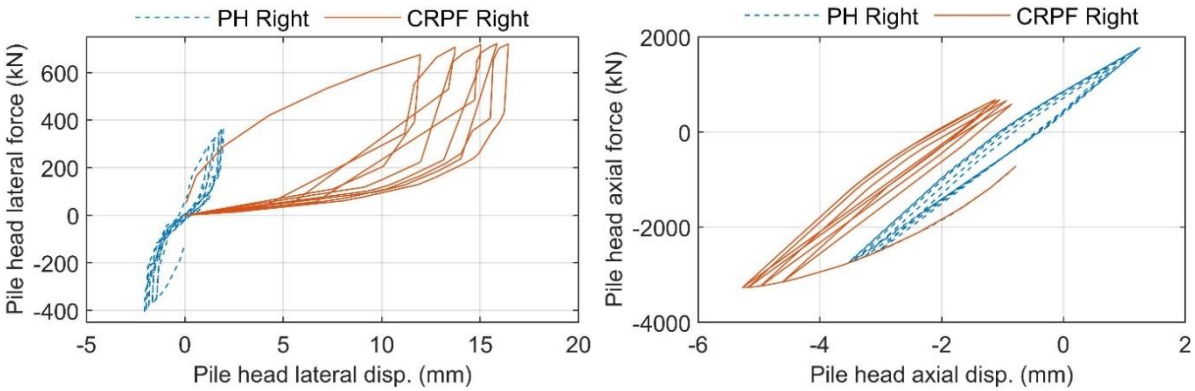

Figure 6.10 *Force-displacement response of the exterior piles in (a) lateral direction and (b) axial direction*

Response to Dynamic Free Vibrations

The CRPF and PH piers experienced free vibrations to examine their dynamic characteristics. Two rectangular pulse accelerations were applied laterally as the base excitations to the CRPF and PH piers. As shown in Figure 6.11a, the duration of the excitations was 0.5 sec., and the amplitude of the low-intensity excitation and high-intensity excitation was 0.1 g and 0.5 g, respectively. Figure 6.11b shows the column lateral displacement time histories for the CRPF and PH piers when subjected to the two excitations, and Figure 6.11c depicts the force-displacement responses of the two piers. To demonstrate

the rocking response of the CRPF pier, the pile cap uplift with respect to the exterior piles was plotted in Figure 6.11d as a function of time. When subjected to the low-intensity excitation, no pile cap uplift occurred in the CRPF pier, and the column top displacement primarily resulted from the elastic deformation of the column. The PH pier also behaved in an elastic manner. Because of the similarity of their elastic characteristics, the CRPF and PH piers exhibited comparable column displacement time history responses.

As the amplitude of the excitation increased to 0.5 g, both the CRPF and PH piers underwent the maximum displacement of approximately 0.44 m (17 in.), corresponding to a column drift ratio of 3.9%. The large displacement caused the plastic deformation in the column of the PH pier, leading to a considerable residual displacement of 0.18 m (7 in.), corresponding to a column drift ratio of 1.6%. In contrast, the CRPF pier recentered following the excitation. Its force-displacement response displayed the characteristic flag-shape with a fat hysteretic loop, indicating that a significant amount of energy dissipated during the large displacement cycle, but minimal energy dissipation took place for small displacement cycles. Consequently, the rocking response of the CRPF pier was abruptly decayed during the first displacement cycle, but afterward the pier continuously rocked at the small displacement amplitude for a number of cycles. The rocking mechanism excited the vertical inertia effects and induced impact between the pile cap and piles, causing the change in column axial force. As shown in Figure 6.11e, when subjected to the high-intensity excitation, the changes in the column axial force were more pronounced for the CRPF pier than those of the PH pier, and the impulses can be detected when the impacts occurred.

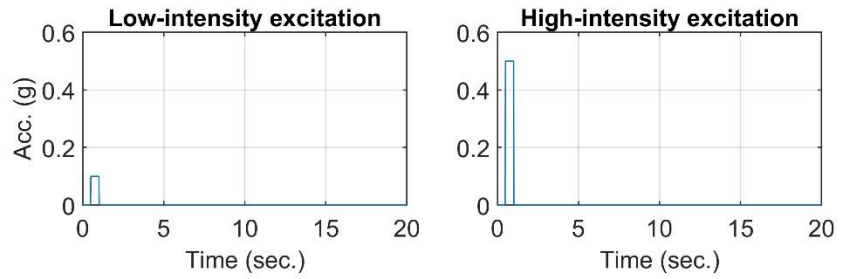

(a)

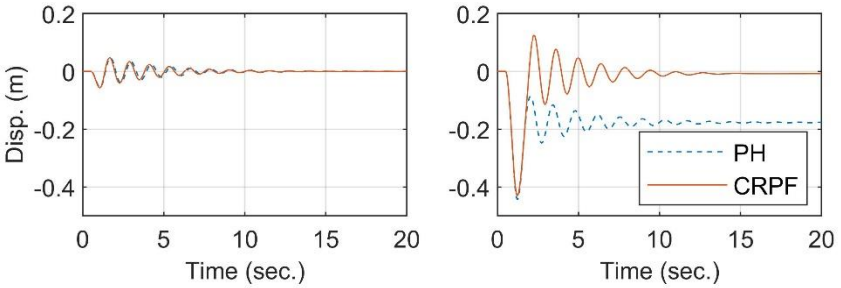

(b)

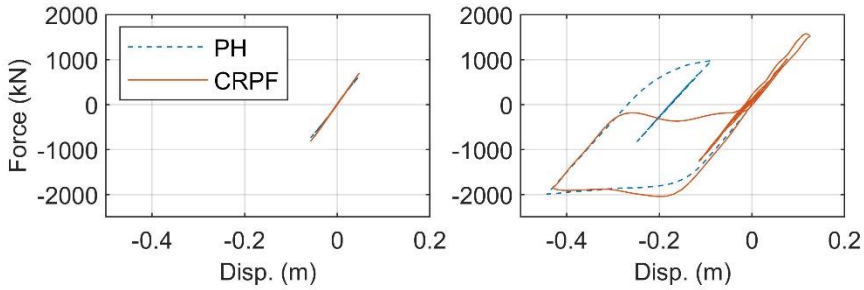

(c)

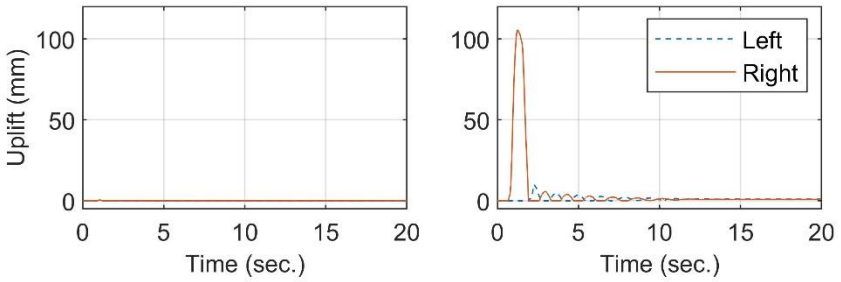

(d)

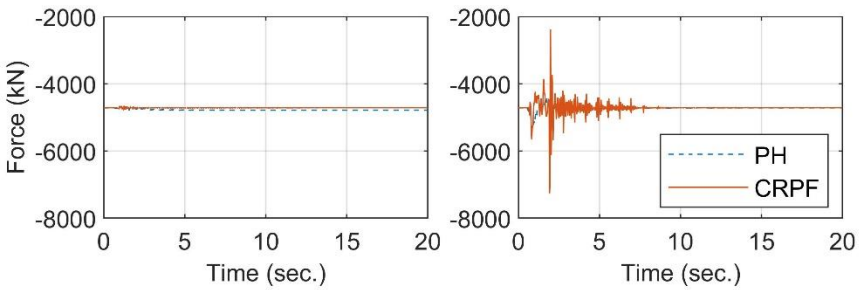

(e)

Figure 6.11 *Free vibration responses: (a) base excitation; (b) column displacement; (c) pile cap uplift for the CRPF pier; (d) force-displacement response; and (e) axial force in the column*

Response to Earthquake Ground Motions

To further analyze the behavior of the CRPF pier, the numerical models were subjected to a total of six earthquake ground motions with the details presented in Table 6.1. All records were sourced from the PEER strong motion database (PEER 2019). The ground motions were selected to represent a wide range of excitation that was expected for a high seismic zone. The 5% damped acceleration response spectra of the selected ground motions are plotted as shown in Figure 6.12.

Table 6.1 *Summary of selected earthquake ground motions*

Motion	Earthquake	Year	Magnitude	Station component	PGA (g)
EQ 1	Chi-chi	1999	7.6	CHY080-N	0.86
EQ 2	Chi-chi	1999	7.6	CHY028-N	0.69
EQ 3	Tabas	1978	7.4	TAB-L1	0.85
EQ 4	Kobe	1995	6.9	TAK000	0.62
EQ 5	Loma Prieta	1989	6.9	LGP000	0.57
EQ 6	Northridge	1994	6.7	JGB292	0.99

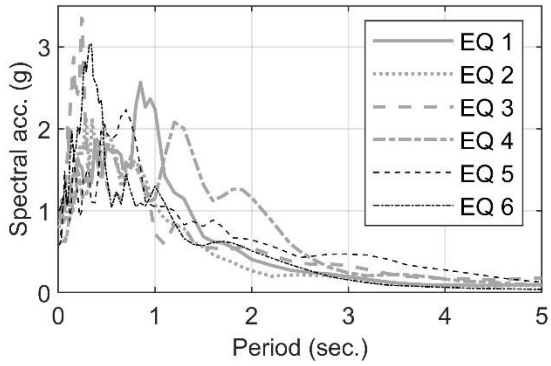

Figure 6.12 *Spectral acceleration versus period*

Table 6.2 summarizes the response parameters of the CRPF and PH piers for each of the ground motions. The maximum column drifts of the CRPF were comparable or slightly higher than those of the PH pier. This behavior was attributed to the lower hysteretic damping in the CRPF pier. The residual drift of the CRPF pier remained below 0.1%, benefiting from its recentering capacity. However, the residual drifts of the PH pier were up to 0.7%. For the CRPF pier, the strains of the bar fuses were less than 0.076, corresponding to 44.7% of the ultimate strain capacity of the bar steel. As the rocking mechanism causing the change in the column axial force, Table 6.2 also lists the maximum compressive axial force in the column of the CRPF pier. The maximum force was 17370 kN (3905 kips), corresponding to an axial load ratio of 24%.

Table 6.2 *Response parameters for the CRPF and PH piers subjected to the ground motions*

Motion	PH		CRPF			
	Max. drift ratio (%)	**Residual drift ratio (%)**	**Max. drift ratio (%)**	**Residual drift ratio (%)**	**Max. strain of fuses (ε)**	**Max. comp. axial force in column (kN)**
EQ 1	3.56	0.70	3.56	0.10	0.047	11116
EQ 2	2.05	0.14	2.14	0.03	0.022	10880
EQ 3	2.67	0.14	2.73	0.01	0.031	8683
EQ 4	4.67	0.04	5.12	0.07	0.076	17370
EQ 5	2.42	0.40	2.42	0.01	0.027	13206
EQ 6	2.37	0.23	2.38	0.07	0.025	11859

Figure 6.13 compares the force-displacement hysteresis behaviors of the CRPF and PH piers for each of the ground motions. All the hysteresis curves exhibited no major strength degradation, indicating that both piers ensured life safety and collapse prevention. For the PH pier, given that the lateral displacement corresponding to damage level III were approximately 0.3 m (11.8 in.), it experienced moderate-to-significant damages when subjected to the ground motions of EQ 1 and EQ 4 and required closures for repairing. Despite the inelastic yielding of the bar fuses as expected, the CRPF pier did not experience inelastic deformations in the column, pile cap, and pile foundation for the ground motions, thus was immediately accessible for normal traffic.

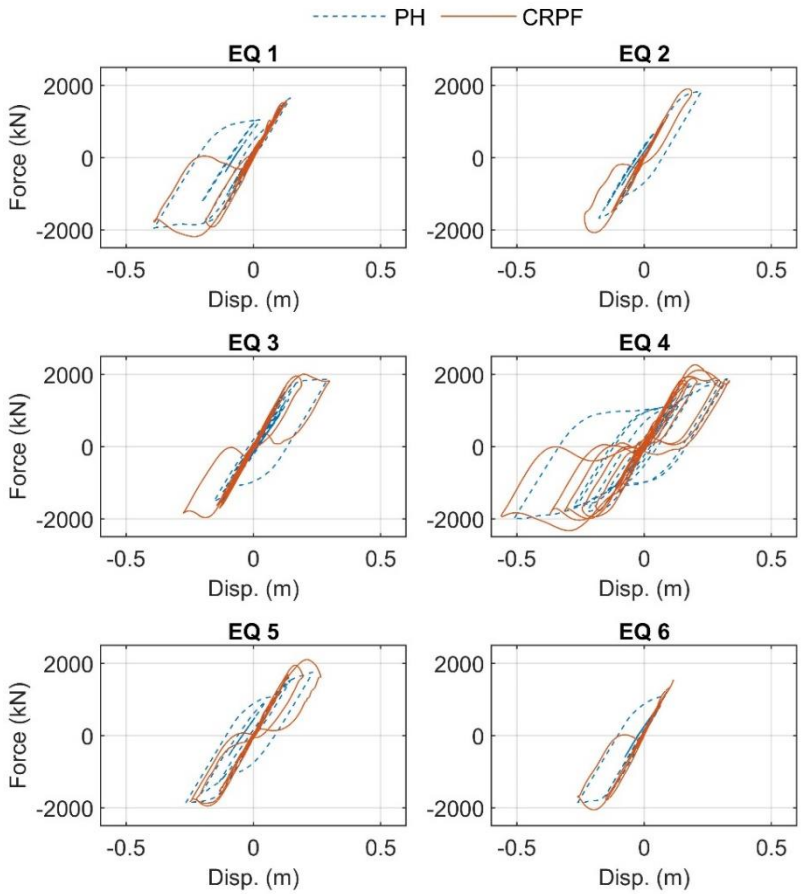

Figure 6.13 *Force-displacement behaviors of the CRPF and PH piers for each of the ground motions*

Conclusions

This paper presents the controlled rocking pile foundation (CRPF) system with replaceable bar fuses designed for seismic resilience. The CRPF system features the precast pile cap that is allowed to uplift with respect to the piles and the replaceable bar fuses connecting the pile cap and piles. When subjected to a strong earthquake excitation, the pile cap is uplifted from the top of the pile foundation, causing the fuses to undergo inelastic deformation to dissipate seismic energy. The superstructure weight acting on the CRPF system provides restoring force to recenter the system. The CRPF system can be constructed on different types of pile foundations. For the different pile types, the conceptual connections are developed to efficiently attach the bar fuses. The seismic response of a bridge pier utilizing the CRPF system (CRPF pier) was numerically investigated and compared with that of a bridge pier designed to develop a flexural plastic hinge in the column (PH pier). The three-dimensional nonlinear analytical models of the CRPF and PH piers were subjected to static cyclic loads, dynamic free vibrations, and earthquake ground motions. The following conclusions were made based on the findings of this analytical study:

- The CRPF system designed following the simplified approach successfully achieved the design objectives. When subjected to the cyclic lateral loads acting at the top of the column, the resistance of the CRPF pier was comparable to that of the PH pier as designed. The CRPF pier reached a column drift ratio of 8.6% without significant strength degradation and exhibited sufficient recentering capacity. The CRPF pier resulted in an elastic response of the column, pile cap, and pile foundation. The inelastic behavior only occurred in the bar fuses as expected. The inelastic deformation of the bar fuses provided the equivalent viscous damping ratio more than 10% and reached approximately 20% before the

bar fuses fractured. It is worth noting that the damping ratio corresponds to the configuration of the pile foundation and bar fuses, thus can be correspondingly adjusted according to the design requirements.

- When subjected to the low-intensity excitation with a duration of 5 sec. and an amplitude of 0.1 g, the CRPF and PH piers deformed in an elastic manner and exhibited comparable free vibration behavior because of their similar elastic characteristics. As the amplitude of the excitation increased to 0.5 g, the pile cap of the CRPF pier uplifted with respect to the pile foundation, causing the bar fuses to undergo inelastic deformation and providing a large amount of hysteretic damping, thus abruptly decaying the free vibration of the CRPF. The energy dissipation of the CRPF pier significantly reduced after the first cycle of the free vibration because the fuses remained elastic during the following cycles.
- Both the CRPF and PH piers provided life safety and collapse prevention when subjected to the earthquake ground motions. The column drift ratio of the CRPF pier did not exceed 5.12% for the duration of the shakings, and the residual drift ratio was less than 0.1%. In addition, all components except the bar fuses retained elastic response, and the strain of the bar fuses stayed below the acceptable limits suggested by the PRESSS design handbook (Pampanin et al. 2010), confirming the seismic resilience of the CRPF system. In contrast, the PH pier experienced the significant damage in the column and exhibited a residual drift up to 0.7%. Note that as the pile cap of the CRPF pier rocked on the top of the pile foundation, the axial force in the column was varied up to 4 times the design

value, suggesting the necessity of keeping a low column axial load ratio for design.

Reference

Acikgoz, S., and DeJong, M. J. (2012). "The interaction of elasticity and rocking in flexible structures allowed to uplift." *Earthquake Eng. Struct. Dyn.*, 41(15), 2177–2194.

Allmond, J., and Kutter, B. L. (2012). "Centrifuge testing of rocking foundations on saturated and submerged sand: Centrifuge Data Report for JDA01." *UCD/CGMDR-12/01*, Univ. of California at Davis, Davis, CA.

Allmond, J., and Kutter, B. L. (2013). "Centrifuge testing of rocking foundations on saturated and submerged sand: Centrifuge Data Report for JDA02." *UCD/CGMDR-13/01*, Univ. of California at Davis, Davis, CA.

Allmond, J. D., and Kutter, B. L. (2014). "Design considerations for rocking foundations on unattached piles." *J. Geotech. Geoenviron. Eng.*, 140(10), 04014058.

Antonellis G, and Panagiotou M., "Seismic response of bridges with rocking foundations compared to fixed-base bridges at a near-fault site." *J. Bridge Eng.*, 19(5), 04014007.

Antonellis, G., Gavras, A. G., Panagiotou, M., Kutter, B. L., Guerrini, G., Sander, A. C., and Fox, P. J. (2015). "Shake table test of large-scale bridge columns supported on rocking shallow foundations." *J. Geotech. Geoenviron. Eng.*, 141(5), 04015009.

API (2002). "Recommended practice for planning, designing and constructing fixed offshore platforms-working stress design." *RP 2A-WSD,* American Petroleum Institute.

Caltrans. (2019). *Seismic design criteria version 1.7*, Sacramento, CA.

Chopra, A. K. and Yim, C. S. (1985). "Simplified earthquake analysis of structures with foundation uplift." *J. Structural Eng.*, 11(4), 906–930.

Chou, C. C., and Chen, Y. C. (2006). "Cyclic tests of post-tensioned precast CFT segmental bridge columns with unbonded strands." *Earthquake Eng. Struct. Dyn.*, 35(2), 159–175.

Culmo, M. P. (2011). "Accelerated Bridge Construction- Experiences in Design, Fabrication and Erection of Prefabricated Bridge Elements and Systems." *FHWA-HIF-12-013*, Federal Highway Administration, U.S. Department of Transportations, Washington, DC.

Deng, L., Kutter, B. L., and Kunnath, S. K. (2012). "Probabilistic seismic performance of rocking-foundation and hinging-column bridges." *Earthquake Spectra*, 28(4), 1423–1446.

Espinoza, A., and Mahin, S. A. (2008). "Shaking table and analytical investigation of reinforced concrete bridge piers with foundations allowed to uplift during earthquakes." *Rep. No. UCB/SEMM-08/03,* Dept. of Civil and Environmental Engineering, Univ. of California, Berkeley, CA.

Kalliontzis, D., Sritharan, S., and Schultz, A. (2016). "Improved coefficient of restitution estimation for free rocking members." *J. Structural Eng.*, 142(12), 06016002.

Kalliontzis, D., and Sritharan, S. (2018). "Characterizing dynamic decay of motion of free-standing rocking members." *Earthquake Spectra*, *34*(2), 843-866.

Gajan, S., and Kutter, B. L. (2008). "Capacity, settlement, and energy dissipation of shallow footings subjected to rocking." *J. Geotech. Geoenviron. Eng.*, 10.1061/(ASCE)1090-0241(2008)134:8(1129), 1129–1141.

Guan, Z., Chen, X., and Li, J. (2018). "Experimental investigation of the seismic performance of bridge models with conventional and rocking pile group foundations." *Eng. Struct.*, 168, 889-902.

Guo, T., Cao, Z., Xu, Z., and Lu, S. (2015). "Cyclic load tests on self-centering concrete pier with external dissipators and enhanced durability." *J. Structural Eng.*, 142(1), 04015088.

Hewes, J. T., and Priestley, M. J. N. (2002). "Seismic design and performance of precast concrete segmental bridge columns." *Rep. No. SSRP2001/25*, California Dept. of Transportation, Sacramento, CA.

Hose, Y.D. and Seible. F. (1999). "Performance evaluation database for concrete bridge components and systems under simulated seismic loads." Pacific Earthquake Engineering Research Center, Berkeley, CA.

Housner, G. W. (1963). "The behavior of inverted pendulum structures during earthquakes." *Bull. Seismol. Soc. Am.*, 53(2), 403–417.

Mander, J. B., Priestley, M. J. N. and Park R. (1984). "Theoretical stress strain model for confined concrete." *J. Struct. Eng.*, 114(3). 1804-1826.

Marriott, D., Pampanin, S., and Palermo, A. (2009). "Quasi-static and pseudo-dynamic testing of unbonded post-tensioned rocking bridge piers with external replaceable dissipaters." *Earthquake Eng. Struct. Dyn.*, 38(3), 331–354.

Marsh, M. L., and Stringer, S. J. (2013). "Performance-based seismic bridge design." *NCHRP Synthesis 440*, Transportation Research Board, Washington, DC.

Meek, J. W. (1975). "Effects of foundation tipping on dynamic response." *J. Struct. Div.*, ASCE, 101(7), 1297-1311.

Mergos, P. E., and Kawashima, K. (2005). "Rocking isolation of a typical bridge pier on spread foundation." *J. Earthquake Eng.*, 9(supplement 2), 395–414.

Ou, Y. C., Tsai, M. S., Chang, K. C., and Lee, G. C. (2010). "Cyclic behavior of precast segmental concrete bridge columns with high performance or conventional steel reinforcing bars as energy dissipation bars." *Earthquake Eng. Struct. Dyn.*, 39(11), 1181–1198.

Pampanin, S., Marriott, D., and Palermo, A. (2010). PRESSS design handbook. *New Zealand Concrete Society*.

PEER (Pacific Earthquake Engineering Research Center). (2019). "Welcome to the PEER ground motion database." <http://ngawest2 .berkeley.edu/> (May 10, 2019).

Priestley, M. J. N., Sritharan, S., Conley, J. R., and Pampanin, S. (1999). "Preliminary results and conclusions from the PRESSS five-story precast concrete test building." *PCI Journal*, 44(6), 42-67.

Restrepo, J. I., and Rahman, A. (2007). "Seismic performance of self-centering structural walls incorporating energy dissipators". *J. Structural Eng.*, 133(11), 1560-1570.

Restrepo, J. I., Tobolski, M. J., and Matsumoto, E. E. (2011). "Development of a precast bent cap system for seismic regions." *NCHRP Rep. No. 681*, Transportation Research Board, Washington, DC.

Roh, H., and Reinhorn, A. M. (2010). "Hysteretic behavior of precast segmental bridge piers with superelastic shape memory alloy bars." *Eng. Struct.*, 32(10), 3394–3403.

Saidi, M., Gopalakrishnan, B., and Siddharthan, R. (2002). "Shake table studies of effects of foundation flexibility on seismic demand in substandard bridge piers." *ACI 5th Int. Conf., Special Publication*, American Concrete Institute, Detroit, 553–569.

Sritharan, S., Aaleti, S., Henry, R. S., Liu, K. Y., and Tasi, K. C. (2015). "Precast concrete wall with end columns (PreWEC) for earthquake resistant design." *Earthquake Eng. Struct. Dyn.*, 44(12), 2075-2092.

Wang, J. C., Ou, Y. C., Chang, K. C., and Lee, G. C. (2008). "Large-scale seismic tests of tall concrete bridge columns with precast segmental construction." *Earthquake Eng. Struct. Dyn.*, 37(12):1449–1465.

Welch, R. C. and Reese L. C. (1972). "Laterally loaded behavior of drilled shafts." *Research Report 3-5-65-89*, Center for Highway Research, University of Texas, Austin.

White, S. L. (2014). "Controlled damage rocking systems for accelerated bridge construction." M.E. thesis, Univ. of Canterbury, Christchurch, New Zealand.

CHAPTER 7. SUMMARY AND CONCLUSIONS

Summary

The focus of the studies presented in this dissertation was to investigate the seismic performance of the prefabricated bridge piers supported on pile foundations. Given that the widely adopted seismic design approach relies on the formation of plastic hinges in preselected locations (column ends in most of the cases) to protect bridges from collapse, the connections between prefabricated components must be able to remain elastic when the bridges are subjected to earthquakes. In response to these requests, a prefabricated column-pile cap-pile system suitable for seismic regions was developed in light of the current state of the art. The system consists of precast column, precast pile cap, and pile foundation. The components are integrally connected utilizing column socket connection and pile pocket connections that are preformed in the pile cap with corrugated steel pipes (CSPs). To evaluate the side shear strength of the column socket connection with various connection parameters, an experimental study was performed using eight specimens that modeled the full-scaled connection interfaces. Each specimen consisted of a short precast column segment that was embedded in a socket on a precast foundation. When a compressive force is applied to the top of the column segment, the side shear acting on the connection interface produced the resistance. Thus, the side shear strength could be evaluated by loading the column segment until it experiences a sliding failure with respect to the foundation. The specimens were constructed with different surface texture for the embedded portion of the column segment and CSP-to-column segment clearance and were tested by subjecting them to monotonic and cyclic axial loading. Test results show that side shear mechanism in the

column socket connections can provide significant resistance, facilitating transfer of large vertical loads.

An outdoor test was subsequently conducted on the column-pile cap-pile system at a cohesive soil site. The test unit was constructed as a half-scale representation of the column-pile cap-pile system utilizing a precast column, a precast pile cap, four vertical steel piles, and four battered piles. The test unit was subjected to combined vertical and lateral loads applied to the top of the column, and a plastic hinge was formed in the column as the lateral load and column displacement gradually increased. The column socket connection and pile pocket connections maintained fixity with the formation of a plastic hinge in the column, evidencing that the seismic sufficiency of the system.

After casting a concrete block on top of the pile cap surrounding the damage column, the foundation of the test unit was further tested under different combinations of vertical and lateral loads. Not only the magnitude of the loads were changed, but the height of lateral load was also varied to produce different overturning moment-to-lateral load ratio. The foundation exhibited significant resistance to the combined vertical and lateral loads and eventually failed due to the combined effects of pile buckling, damage in the pile pocket connections, and formation of the permanent gaps between the piles and cohesive soil. A numerical model with nonlinear springs representing soil resistances was developed for helping better understanding understand the behavior of the pile foundation. The experimental and analytical results show that the battered piles were subjected to larger axial forces but less bending moments than the vertical piles.

In addition to ensure life safety and prevent collapse, seismic performance objectives such as immediately openings after an earthquake, shorter repair times, and lower repair

costs are also desired for bridges. Therefore, the controlled rocking pile foundation (CRPF) system with replaceable bar fuses was developed. The CRPF system allows the precast pile cap to rock on the top of pile foundation and dissipates seismic energy through the inelastic deformations of the bar fuses connecting the pile cap and piles. Its seismic performance was studied through the numerical approach and compared with that of a bridge pier designed to develop a flexural plastic hinge in the column. The analysis results show that, subjected to a severe earthquake, the CRPF system showed negligible residual displacement and maintained elastic behavior except the bar fuses as designed. The damaged fuses can be rapidly replaced to recover the bridge seismic resistance after the earthquake.

Conclusions

Conclusions drawn from the studies presented in this dissertation are presented below:

Side shear strength of column socket connection

- The intentionally roughened column surface, as required by AASHTO, is necessary to develop satisfactory side shear strength to sustain axial loads used in routine design practice. However, surface roughness smaller than an amplitude of 6-mm is adequate, which can be easily achieved by exposing the aggregates.
- The column surface textures with deep amplitude (e.g., fluted fins) exhibited softer connection responses compared to the one with exposed aggregate surface finish. Thicker grout closure pour resulting from wider CSP-to-column clearance also reduced the stiffness of the socket connection.
- For the column segment surface textures with deeper amplitude, the force transfer was more efficient when subjecting to high loads due to the increased surface roughness, enabling the load to be resisted over a shorter length.

- Exposed aggregate for column surface preparation, standard CSP, and high-strength grout are recommended for establishing socket connections effectively. For connections established as described in this study, the side stress limitations of 6.89-MPa (1000-psi) and 4.83-MPa (700-psi) suggested, respectively, for the column-to-grout interface and CSP-to-surrounding concrete interface to determine the minimum depth of the preformed socket.

Performance of prefabricated column-pile cap-pile system

- The system exhibited stable energy dissipation capacity as the plastic hinge was fully developed in the column, and the pile cap and connections remained undamaged throughout the test. This proved that the performance of the prefabricated column-pile cap-pile system was excellent and is believed to be at least as good as, if not better than, that of a conventional cast-in-place system. For the column socket connection, the embedment length equal to one times the column diameter is sufficient to allow a plastic hinge to be developed in the column. The pile embedment length of 1.5 times the depth of pile is also sufficient to maintain the fixity of the pile pocket connection.
- Foundation flexibility produced a significant effect on the system response. About 40% of column top displacement was due to the foundation flexibility prior to development of the column plastic hinge. As the damage progressed in the column, the foundation flexibility caused less effect in terms of column top displacement, while it still accounted for an important component when the effective lateral load reached its maximum.
- The constructability advantages of the prefabricated column-pile cap-pile system are that it is quick and simple to build. The precast column and precast pile cap with no

projected reinforcement are easy to transport and are unlikely to be damaged during construction. Given the friction collar and grout with desirable characteristics (including high-early-strength, extended working time, and appropriated fluid consistency), construction of a column-pile cap-pile system can be completed within one day.

Performance of pile foundation including battered piles

- The pile group exhibited significant load resistances to the combined vertical and lateral loads. Under the load combinations with high overturning moment-to-lateral load ratio [i.e., the lateral load was applied at 2.13 m (7 ft) above the pile cap], the bending moments at the head of piles was negligible, and the applied loads were primarily resisted by the vertical reactions provided by the piles. When the overturning moment-to-lateral load ratio was reduced [i.e., the lateral load was applied at 0.30 m (1 ft) above the pile cap], in addition to the axial forces, the considerable bending moments were developed at the pile heads.
- Precast pile cap showed a satisfactory performance and remained essentially undamaged under the different combinations of vertical and lateral loads. Sufficient pile-to-pile cap connections were established by embedding the pile heads into the preformed pockets. With the embedment length of 1.5 times the depth of the piles, the connections developed considerable resistances to the axial force and bending moment acting in the piles. Under the very large lateral loads, the significant tensile forces were induced to the piles, and the connections were damaged in a ductile manner.

- The numerical model adequately captured the behavior of the tested pile group. The nonlinear response of the piles and pile-to-pile cap connections was accounted for using the concentrated hinges and zero-length springs assigned to the pile elements. The soil resistances were represented by the nonlinear springs prescribed by *p-y* curves and *t-z* curves. These nonlinear curves developed from empirical formulations were adjusted using multipliers to account for the effects of the pile batter, plugin holes surrounding the piles, and group interaction.
- Based on the results of analyses and the test observations, the battered piles were subjected to larger axial forces but less bending moments than the vertical piles. The role of batter was more prominent when the lateral load was applied close to the pile cap.

Performance of CRPF system

- The performance of a bridge pier supported on the CRPF system (CRPF pier) was numerically investigated and compared to that of a pier designed to form a plastic hinge in its column (PH pier). The CRPF system designed following the simplified approach successfully achieved the design objectives. When subjected to the cyclic lateral loads acting at the top of the column, the resistance of the CRPF pier was comparable to that of the PH pier as designed. The CRPF pier reached a considerable column drift ratio without significant strength degradation and exhibited sufficient recentering capacity. The CRPF pier resulted in an elastic response of the column, pile cap, and pile foundation. The inelastic behavior only occurred in the bar fuses as expected. The inelastic deformation of the bar fuses provided the equivalent viscous damping ratio up to approximately 20% before the bar fuses fractured. It is worth

noting that the damping ratio corresponds to the configuration of the pile foundation and bar fuses, thus can be correspondingly adjusted according to the design requirements.

- When subjected to the low-intensity excitation with a duration of 5 sec. and an amplitude of 0.1 g, the CRPF and PH piers deformed in an elastic manner and exhibited comparable free vibration behavior because of their similar elastic characteristics. As the amplitude of the excitation increased to 0.5 g, the pile cap of the CRPF pier uplifted with respect to the pile foundation, causing the bar fuses to undergo inelastic deformation and providing a large amount of hysteretic damping, thus abruptly decaying the free vibration of the CRPF. The energy dissipation of the CRPF pier significantly reduced after the first cycle of the free vibration because the fuses remained elastic during the following cycles.
- Both the CRPF and PH piers provided life safety and collapse prevention when subjected to the earthquake ground motions. The column drift ratio of the CRPF pier did not exceed 5.12% for the duration of the shakings, and the residual drift ratio was less than 0.1%. In addition, all components except the bar fuses retained elastic response, and the strain of the bar fuses stayed below the acceptable limits suggested by the PRESSS design handbook (Pampanin et al. 2010), confirming the seismic resilience of the CRPF system. In contrast, the PH pier experienced the significant damage in the column and exhibited a residual drift up to 0.7%. As the pile cap of the CRPF pier rocked on the top of the pile foundation, the axial force in the column was varied up to 4 times the design value, suggesting the necessity of keeping a low column axial load ratio for design.